Title
The HVEM-BTLA axis restrains T cell help to germinal center B cells and functions as a cell-extrinsic suppressor in lymphomagenesis

Author
Mintz, Michelle Amy

Publication Date
2019

Peer reviewed|Thesis/dissertation

The HVEM-BTLA axis restrains T cell help to germinal center B cells and functions as a cell-extrinsic suppressor in lymphomagenesis

by
Michelle Amy Mintz

DISSERTATION
Submitted in partial satisfaction of the requirements for degree of
DOCTOR OF PHILOSOPHY

in

Biomedical Sciences

in the

GRADUATE DIVISION
of the
UNIVERSITY OF CALIFORNIA, SAN FRANCISCO

Approved:

DocuSigned by:
Arthur Weiss
69EA7B8D002043D...

Arthur Weiss
Chair

DocuSigned by:
Christopher Allen
DocuSigned by:

CHRISTOPHER ALLEN

Jason Cyster
5FFFC327038A40D...

Jason Cyster

Committee Members

This dissertation is dedicated to my parents,

Barbara Mintz and Donald Mintz,

for their endless support

ACKNOWLEDGEMENTS

The work described in this dissertation was done under the direct supervision of Dr. Jason Cyster, PhD. Dr. Jason Cyster has shown me, through his actions, an excellent example of how to lead a scientifically rigorous lab. He has provided critical feedback throughout my training that I will continue to carry with me through the entirety of my career. Additional guidance was provided by members of the thesis committee: Dr. Arthur Weiss MD, PhD and Dr. Chris Allen, PhD.

Dr. Jagan Muppidi, MD, PhD mentored me during my rotation in the lab and during the initial portions of my project. He has continued to provide scientific and career advice. Marissa Chou was instrumental in adding to our understanding of how HVEM and BTLA moderate T cell help through CD40L, and has provided helpful discussions on many portions of my project, paper, and work. Dr. Eric Dang, PhD was an excellent colleague, who provided critical feedback and was always happy to brainstorm ideas. I had a great collaboration with Dr. James Felce, PhD along with Dr. Viveka Mayya, PhD and Dr. Michael Dustin, PhD, who added to our understanding of how BTLA regulates T cell signaling. Ying Xu provided instrumental support and advice regarding my molecular biology work, sequencing, mouse development, and protocol trouble shooting. JinPing An provided invaluable assistance in genotyping and taking care of the mouse colony. Zhongmei Li in Dr. Alexander Marson's lab provided expertise to develop our new mouse line BTLA Y3. Dr. Brian Laidlaw, PhD has provided insightful germinal center discussions and career advice. Dr. Erick Lu, PhD and Dr. Lauren Rodda, PhD were great colleagues who were always helpful at bouncing ideas off of and providing advice for analyzing

large datasets and staining sections. Dr. Hsin Chen, PhD provided excellent training in 2-photon microscopy. Dr. Andrea Reboldi, PhD and Dr. Jiaxi Wu, PhD provided advice early on in my PhD. Dr. Dan Liu, PhD provided helpful discussions about germinal center biology. Dr. Lihui Duan, PhD provided assistance in analyzing single cell data and advice on analyzing large datasets. Benchmates Antonia Gallman and Elise Wolf have been crucial in sharing in the joys of exciting of new data and disappoints of negative data and discussing ideas throughout the later part of my PhD. Trisha Macrae has been a fantastic friend and has provided help in my understanding of GSEA analysis. Dr. Sophie Levan, PhD has been a helpful friend one step ahead along the MSTP track and has provided excellent path in which to follow. Dr. Mark Anderson, MD PhD has served as my graduate school advisor and provided excellent advice. Geri Ehle, Demian Sainz, Ned Molyneaux, Amanda Andonian, and Andres Zepeda have been essential to helping me progress throughout the MSTP and BMS programs. Bernarda Lopez has provided help in keeping our projects running in lab. Claire Chan, Kenna Fowler, and Viviana Davila have kept the labs running through administrative support. The LARC staff has been essential to be maintaining healthy mouse lines and the ensure the success of my projects. Additional support for this project came from collaborators who provided us with essential mouse tools: Dr. Takaharu Okada, PhD, Dr. Carl Ware, MD, PhD, Dr. Mitchell Kronenberg, PhD, and Dr. JR-WeN Shui, PhD.

My husband Alex Roth has provided endless support, encouragement, and companionship that was essential to my success in completing my graduate work. My sister Melissa Morgan and her family, JP, Hannah, and Henry, also have offered support and encouragement. Lastly, I want to

thank my mother Barbara Mintz and my father Donald Mintz for being my lifelong supporters and my confidants with whom to debrief with at the end of nearly every day in the lab.

CONTRIBUTIONS TO PRESENT WORK

The work described in this dissertation was done under the direct supervision of Dr. Jason Cyster, PhD. Funding for this research was acquired through the F30 NIAID as well as additional funding acquired through Dr. Cyster. Additional contributions are described below.

The Introduction and conclusion have been adapted from a review I conceived and wrote that are in development for submission, entitled "T follicular helper cells in germinal center B cell section and lymphomagnesis" to *Immunological Reviews*. Dr. Jason Cyster has provided critical feedback and edits on this manuscript.

Chapter 1 was published as Mintz, M. A., Felce, J. H., Chou, M. Y., Mayya, V., Xu, Y., Shui, J.-W., et al. (2019). The HVEM-BTLA Axis Restrains T Cell Help to Germinal Center B Cells and Functions as a Cell- Extrinsic Suppressor in Lymphomagenesis. *Immunity*, *51*(2), 310–323.e7. http://doi.org/10.1016/j.immuni.2019.05.022

Michelle A Mintz and Jason G Cyster conceptualized the project, designed the experiments, interpreted the results and wrote the manuscript. Michelle A Mintz performed the experiments. James H Felce, Viveka Mayya and Michael L Dustin designed and performed the lipid bilayer experiments, interpreted the results and helped prepare the manuscript. Marissa Y Chou performed CD40L induction studies, interpreted data and helped prepare the manuscript. Ying Xu performed molecular biology experiments. JinPing An genotyped mice. Zhongmei Li and Alexander Marson generated the BTLA Y3 mutant mouse line. Takaharu Okada, Jr-Wen Shui, Carl F Ware and Mitchell Kronenberg provided gene targeted mouse lines and provided input on the manuscript.

The HVEM-BTLA axis restrains T cell help to germinal center B cells and functions as a cell-extrinsic suppressor in lymphomagenesis

Michelle Amy Mintz

ABSTRACT

TNF receptor family member HVEM is one of the most frequently mutated surface proteins in germinal center (GC) derived B cell lymphomas, yet the role of HVEM in normal GCs is unknown. We found that HVEM-deficiency intrinsically increased B cell competitiveness during pre-GC and GC responses. The Ig superfamily molecule BTLA was identified as the ligand regulating these responses, and B cell-intrinsic signaling via HVEM and BTLA was not required. Instead, BTLA signaling into the T cell through SHP1 reduced TCR signaling and the amount of preformed CD40L mobilized to the immunological synapse and thus diminished the help delivered to B cells. Moreover, T cell-deficiency in BTLA cooperated with B cell Bcl-2-overexpression in leading to GC B cell outgrowth. These results establish that HVEM restrains the T helper signals delivered to B cells in a manner that influences GC selection outcomes, and they suggest that BTLA functions as a cell-extrinsic suppressor of GC B cell lymphomagenesis.

TABLE OF CONTENTS

CHAPTER 1: Introduction *1*

Introduction **2**

Mutations in B cell lymphomagenesis **4**

Tfh cell participation in follicular lymphoma **5**

IL-4 – STAT-6 ..... **7**

CD40L – CD40 ..... **9**

PD-1 – PD-L1/PD-L2 ..... **11**

ICOS – ICOSL **14**

FasL – Fas **16**

SAP – SLAMF **18**

Tfh cell derived lymphomas **19**

BTLA – HVEM **21**

CHAPTER 2: The HVEM-BTLA axis restrains T cell help to germinal center B cells and functions as a cell-extrinsic suppressor in lymphomagenesis *24*

Summary **25**

Introduction **25**

Results **27**

HVEM-deficiency increases GC B cell competitiveness 27

HVEM-deficiency provides the earliest GC B cells with a proliferation advantage 31

Loss of HVEM in an ongoing GC provides B cells with a competitive advantage 31

HVEM signaling intrinsic to the B cell is not required for GC B cell suppression 34

BTLA on CD4$^+$ T cells is required for HVEM-deficient GC B cell competitiveness ... 36

BTLA-HVEM at the immunological synapse recruits SHP1 to inhibit signaling in Tfh cells 38

BTLA signaling into the T cell through SHP1 is required for HVEM-deficient GC B cell competitiveness 41

HVEM-BTLA interaction reduces the amount of CD40-CD40L brought to synaptic interface 43

BTLA-deficiency in T cells leads to GC B cell expansion in the setting of Bcl-2-overexpression 45

Discussion 47

SUPPLEMENTAL FIGURES AND LEGENDS 53

MATERIALS AND METHODS..... 58

Mice 59

Generation of BTLAY3 mice 59

Bone marrow chimeras 60

Retroviral constructs and transductions 60

Cell isolation, adoptive transfer 61

Immunizations 61

Flow cytometry 62

qPCR and RNA-sequencing 62

GSEA and Gene Ontology 63

NP V_H186.2 mutation analysis 63

Tfh cell CD40L surface mobilization 64

Assessment of BCR clonality by PCR 65

Human $CD4^+$ T cell isolation, stimulation, and transfection 65

Human Tfh cell isolation 66

Quantification of BTLA and HVEM surface expression 67

Supported lipid bilayer preparation and use 68

Immunofluorescence staining 69

TIRF and confocal imaging 69

Image analysis 70

In-situ analysis of interaction of SHP1 and SHP2 with PD-1 70

Quantification and statistical analysis 72

Data availability 72

Acknowledgements **72**

Declaration of interests **73**

CHAPTER 3: CONCLUSION ***74***

Therapeutic approaches **81**

Concluding remarks **82**

REFERENCES ***83***

TABLE OF FIGURES

CHAPTER 1:

FIGURE 1.1 7

CHAPTER 2:

FIGURE 2.1 29

FIGURE 2.2 32

FIGURE 2.3 34

FIGURE 2.4 37

FIGURE 2.5 39

FIGURE 2.6 41

FIGURE 2.7 46

SUPPLEMENTAL FIGURES:

FIGURE S1. 54

FIGURE S2. 55

FIGURE S3. 56

FIGURE S4. 57

FIGURE S5. 58

CHAPTER 3:

FIGURE 3.1 74

CHAPTER 1: Introduction

Introduction

Germinal centers (GCs) are anatomic regions in lymphoid organs where activated B cells undergo somatic mutation and rapid proliferation, and give rise to memory B cells and long-lived antibody secreting plasma cells. GCs are organized into two main anatomical compartments, named based on their histological appearance in early staining techniques, a dark zone (DZ) and light zone (LZ). In the DZ, B cells express activation induced cytidine deaminase (AID) which mutates immunoglobulin (Ig) genes through deamination of cytosines, leading to Ig diversification. In the LZ, GC B cells test their newly mutated Ig proteins for improved affinity to antigen presented on the surface of specialized stromal cells called follicular dendritic cells (FDCs). If the B cell recognizes antigen, it internalizes the antigen for presentation to the limited number of $CD4^+$ T follicular helper (Tfh) cells that reside in the LZ. Tfh cell positive selection drives expression of Myc, which determines GC B cell size and subsequent numbers of clonal cell divisions that occur in the DZ (Mayer et al., 2017). Just as GC B cells are some of the most proliferative mammalian cells, dividing every 4-6 hours, they are also particularly sensitive to cell death with ~50% of GC B cells dying in 6 hours. DZ GC cells die due to deleterious AID-induced mutations and LZ GC B cells die by default if there is a lack of antigen engagement and subsequent T cell help.

Tfh cells are a subset of $CD4^+$ T cells that require the transcription factor Bcl-6, localize to B cell follicles and GCs, and depend on GC B cells for their maintenance (Crotty, 2019; Wan et al., 2019). Tfh cells are not necessarily defined by their production of particular cytokines, but rather by their ability to support GC formation, select GC B cells, and determine GC B cell differentiation into memory B cells and plasma cells through cognate interactions. Tfh cell positive selection of GC B cells occurs predominantly through CD40L engagement of CD40 on

the GC B cell. However, several cytokine and cell surface proteins contribute to the Tfh cell's ability to promote the clonal expansion and selection of GC B cells.

Despite the fragility of GC B cells in the absence of sufficient Tfh cell positive selection signals, GC B cell selection can go awry. While overexpression of anti-apoptotic molecules such as Bcl-2 and cell cycle promoting molecules such as c-Myc have long been recognized to drive lymphomagenesis, whether mutations occur that lead to exaggerated T cell help has been less clear (Mlynarczyk et al., 2019). There are three main types of non-Hodgkin B cell lymphomas that originate in the GC and maintain a GC B cell transcriptional identity: follicular lymphoma (FL), GC-type diffuse large B cell lymphoma (GC-DLBCL), and Burkitt lymphoma (BL). Follicular lymphoma, in particular, maintains the normal GC architecture, such as the presence of Tfh cells and stromal cells, despite dyssynchronous LZ and DZ cycling (Bende et al., 2007; Milpied et al., 2018; Ochando and Braza, 2017). However, GCB-DLBCL also maintains a $CD4^+$ T cell and Tfh cell signature, compared to Activated B cell (ABC)-DLBCL (Iqbal et al., 2011; Schmitz et al., 2018). This has led to the hypothesis that non-malignant immune cells support lymphomagenesis. Large scale sequencing of patient samples provided novel insights about the regulatory pathways that are commonly targeted during GC B cell lymphomagenesis (Lackraj et al., 2018; Schmitz et al., 2018). In this introduction, we present evidence for participation of Tfh cells in the formation and progression of GC B cell lymphomagenesis with a focus on the key molecular mediators of Tfh cell help. We will also examine the role of GC B cells in supporting Tfh cell lymphomagenesis. Lastly, we will introduce the BTLA and HVEM signaling axis, which will be the focus on Chapter 2.

Mutations in B cell lymphomagenesis

In follicular lymphoma, the first genetic hit in 90% of cases is the t(14;18)(q32;q21) chromosomal translocation of the anti-apoptotic Bcl-2 gene with the IgH locus during Ig gene recombination in the bone marrow (BM). Although Bcl-2 overexpression provides B cells with a survival advantage, it is not sufficient for lymphomagenesis as 10-100 per million circulating peripheral blood B cells in a healthy adult have this translocation (Rabkin et al., 2008). Bcl-2-overexpressing GC B cells have increased survival and this is likely associated with an increased risk of abnormal selection and AID-induced transformation to a malignant state (Bende et al., 2007). Indeed, Bcl-2 overexpression can occur in all three forms of GC B cell-derived lymphomas, driving survival of GC B cells that normally do not express Bcl-2. Interestingly, Bcl-2 overexpression is more common in the adult form of BL compared to the pediatric form (Bouska et al., 2017). This correlates with the increased frequency of Bcl-2 translocations in older people, and the evidence that Bcl-2-overexpressing B cells give rise to memory B cells that can undergo iterative rounds of GC entry, allowing for multiple rounds of mutagenesis and potential errors in selection (Liu et al., 1994; Sungalee et al., 2014).

AID-mediated cytidine deamination can be recognized by base excision repair or mismatch repair mechanisms leading to either point mutations or double strand breaks followed by recombination. While AID is hypothesized to drive the majority of mutations that transform a mature B cell into a malignant cell, some lymphoma-associated mutations may arise independently of AID, perhaps as a consequence of the increased error prone DNA repair in GC B cells (Álvarez-Prado et al., 2018; Tsukamoto et al., 2017). Extensive sequencing has been done in GC-derived lymphomas to understand what mutations are driving lymphomagenesis. Surprisingly, only around half a dozen are common targets of mutation in all three types of GC

lymphomas (Bouska et al., 2017; Lackraj et al., 2018; Schmitz et al., 2018). These include *BCL-2*, *TNFRSF14*, *SOCS1*, *STAT6*, *CREBBP*, *EZH2*, and *GNA13*.

Loss of function mutations in *TNFRSF14* and *SOCS1* and activating mutations in *STAT6* enhance or override Tfh cell helper signals to GC B cells (Losman et al., 1999; Mintz et al., 2019; Turqueti-Neves et al., 2014) and will be discussed in detail below. *CREBBP* and *EZH2* are epigenetic modifiers that have complex effects on GC B cell signaling and gene expression. Loss of function mutations in *CREBBP* promotes unrestricted GC growth, in part through increasing CD40 signaling, and also reducing MHC-II expression, which alters mutant FL cell ability to present antigen to $CD4^+$ T cells (Hashwah et al., 2017). Gain of function mutations in polycomb repressor complex-2 (PRC2) component *EZH2* inhibits cell cycle checkpoints, promoting uncontrolled GC B cell proliferation (Béguelin et al., 2013; 2017). *GNA13* is a signaling protein downstream of transmembrane G-protein coupled receptors S1PR2 and P2RY8 that confines B cells to the GC and inhibits Akt and possibly other signaling molecules, limiting survival signals (Green et al., 2011; Lu et al., 2019; Muppidi et al., 2014). While mutations in some of the key positive regulators of GC B cells, such as CD40, ICOSL, and SLAMF and negative regulators of GC B cells, such as PD-L1/2 and Fas, are less selected in GC lymphomas, we suggest that these molecular mediators may often play an important, and yet underappreciated role in disease pathogenesis.

Tfh cell participation in follicular lymphoma

Tfh cells, defined by surface expression as $CXCR5^+PD\text{-}1^+ICOS^+CD4^+$ T cells, support GC B cells, which in turn maintain Tfh cells, providing a feedforward positive selection loop. In a mouse model of follicular lymphoma, in which the Vav promoter drives Bcl-2 overexpression in hemopoietic cells, depletion of $CD4^+$ T cells reduced the size of the GCs, suggesting that

disease initiation and likely progression depends on T cells (Egle, 2004). Tfh cells in the FL tumor microenvironment have been demonstrated by several studies (Ochando and Braza, 2017). Tfh cell gene signatures are also maintained in Bcl-2-positive GCB-DLBCL cases (Iqbal et al., 2011). An association of Tfh cells with EBV^+ BL cases has not been reported (Schmitz et al., 2012), although interestingly EBV transformed GC B cells may support Tfh cell type lymphomas (Schmitz and de Leval, 2016). We will focus our introduction on what is known about the key molecular regulators of Tfh cell help to GC B cells and how they may play a role in GC B cell outgrowth and lymphomagenesis (Fig. 1.1).

Before discussing CD4 T helper molecules, the role of cytotoxic lymphocytes in lymphomas should be mentioned. GC lymphoma cells have a high mutation burden and are susceptible to killing by cytolytic CD8 T cells and NK cells (Basso and Dalla-Favera, 2015). It is therefore not surprising that GC lymphomas commonly show mutations in beta-2-microglobulin (b2m) and CD58 (LFA3). B2m is a component of all MHC class I molecules, and loss of this protein leads to loss of MHC class I expression and protection from CD8 mediated killing. Loss of MHC class I can, however, lead to recognition by NK cells. GC lymphomas can become resistant to NK cells through loss of CD58 expression, a surface counter receptor for CD2, an adhesion and activating molecule expressed on NK cells (Challa-Malladi et al., 2011). Cytotoxic cells usually have very limited access to B cell follicles and GCs and it is possible that another mode of GC lymphoma evasion of cytotoxic cells is through continued CXCR5-CXCL13 mediated compartmentalization within the follicular microenvironment. CXCL13 is made by several types of stromal cells, including FDCs and marginal reticular cells (MRCs) and GC lymphomas, especially FLs, maintain their FDC networks and have strong expression of CXCL13. A signature feature of Tfh cells is their expression of CXCR5 and efficient ability to

access lymphoid follicles (Chang et al., 2003). Human Tfh cells are also a source of CXCL13 though the role of Tfh CXCL13 in GCs remains unclear. While most cytotoxic cells are CXCR5 negative, in some situations they can be induced to express CXCR5 and this facilitates their access to GC microenvironments and elimination of GC lymphoma cells (Tang et al., 2017).

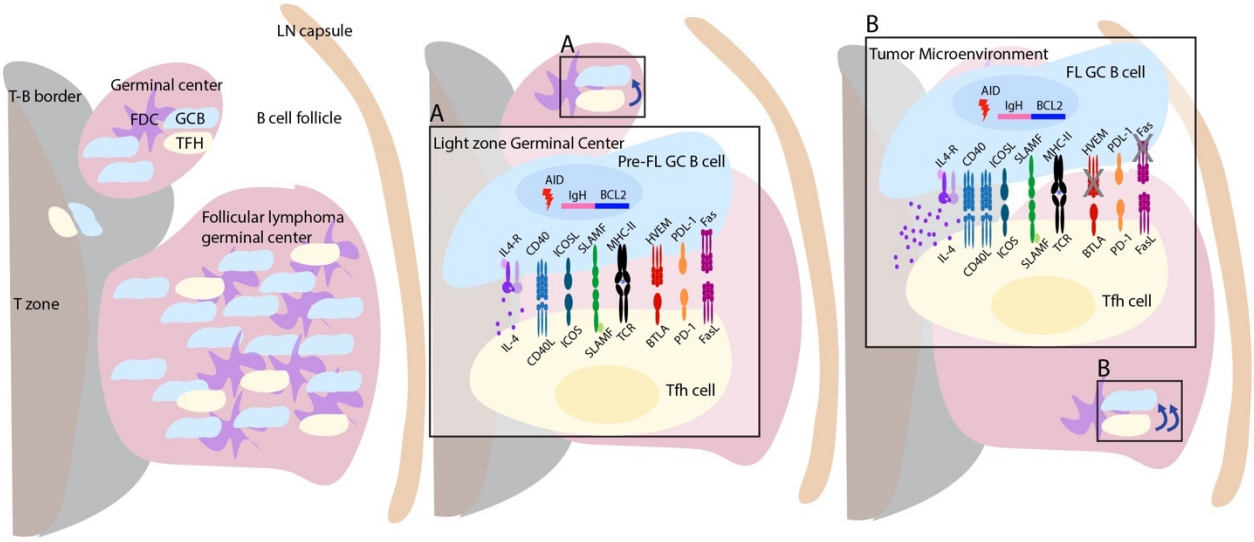

Figure 1.1. Follicular lymphoma (FL) germinal center B cells receive exaggerated helper cues from T follicular helper cells
Germinal center microenvironment in a LN with a follicular lymphoma tumor. The follicular lymphoma germinal center contains stromal follicular dendritic cells (FDC, purple), germinal center (GC) B cells (blue), and T follicular helper (Tfh) cells (yellow). (A) Magnification of light zone germinal center where a Bcl-2 translocated GC B cell is presenting antigen to a Tfh cell and is receiving normal positive selection (left of TCR) and negative selection (right) signals. (B) Magnification of a FL GC B cell's interaction with a Tfh cell in which several of the key molecular regulators are altered as will be discussed below. Briefly, there is increased IL-4 production, increased Tfh cell help via CD40L due to the absence of BTLA-HVEM, and mutations in Fas death domain that prevents FasL mediated cell death.

IL-4 – STAT-6

IL-4 is a CD4 T cell derived cytokine known to support B cell proliferation, class-switching, and survival (Paul, 2015). Sequencing of human FL identified activating mutations in *STAT6*, the main IL-4R signaling mediator, and loss of function mutations in a suppressor of cytokine signaling, including IL-4R signaling, *SOCS1* (Lackraj et al., 2018). This is consistent

with increased STAT6 signaling measured by p-STAT6 in formalin fixed FL sections compared to tonsil (Rawal et al., 2013). Furthermore, IL-4 protein was identified to be 5-fold more abundant in FL samples compared to tonsils (Calvo et al., 2008). Interestingly, normal Tfh cells express high amounts of IL-4 mRNA, yet produce small amounts of IL-4 protein (Crotty, 2019). When malignant B cells and bystander healthy immune cells were sorted and their transcriptional signatures analyzed, Tfh cells were found to express high levels of IL-4 transcripts in FL (Pangault et al., 2010). Furthermore, FL B cells in close proximity to Tfh cells were actively signaling through STAT-6 as measured by p-STAT6, suggesting Tfh cells in FL are the major producers of IL-4. A follow up study, confirmed the high expression of IL-4 in CD25-low Tfh cells (Ame-Thomas et al., 2012).

It remains unknown what is driving the elevated expression of IL-4 transcripts by FL Tfh cells compared to tonsillar Tfh cells. Unlike the increase seen in IL-21 expression, IL-4 expression was unchanged when the amount of antigen GC B cells presented to Tfh cell was increased, suggesting that TCR signaling in Tfh cells is not sufficient to increase IL-4 mRNA expression (Shulman et al., 2014). IL-4 production in Tfh cells is uniquely regulated compared to Th2 IL-4, as Tfh cell IL-4 is transcriptionally regulated by CNS2, a 3' enhancer in the IL-4 locus, but not by GATA-3 (Vijayanand et al., 2012). Understanding the production of IL-4 by Tfh cells and its consequential IL4-R – STAT-6 signaling in FL B cells is further complicated by the results that the blockade or deletion of these signaling pathways results in minor alterations in the normal GC response (Kopf et al., 1995). In the mouse, production of both IL-4 and IL-21 are required for a robust GC B cell response (Reinhardt et al., 2009; Zotos et al., 2010). Two recent studies have found that IL-4 is preferentially expressed by Tfh cells later in the immune response, compared to IL-21 which is preferentially expressed early in the GC (Gonzalez et al.,

2018; Weinstein et al., 2016). IL-4 has also recently been shown to be uniquely able to induce high levels of Bcl6 protein, which is the transcription factor that is required for GC B cell formation and maintenance (Chevrier et al., 2017).

These data support a model in which Tfh cells in FL are most similar to late GC-Tfh cells. The independent data supporting high IL-4 and selection for activating *STAT6* and loss of function *SOCS1* mutations adds further support to the notion that IL-4 production by Tfh cells is supportive of FL B cells. Additionally, IL-4's ability to stabilize Bcl-6 protein may play an important role in maintaining GC B cell identity and preventing transformation into a post-GC B cell lymphoma. While the effect of IL-4 alone in driving GC B cell outgrowth is less clear based on the normal GC B cell evidence, it remains to be studied whether IL-21 is being co-produced by FL Tfh cells, such that FL B cells are receiving two complementary cytokine signals known to support GC B cell expansion.

CD40L – CD40

CD40, a TNFRSF member, predominantly promotes B cell survival, proliferation and class switching through its ability to signal via NFκB. In humans with mutations in CD40L-CD40 signaling, GCs cannot form and hyper-IgM immunodeficiency develops. FL B cells express CD40 and respond to CD40L. CD40 signaling in FL B cells increased the anti-apoptotic protein Bcl-XL and prolonged FL B cell survival *in vitro*, suggesting CD40 promotes the survival of FL B cells complementary to their overexpression of Bcl-2 (Ghia et al., 1998; Travert et al., 2008). CD40 signaling can promote differentiation into plasma cells and CD40 amplifications occur in human plasma cell malignancies, yet none have been described in GC-derived lymphomas (Hömig-Hölzel et al., 2008).

CD40L is expressed by naïve and activated $CD4^+$ T cells, but not by $CD8^+$ T cells (Lesley et al., 2006; MacLennan, 1994). CD40L expression was increased after TCR signaling (Casamayor-Palleja et al., 1995; Iezzi et al., 2009), and the amount of preformed CD40L mobilized to the surface of Tfh cells increased with the amount of antigen presented (Mintz et al., 2019). One study found FL Tfh cells expressed 2.5-fold higher amounts of CD40L mRNA compared to tonsillar Tfh cells, suggesting FL Tfh cells may receive stronger TCR signals though it is also possible that the FL samples were more enriched for the type of Tfh cells associated with GCs (GC-Tfh) that correspond to only a fraction of Tfh cells in healthy lymphoid tissue (Ame-Thomas et al., 2012). CD40L protein is also expressed on T cells in the FL environment (Carbone et al., 1995). Strong evidence for a positive role of CD40L in promoting lymphomagenesis comes from a mouse study in which constitutive CD40L expression in mature T cells was driven by LTR of HTLV1 (Sacco et al., 2000). At 6 months of age, one third of the mice developed palpable inguinal masses that were indistinguishable from GC-derived BL (Sacco et al., 2000). These data are in contrast to B cell constitutive CD40L transgenic mice which do not maintain the GC B cell response (Kishi et al., 2010), suggesting that the cellular source and regulation of CD40L delivery is crucial to the signaling outcome.

As CD40 signaling is a master regulator of B cell responses, therapeutics have been developed for the purposes of immune modulation in transplantation, autoimmunity, and lymphoma. While several CD40 agonists have been developed to stimulate the immune response via costimulation of antigen presenting cells, CD40 blocking agents have also been developed. In a Phase I/II trial with a CD40 antagonist HCD122, CD40 blockade induced a response in a third of FL patients with refractory disease to rituximab treatment (Fanale et al., 2013). Since HCD122 has been shown to induce antibody dependent cellular cytotoxicity (ADCC), it remains

to be determined if the clinical efficacy is due to ADCC, blockade of CD40L-CD40 signaling, or both.

PD-1 – PD-L1/PD-L2

The inhibitory immunoglobulin superfamily (IgSF) member PD-1 is a defining marker of normal and FL Tfh cells (Myklebust et al., 2013). PD-1 is also highly upregulated on exhausted $CD8^+$ T cells that cannot appropriately perform cytotoxic functions, which has led to impressive immunotherapy benefit by blocking PD-1 to restore TCR sensitivity and T cell function in some cancers (Mulder et al., 2019; Xu-Monette et al., 2019). Several studies have attempted to correlate the outcome of FL with PD-1^+ T cells, but the results have not been consistent likely due to heterogeneity of PD-1^+ T cells within the FL environment (Smeltzer et al., 2014; Yang et al., 2019). While the number of PD-1^+ T cells did not correlate with outcome, the location of PD-1^+ T cells in a follicular pattern was associated with a shorter time to transformation compared to a diffuse pattern (Smeltzer et al., 2014). Although these results are difficult to interpret as the authors did not stain for CD4 or CD8, the finding that the diffuse PD-1^+ cells co-stained for TIM-3, a marker of $CD8^+$ T cell exhaustion, whereas the follicular PD-1^+ cells did not, suggests that the diffuse T cells are $CD8^+$ cells whereas the follicular cells may be Tfh cells. In another study, higher levels of PD-1 expression were found in $CD4^+$ T cells compared to $CD8^+$ T cells in FL (Yang et al., 2019). Amongst the $CD4^+CD25^-$ PD-1^+ cells in FL, there were 4 subsets: (1) $CXCR5^+$ Tfh cells, (2) $CD27^+CXCR5^-$ cells, (3), $CD28^-CCR4^+$ cells, (4) $CD28^-CCR4^-$ cells. Interestingly, $CD27^+CXCR5^+$ Tfh cells and $CD27^+CXCR5^-$cells were correlated with better overall survival while $CD28^-CCR4^+$ cells and $CD28^-CCR4^-$ cells were correlated with poor overall survival. These data suggest that non-Tfh $CD4^+$ T cells with low expression of

costimulatory molecules likely prevent a productive immune response to the FL or, alternatively, directly support FL B cell proliferation. While a higher frequency of PD-1$^+$ Tfh cells in the FL microenvironment did not correlate with poor survival, these data do not rule out a possibility that PD-1 may be restraining the Tfh cell's ability to support FL B cell survival. Interestingly, 40% of ABC-DLBCL have mutations or copy number gains of *PD-L1*, whereas only 10% of GCB-DLBCL have increased PD-L1 expression (Godfrey et al., 2019; Xu-Monette et al., 2019). Increased expression of PD-L1 is associated with increased numbers of activated and exhausted CD8$^+$ T cells in the tumor microenvironment. However, these data suggest that increased PD-L1 is not as prevalent of a selection mechanism in GCB-DLBCL compared to post-GC ABC-DLBCL, perhaps due to the inhibition of PD-1$^+$ Tfh cells in GCB-DLBCL tumors. It remains to be determined if PD-L1 expression alters Tfh cells in the GCB-DLBCL tumor microenvironment and if PD-L1 is mutated in a manner that leads to loss of expression in some GCB-DLBCL cases (Godfrey et al., 2019).

During the normal GC response, the majority of evidence suggests that PD-1's interaction with PD-L1 restrains the response. However, PD-1's function in the Tfh cell and how it restrains the amount of help provided to GC B cells remains unclear despite several studies. PD-L1 is expressed in naïve B cells, and upregulated in GC B cells, whereas PD-L2 is not expressed in naïve B cells, but slightly increased in GC B cells (Good-Jacobson et al., 2010). In one study, where PD-1 or its ligands were deficient, plasma cell output was decreased at 2 weeks and this decrease was sustained for greater than 1 year after NP-CGG immunization. In discordance with PC output, GC B cells were not increased, likely due to their increased cell death in the absence of PD-1 during this immunization. Interestingly, while the authors found that PD-1 deficiency led to increased Tfh cell numbers, these Tfh cells had reduced expression of

helper cytokines such as IL-21 (Good-Jacobson et al., 2010). In another study, after helminth infection, PD-L1-deficiency led to increased GC B cells and Tfh cells (Hams et al., 2011). After immunizing with KLH/CFA and blocking PD-1, PD-L1, or PD-L2, it was found that PD-L1 blockade increased Tfh cells 5-fold, whereas PD-L2 blockade had no effect, and PD-1 blockade provided an intermediate 2-fold increase in Tfh cells, suggesting that PD-L2 is not upregulated during KLH/CFA or the blocking agent is not sufficient to reveal an effect (Hams et al., 2011). These data are further complicated as PD-1 is also expressed by T follicular regulatory (Tfr) cells, $CD4^{+}Foxp3^{+}$ cells that express CXCR5. PD-1 or PD-L1 deficiency, but not PD-L2 deficiency, led to increased Tfr cells rather than Tfh cells after immunization with MOG (Sage et al., 2012). Interestingly, PD-1 or PD-L1-deficiency or blockade increased GC B cell responses in a mouse model of type I diabetes, whereas PD-L2 blockade had no effect (Martinov et al., 2019). While these studies suggest that PD-1 restrains Tfh cells, together they do not point to a mechanism of how PD-1 on the T cell restrains help to GC B cells. In a more recent study, mixed chimeras were generated with PD-L1 deficient and wild-type BM. While PD-L1 deficient B cells were increased in representation in the GC, memory B cell, and plasma cell compartments, they had reduced affinity to the immunogen, the hapten NP (Shi et al., 2018; Wan et al., 2019). These data most clearly suggest that PD-L1 expression on the GC B cell restricts the amount of T cell help and the stringency of GC B cell selection by Tfh cells. While the authors did not directly show PD-L1 in the GC B cell was regulating PD-1 in Tfh cells, they observed that PD-1 mutant antigen-specific Tfh cells supported larger GC B cell responses.

PD-1 is known to dampen T cell signaling by inhibiting TCR and CD28, and has been shown to signal predominantly through the phosphatase SHP2 (Hui et al., 2017; Mintz et al., 2019; Yokosuka et al., 2012). Although T cell deficiency in SHP2 did not phenocopy many of

PD-1's known roles in $CD8^+$ T cells, in the absence of SHP2, the inhibitory phosphatase SHP1 was capable of replacing SHP2 in mediating inhibition (Celis-Gutierrez et al., 2019; Rota et al., 2018). The relative importance of SHP1 and SHP2 for PD1 function in Tfh cells remains to be determined. Another set of recent observations has shown the existence of *cis*-interactions between PD-1/PD-L1 and PD-L1/CD80 on dendritic cells (Sugiura et al., 2019). Since B cells can express PD-1 and CD80 (Good-Jacobson et al., 2010), it may be the case that not all PD-L1 molecules expressed on GC B cells are capable of engaging with PD-1 on Tfh cells to restrain their TCR signaling.

The heterogeneity of PD-1^+ T cells in FL and the role of PD-1 in restraining Tfh cell help to GC B cells may provide an explanation for the modest effects of PD-1 blockade in FL. If the majority of PD-1^+ T cells in the FL microenvironment are exhausted $CD8^+$ and $CD4^+$ T cells that are failing to perform cytotoxic or immune priming functions, we would hypothesize that FL patients would likely have good clinical responses to anti-PD-1 therapy. However, if PD-1^+ Tfh cells are present in nearly all FL microenvironments, we would hypothesize that blocking PD-1 in Tfh cells would increase helper signals to FL B cells and lead to poor clinical responses. In agreement with the diversity of PD-1^+ T cells, while FL clinical responses to PD-1 have only been effective in a third of patients, in classical Hodgkin's lymphoma nearly 90% of patients exhibit a response (Mulder et al., 2019; Xu-Monette et al., 2019). This suggests that additional immunotherapy approaches that do not unleash Tfh cell helper signals need to be tested in FL, such as CD47 blockade, where combination therapy with rituximab has shown a response in 70% of patients in a small clinical trial (Mulder et al., 2019). CD47 is present on GC B cells and and is often upregulated on DLBCL and FL cells (Chao et al., 2010). CD47 binds SIRPα, an ITIM containing inhibitory receptor that is expressed on myeloid cells, transmitting an anti-

phagocytic ‘don’t eat me signal’. Blockade of CD47 maybe an approach to enhance rituximab mediated ADCC. SIRPa is not expressed on T cells and therefore blocking antibodies to CD47 are unlikely to lead to augmented Tfh cell responses.

ICOS – ICOSL

ICOS, or inducible T cell co-stimulator, is required for Tfh cell differentiation and maintenance (Wan et al., 2019). ICOS, which signals through PI3K, is the dominant co-stimulatory molecule for Tfh cells and it functions analogously to CD28 once T cells are in the GC (Wan et al., 2019; Weber et al., 2015). ICOSL is not known to signal and is downregulated on GC B cells compared to follicular B cells. However, ICOSL is upregulated after CD40 signaling on GC B cells, suggesting that GC B cells that have received the most T cell help enter into a positive feedback loop that amplifies this help. Indeed, when ICOSL-high cells versus -low cells were analyzed for high affinity NP-binding mutations, the highest ICOSL expressing GC B cells had increased high affinity mutations. When Tfh cells were stimulated *in vitro* with activating antibodies to CD3 and ICOS, Tfh cells increased their mobilization of CD40L to the T cell surface compared to cells activated by anti-CD3 alone, suggesting ICOS signaling enhances T cell helper signals to GC B cells (Liu et al., 2014; Wan et al., 2019). While in a competitive setting with WT cells, ICOSL-deficient GC B cells formed brief immune synapses with decreased surface area of engagement with Tfh cells (Liu et al., 2014; Wan et al., 2019). Together these data suggest that ICOSL expression on GC B cells is crucial for positive selection by ICOS-expressing Tfh cells.

Surprisingly, increases in ICOSL expression have not been reported in GC B cell lymphomas. However, ICOSL is more highly expressed in GCB-DLBCL compared to ABC-DLBCL, suggesting ICOSL may be maintained and beneficial in a more GC-like lymphoma

microenvironment (Xu-Monette et al., 2016). Although ICOSL transcripts were expressed highly in FL cells compared to a B cell line, ICOSL protein was not detected on FL cells in sections. Despite this, ICOS has been shown to be highly expressed on FL T cells and specifically on a subset of $CD25^{+}CXCR5^{+}PD\text{-}1^{+}$ $CD4^{+}$ T cells (Le et al., 2016). While Le et al. suggested that ICOS is defining a Treg population that is directly suppressing FL B cells through *in vitro* experiments, it has also been shown that ICOS expressing $CD4^{+}$ T cells in the FL microenvironment are IL4-expressing non-regulatory Tfh cells (Ame-Thomas et al., 2012). Further study on the role of ICOS-ICOSL signaling in GC lymphomas is needed.

FasL – Fas

GC B cells are known to be intrinsically prone to cell death given their low expression of Bcl-2. Another feature that poises the cells for apoptosis is their high expression of the cell death receptor Fas. Fas is a TNFRSF molecule that, upon engagement by FasL, initiates the death inducing signaling complex, leading to Caspase-8 activation and apoptosis (Koncz and Hueber, 2012). Fas is selectively lost in a number of GC-derived lymphomas, as well as antibody driven autoimmune diseases. Fas mutations are found in GCB-DLBCL and in some cases of FL and transformed FL (Lossos and Gascoyne, 2011; Schmitz et al., 2018). Fas mutations likely arise during the GC response and can lead to dominant negative mutations in the death domain or loss of expression (Müschen et al., 2002). In autoimmune lymphoproliferative syndrome (ALPS), patients with mutations in the Fas death domain have a 14-fold increased likelihood in developing non-Hodgkin B cell lymphomas later in life (Straus et al., 2001). Interestingly, healthy family members of ALPS patients that have Fas mutations are at increased risk of

lymphomagenesis likely due to their accumulation of somatic hypermutations during GC responses (Bride and Teachey, 2017).

In mice, Fas has varying impacts on GC size and B cell affinity maturation. Fas is highly expressed on activated and GC B cells. A Fas mutation in the mouse called *lpr* leads to lymphoproliferation and autoimmunity, yet normal sized peak GC responses after acute immunization. However, while wild-type GCs begin to contract three weeks post immunization Fas-deficient GCs are maintained (Takahashi et al., 2001). In another study, conditional deletion of Fas in class-switched B cells was sufficient to lead to increased GC B cell responses (Hao et al., 2008). Although FasL transcript was increased in activated T cells and presumably present on Tfh cells (Kondo et al., 1997), FasL is difficult to stain for and it has yet to be shown that Tfh cells can negatively select GC B cells through FasL. In addition to the elusive source of FasL in the GC, contradictory results have been reported for the role of Fas in the GC. Loss of Fas in GC B cells led to increased somatic hypermutation, loss of antigen reactivity, and preferential differentiation into plasma cells late in the response in a more recent study (Butt et al., 2015). Together, these data are inconclusive on whether Fas is a crucial negative regulator of ongoing GC responses, but suggest Fas is necessary for the proper contraction of the late GC response and suppression of lymphomagenesis. In a setting in which the intrinsic mitochondrial sensitivity to cell death is askew, such as in t(14;18) GC B cells, Fas may play a heightened role in maintaining stringent GC B cell selection. Such a role has been demonstrated in the setting of c-Myc overexpression (Totten et al., 2014).

Due to the downregulation of Fas and its apoptosis promoting signaling in many GC-derived lymphomas, it is not straightforward to consider how FasL-Fas signaling might be restored. One group has suggested that CD74 (the invariant chain) might be a regulator of Fas

signaling and that an anti-CD74 antibody, milatuzumab, might act to enhance Fas mediated cell death (Berkova et al., 2009), though other mechanisms of anti-CD74 action are likely. Another approach might be to inhibit NFκB signaling, which provides resistance to extrinsic cell death signaling through a Nedd8-activating inhibitor called Pevonedistat (Paiva et al., 2017). It remains to be determined how Fas-mediated cell death can best be enhanced as a treatment for lymphomagenesis.

SAP – SLAMF

Signaling lymphocytic activation molecule (SLAM)-associated protein or SAP (encoded by *SH2D1A*) is a T cell signaling molecule that is mutated or lost in patients with X-linked lymphoproliferative (XLP) syndrome (Engel et al., 2003). SAP is composed of a single SH2 domain and its functions include blocking the recruitment of SHP1 and SHP2 to SLAM proteins. SLAM family members are homotypic adhesion receptors that are involved in the formation of immune synapses between T and B cells, with SLAMF6 (Ly108) and SLAMF5 (CD84) being most important. XLP is thought to arise because NK and $CD8^+$ T cells in SAP-deficient patients are ineffective in killing EBV-infected B cells due to exaggerated negative signaling via SLAM-family proteins. As well as an extreme susceptibility to EBV infection, patients harboring *SH2D1A* mutations have a 200-fold increased risk in developing lymphoma compared to the normal population and 30% have an extranodal BL type presentation in the ileum. XLP patients have not been reported to have increases in other types of GC-derived lymphomas (Fouquet et al., 2018).

In the mouse, loss of SAP prevents T cells from forming stable conjugates with B cells, but not other APCs (Qi et al., 2008). Despite the relatively normal expression of helper

molecules, SAP-deficient Tfh cells are altered in their ability to engage GC B cells because SLAMF6 and SLAMF5 send inhibitory signals into SAP-deficient T cells, and as a result the GC response fails. The importance of SAP in Tfh cell function in supporting GC cells might explain why XLP patients do not have an increased incidence of non-EBV associated GC lymphomas. In this regard, it is interesting to consider that a lack of B cell killing ability might be expected to have a similar effect to loss of b2m or LFA3/CD58, which are common mutations in GC-derived lymphomas (Basso and Dalla-Favera, 2015); that SAP-deficiency doesn't may reflect the need for Tfh cells to be able to provide positive signals during lymphomagenesis. While the negative role of SLAM family molecules is clearly evident when SAP is lacking, the physiological role of SLAM molecules in SAP replete T cells is less clear. SLAM signaling can contribute to Tfh cell IL-4 production (Yusuf et al., 2010) though recent analysis of mice lacking all SLAM family members did not reveal an essential role for these molecules in the GC response (Huang et al., 2016). More studies of these SLAM-family deficient mice may help reveal how these molecules influence events necessary for antibody diversification and affinity maturation in GCs (Cannons et al., 2010).

Tfh cell derived lymphomas

In additional to GC B cell derived lymphomas, two types of Tfh cell-derived lymphomas, angioimmunoblastic T cell lymphoma (AITL) and Tfh-type peripheral T cell lymphoma (Tfh-PTCL), originate from the GC reaction. Tfh lymphomas frequently maintain a GC microenvironment and around half maintain EBV^+ B cells and clonal outgrowths of blasting B cells in the tumor microenvironment (Schmitz and de Leval, 2016). A case study reported depletion of B cells using rituximab combined with chemotherapy was a successful treatment for

a relapsed AITL patient with EBV reactivation (Kasahara et al., 2013) making it important to determine how broadly these T lymphomas depend on B cells. Tfh-derived lymphomas are characterized by epigenetic modifications and often have inactivating mutations in *TET2* and *DNMT2* and activating mutations in *IDH2*. Additionally, several TCR-related signaling genes are mutated and activate the pathway. In 60-70% of AITL and Tfh-PTCL cases, *RHOA* harbors a G17V function altering mutation (Butt et al., 2015). This point mutation was sufficient to increase Tfh cells and drive an AITL like disease in a Tet2-deficient background in mice (Cortes et al., 2018). Additional activating mutations in the TCR signaling pathway, namely *PLCG1*, *PIK3CA*, *VAV*, *FYN*, *LCK* mutations, are found in both AITL and Tfh-PTCL (Berkova et al., 2009). In addition to CD28 mutations, a CTLA4-CD28 fusion gene has been discovered. transforming an inhibitory signal into an activating signal (Schmitz and de Leval, 2016). These data provide further evidence that AITL and Tfh-PTCL cells depend on engaging with antigen presenting GC B cells in the tumor microenvironment.

Given ICOS's ability to drive Tfh cell differentiation and helper signals to B cells, it is not surprising that multiple mechanisms of regulation of *ICOS* mRNA has been described, such as by Roquin and miR-146a (Paiva et al., 2017). It seems reasonable to speculate that the ICOS-ICOSL positive feedback loop contributes to Tfh cell maintenance in the GC-derived lymphoma microenvironment. In a mouse model in which Roquin, a protein that negatively regulates *Icos* mRNA stability, was heterozygously mutated, ICOS expression was increased and Tfh cells and GC B cells spontaneously outgrew; when the mice were aged, AITL developed (Ellyard et al., 2012). Additionally, in a mouse model of AITL driven by RHOA G17V, ICOS was strongly upregulated (Engel et al., 2003). Although Roquin mutations were not reported in a small cohort of human AITL patients (Auguste et al., 2013), analysis of more patients is needed.

An ICOS blocking antibody MEDI 570 is being tested for the treatment of AITL and other Tfh-derived lymphomas in humans (Fouquet et al., 2018). Given that Tfh cell-derived lymphomas often maintain normal GC architecture, similar to their malignant B cell counterparts, it seems likely that blocking this potent positive regulator of GC responses could reduce outgrowth in both B and T cell lymphomas.

The dependence of SAP—SLAMF signaling for Tfh cell interactions with B cells raises the possibility that overexpression of SAP, SLAM, SLAMF5, and SLAMF6 could contribute to GC lymphomagenesis. While alterations in their expression have not been described in GC-derived lymphomas, SLAMF molecules are increased in expression in post-GC chronic lymphocytic leukemia (CLL) (Fouquet et al., 2018). Additionally, SAP expression is maintained in AITL, suggesting productive AITL Tfh cell immune contacts with B cells are beneficial to the tumor cells (Qi et al., 2008).

BTLA – HVEM

As a TNFRSF molecule, HVEM can recruit TRAF2/TRAF5 and signal via NFκB, as well as through NIK and STAT3 (Hsu et al., 1997; Shui et al., 2012; Ward-Kavanagh et al., 2016). Although it is unexpected that a potential NFκB signaling mediator is selectively lost during GC B cell lymphomagenesis, HVEM has been found – as will be described in detail in Chapter 2 – to be a tumor suppressor in mouse models of lymphomagenesis (Boice et al., 2016; Mintz et al., 2019). HVEM has a complex signaling network that can promote reverse signaling through HVEM ligands. HVEM's signaling network is conserved in mouse and human, with the exception of one partner (LTα) which only binds human HVEM. HVEM received its name *H*erpes *v*irus *e*ntry *m*ediator as it is the receptor for the gD subunit of HSV-1 and HSV-2. HVEM

can also bind to two TNFSF members, LIGHT and LTα through its cysteine rich domain 2 (CRD2). HVEM transmits reverse signals through its two IgSF ligands BTLA and CD160, which bind HVEM's CRD1, as well as a more recently identified synaptic adhesion molecule SALM5 (Ward-Kavanagh et al., 2016; Zhu et al., 2016).

BTLA, also known as B and T lymphocyte attenuator, is the most highly expressed HVEM ligand in the GC (Murphy et al., 2006; Sedy et al., 2004). BTLA, an IgSF member, has 50% amino acid sequence homology between mouse and human. BTLA was shown biochemically to recruit the inhibitory phosphatases SHP1 and SHP2 to its cytoplasmic tail (Watanabe et al., 2003). While human BTLA has 4 cytoplasmic tyrosines and mouse only has 3, they are conserved in their ability to recruit SHP1, SHP2, and Grb-2, but do not recruit SHIP-1 (Chemnitz et al., 2004; Gavrieli and Murphy, 2006; Watanabe et al., 2003). In antigen-receptor-BTLA co-crosslinking studies, BTLA directly inhibited CD3ζ phosphorylation in T cells and inhibited BCR signaling by regulating Syk and Fyn in B cells (Vendel et al., 2009; Wu et al., 2007). BTLA is upregulated in Tfh cells compared to naïve $CD4^+$ T cells, and one study has suggested BTLA negatively regulates Tfh cell support of GC B cells by restricting IL-21 production (Chtanova et al., 2004; Kashiwakuma et al., 2010). Although the BTLA-deficient TCR transgenic T cells in this model did support a modestly larger GC B cell response, IL-21 is a notoriously difficult to stain for cytokine and the study did not determine if IL-21 mRNA was elevated, leaving it unclear whether BTLA-mediated inhibition of IL-21 was the key mechanism of action of this HVEM ligand in Tfh cells.

Here we explore the role of HVEM in regulating the GC B cell response. We use mouse models to show HVEM acts as an intrinsic negative regulator of GC B cell responses that depend on a *trans* interaction with BTLA-expressing T cells. We find that BTLA modulates the quality

of Tfh cell help provided to GC B cells through preformed CD40L surface mobilization. Lastly, we show that BTLA expression on Tfh cells regulates Bcl-2-overexpressing GC B cell outgrowth.

CHAPTER 2: The HVEM-BTLA axis restrains T cell help to germinal center B cells and functions as a cell-extrinsic suppressor in lymphomagenesis

Summary

TNF receptor family member HVEM is one of the most frequently mutated surface proteins in germinal center (GC) derived B cell lymphomas, yet the role of HVEM in normal GCs is unknown. We found that HVEM-deficiency intrinsically increased B cell competitiveness during pre-GC and GC responses. The Ig superfamily molecule BTLA was identified as the ligand regulating these responses, and B cell-intrinsic signaling via HVEM and BTLA was not required. Instead, BTLA signaling into the T cell through SHP1 reduced TCR signaling and the amount of preformed CD40L mobilized to the immunological synapse and thus diminished the help delivered to B cells. Moreover, T cell-deficiency in BTLA cooperated with B cell Bcl-2-overexpression in leading to GC B cell outgrowth. These results establish that HVEM restrains the T helper signals delivered to B cells in a manner that influences GC selection outcomes, and they suggest that BTLA functions as a cell-extrinsic suppressor of GC B cell lymphomagenesis.

Introduction

High affinity germinal center (GC)-derived antibodies are crucial for protection from many pathogens. During a T cell-dependent response, antigen-reactive B cells are selected for entry into the GC by $CD4^+$ T cells. The earliest T cell selection of the B cell occurs at the T-B border 1–2 days after antigen exposure. After 3–6 days, T cells residing in the GC, termed T follicular helper (Tfh) cells, are required to select GC B cells. Most data favor a model for high affinity B cell selection where cells with improved affinity internalize and present more of the antigen and win out in receiving more or better-quality T cell help through CD40 ligand (CD40L) or other signals (Bannard and Cyster, 2017; Mesin et al., 2016). However, the factors beyond MHC class II-peptide amounts that determine the quantity and quality of help delivered to GC B cells are incompletely understood.

The tumor necrosis factor (TNF) family receptor HVEM (encoded by the gene *TNFRSF14*) is the most highly mutated surface molecule in GC-derived follicular lymphoma (FL) and diffuse large B cell lymphoma (DLBCL) (Cheung et al., 2010; Lackraj et al., 2018; Launay et al., 2012; Manso et al., 2017; Schmitz et al., 2018). HVEM is expressed in B cells as well as several other cell types, and has multiple ligands. Two ligands, LIGHT and LTα3 are members of the TNF superfamily, whereas two other ligands, BTLA and CD160 are members of the Ig superfamily. BTLA and CD160 bind HVEM's first cysteine rich domain (CRD1), whereas LIGHT binds CRD2 (Ward-Kavanagh et al., 2016). HVEM contains TRAF-binding motifs in its cytoplasmic tail and cross-linking of HVEM can lead to downstream signaling via NFκB (Cheung et al., 2009b; Hsu et al., 1997; Shui et al., 2012). In addition to acting as a receptor and transducing intracellular signals, HVEM can act as a ligand and transmit signals into BTLA-expressing cells (Sedy et al., 2004).

BTLA is widely expressed by immune cells, with high expression on B cells, DCs and some effector T cells (Murphy et al., 2006). BTLA contains ITIM (immunoreceptor tyrosine-based inhibition) motifs in its cytoplasmic domain, and can recruit both SH2-domain containing tyrosine phosphatases, SHP1 and SHP2, but not SHIP or SAP (Chemnitz et al., 2004; Gavrieli et al., 2003; Steinberg et al., 2011; Watanabe et al., 2003). BTLA can negatively regulate both TCR and BCR signaling *in vitro* (Vendel et al., 2009; Wu et al., 2007) and can be recruited to the immune cell interface (Owada et al., 2010). BTLA also contains a Grb2 binding site which may promote $CD8^+$ T cell cytokine production and proliferation (Ritthipichai et al., 2017; Wakamatsu et al., 2013). Therefore, the signaling actions of BTLA may differ between different cell populations and need to be defined on a cell-type by cell-type basis.

BTLA is a Tfh cell marker, yet its role in these cells is not well defined (Chtanova et al., 2004; Kashiwakuma et al., 2010; Nurieva et al., 2009). One study found *Btla*$^{-/-}$ T cells supported a slightly greater IgG2a and IgG2b response following OVA immunization (Kashiwakuma et al., 2010). In a recent study, shRNA targeting of *Hvem* in a Bcl-2-driven model of FL increased lymphomagenesis (Boice et al., 2016). Hematopoietic shRNA targeting of *Btla* also increased lymphomagenesis and it was suggested that this reflected a function of HVEM within B cells engaging BTLA in B cells to transmit BTLA-mediated BCR-repressive signals. Whether such signals occur in normal GC B cells has been unclear.

Here we found that HVEM acts to restrain B cell participation in the GC response by signaling via BTLA on T cells. HVEM-deficiency provided a proliferative advantage to B cells as early as day 3–4 of the response. Interaction of HVEM with BTLA on the T cells decreased the TCR signal and the amount of preformed CD40L mobilized to the T cell surface, thereby limiting B cell help. Thus, HVEM on B cells restrains T cell help to influence GC selection outcomes, and interfering with this regulatory axis provides a competitive advantage in GC B cell lymphomagenesis.

Results

HVEM-deficiency increases GC B cell competitiveness

Hvem (*Tnfrsf14*) transcripts were expressed at similar levels in follicular and GC B cells (Fig. 2.1A) and HVEM protein was present on the surface of both cell types though at lower levels on GC B cells (Fig. 2.1B). To test whether HVEM is an intrinsic regulator of GC B cell responses, we generated mixed bone marrow (BM) chimeric mice where BM from wild-type

(WT) CD45.1 donor mice was mixed with CD45.2 BM from *Hvem*$^{+/-}$ or *Hvem*$^{-/-}$ mice. Following immunization with sheep red blood cells (SRBC), HVEM-deficient B cells were over-represented in GCs compared to the follicular compartment (Fig. 2.1C and Fig. S1A). HVEM heterozygosity led to an intermediate phenotype (Fig. 2.1C). The participation of *Hvem*$^{-/-}$ B cells in the follicular compartment matched that of developing B cells in the BM (Fig. S1B). HVEM-deficiency also provided GC B cells with increased competitiveness in chronic GCs in the mesenteric LN (mLN) and Peyer's Patches (PP) (Fig. S1C). *Hvem*$^{-/-}$ B cells were similarly over-represented in the light and dark zone of the GC (Fig. S1D). While HVEM-deficiency gave GC B cells a competitive advantage in the mixed setting, it did not lead to a significant increase in GC size in competitive or non-competitive conditions (Fig. S1E, F).

To permit tracking of antigen-specific B cells during the GC response, mixed BM chimeras were immunized with the haptenated antigen NP-CGG in alum adjuvant. In the GC response at day 6–7 after immunization, HVEM-deficient GC B cells were increased in frequency compared to the follicular compartment (Fig. 2.1D). Notably, this advantage was more pronounced in the non-hapten binding (NP^{-}) GC B cells compared to the NP^{+} fraction (Fig. 2.1D). HVEM-deficient GC B cells maintained approximately the same magnitude of advantage over the course of the GC response through day 21 (Fig. 2.1D). In full *Hvem*$^{-/-}$ animals the frequency of NP^{+} GC B cells was similar to WT littermate controls, suggesting there is not a baseline repertoire difference (Fig. S1G, H).

Paired-end RNA sequencing and BCR gene usage analysis through MIXCR (Bolotin et al., 2015) at day 11 of the response showed *Hvem*$^{-/-}$ GC B cells had decreased usage of *Iglv1*, the canonical λ chain expanded during NP responses in C57BL/6 mice, compared to the WT competitors (Fig. 2.1E). PCR on sorted GC B cells from mixed BM chimeras was performed to

examine the frequency of high affinity mutations in the canonical NP-responding *VH186.2* gene at days 11–13. When referenced against the WT mixed chimeras, HVEM-deficient GC B cells had a decreased stringency in selection for the W33L mutation compared to WT GC B cells in the same animal (Fig. 2.1F).

The SRBC immunized mixed BM chimeras showed an increased frequency of memory B cells (Bmem) and plasma cells (PCs) at day 8 (Fig. S1A, I). HVEM-deficiency also increased the frequency of NP^+ Bmem and PCs at day 7–21 of the NP-CGG response (Fig. S1J). These data suggest Bmem and PCs were generated approximately in proportion to the GC cells. Additionally, HVEM-deficiency did not affect the frequency of $IgG1^+$ class-switched B cells in the GC (Fig. S1K). One mechanism by which HVEM-deficiency could lead to increased GC B cell accumulation was by reduced cell death. However, the frequencies of apoptotic HVEM-deficient and WT GC B cells as measured by active caspase-3 were similar (Fig. S1L). These findings led us to consider whether B cell proliferation might be affected.

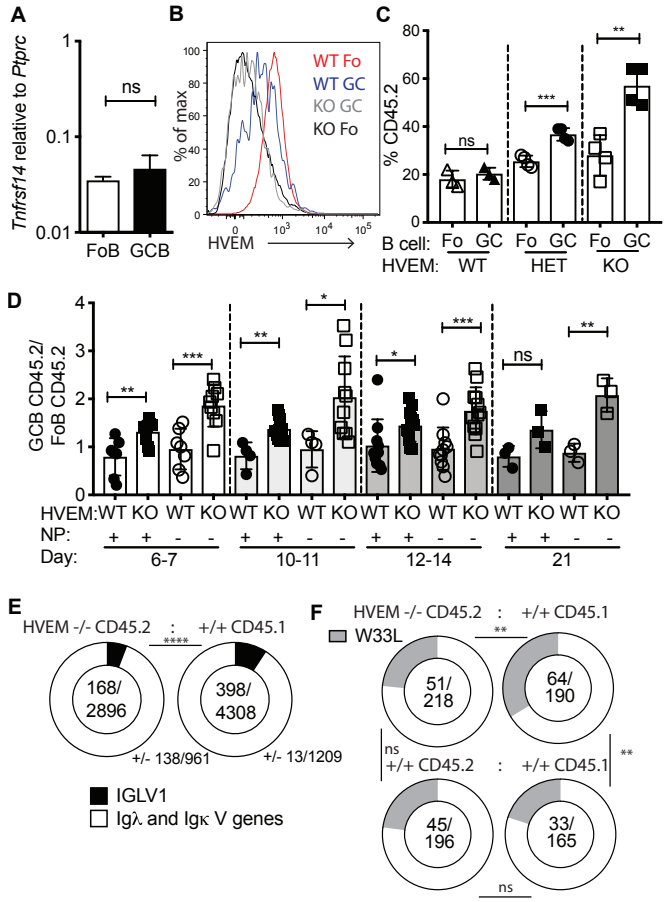

Figure 2.1. HVEM-deficiency increases GC B cell competitiveness

(A) Quantitative PCR analysis of *Hvem* (*Tnfrsf14)* transcript abundance in follicular (Fo) and GC B cells, shown relative to *Ptprc*. **(B)** Representative flow cytometric analysis of HVEM surface expression on $Hvem^{+/+}$ Fo and GC B cells compared to $Hvem^{-/-}$ cells. **(C)** Contribution of $Hvem^{+/+}$, $Hvem^{+/-}$, $Hvem^{-/-}$ CD45.2 cells to Fo and GC populations in spleen of mixed BM chimeras made with ~30% CD45.2 and ~70% WT CD45.1 BM at day 8 after SRBC immunization. Data are representative of >3 independent experiments. **(D)** Ratio of $Hvem^{+/+}$ or $Hvem^{-/-}$ NP^+ or NP^- CD45.2 GC to total CD45.2 Fo B cells in mixed BM chimeras after NP-CGG alum immunization at days 6–21 of the splenic response. Data are shown as ratios to simplify varied mixing of ~20-50% CD45.2 and ~80-50% CD45.1 BM across experiments. Data are pooled from >5 experiments. **(E)** MIXCR BCR repertoire analysis of Ig light chain V gene usage from paired-end bulk RNA sequencing on FACS sorted GC B cells from $Hvem^{-/-}$ CD45.2 (n=3) and WT CD45.1 (n=3) from the same mixed BM chimeras at day 11 after NP-CGG alum immunization, ±SD shown. **(F)** Frequency of W33L mutations in the V_H186.2 heavy chain from sorted CD45.2 $Hvem^{-/-}$ or $Hvem^{+/+}$ and respective CD45.1 WT GC B cells at days 11–13 after NP-CGG immunization of mixed BM chimeras. Data are pooled from 5 experiments. *P<0.05, **P<0.01, ***P<0.001, ****P<0.0001. Unpaired Student's t test, A, C, D. Chi-Squared and Fischer's exact test, E, F. Bars indicate mean ±SD. See also Figure S1.

HVEM-deficiency provides the earliest GC B cells with a proliferation advantage

To determine if HVEM-deficiency increased B cell entry into the GC, we crossed the *Hvem*$^{-/-}$ mouse line to the Hy10 mouse line, which has a BCR specific for hen egg lysozyme (HEL). To test if *Hvem*$^{-/-}$ B cells proliferate more than their competitors during the early response, *Hvem*$^{-/-}$ and WT Hy10 B cell mixes were labeled with cell trace violet (CTV) and co-transferred with OVA-specific OT-II CD4^{+} T cells into WT hosts and immunized with HEL-OVA or a lower affinity antigen, DEL-OVA (Fig. 2.2A). At day 2 the amount of proliferation in each group was similar, but by day 3, *Hvem*$^{-/-}$ Hy10 B cells had an increased frequency of cells that had divided greater than 4 times, as measured by the increase in CTV^{lo} cells (Fig. 2.2B, C). The response to high and low affinity forms of the antigen was similar (Fig. 2.2C). When referenced against the proliferation rates of cells in the control mixed transfers it was evident that the major difference was the lower proliferation rate of the WT cells that were in competition with the HVEM-deficient cells (Fig. 2.2C). At day 4.5–5 after immunization, when both plasmablasts (PB) and GC B cells could be clearly identified by flow cytometry (Fig. S2A), *Hvem*$^{-/-}$ Hy10 B cells had an increased frequency in the GC compartment compared to WT competitors (Fig. 2.2D). There was also an increase in the PB compartment though this effect was often not as marked as observed for the GC B cells in the same animals (Fig. 2.2D). These data suggest that HVEM-deficiency reveals itself in a competitive environment by allowing *Hvem*$^{-/-}$ B cells to outcompete the ability of WT B cells to proliferate.

Loss of HVEM in an ongoing GC provides B cells with a competitive advantage

Tfh cells are involved in supporting the early steps in GC induction as well as the mature GC response. To test if the growth advantage of HVEM-deficient B cells required Tfh cells, we

transferred *Hvem*$^{-/-}$ and WT Hy10 B cell mixes into Tfh cell-deficient Bcl6 $^{f/f}$ *Cd4*^{Cre} hosts. At days 5–7 after immunization with an intermediate affinity HEL conjugated to SRBC, 2x-HEL-SRBC, Hy10 B cells expanded in both control and B*cl6*$^{f/f}$ *Cd4*^{Cre} hosts (Fig. S2B). While *Hvem*$^{-/-}$ Hy10 B cells had an increased frequency compared to their WT competitors in control hosts, the HVEM-deficient advantage was lost in the Tfh cell-deficient hosts (Fig. 2.2E).

To determine if HVEM-deficiency provided B cells with a competitive growth advantage once the cells were within the GC, we crossed *Hvem* floxed animals to the inducible GC Cre line, *S1pr2*^{ERT2Cre}, and to tdTomato$^{f/f}$ reporter animals. We then made mixed BM chimeras with the *Hvem* floxed line and respective controls, immunized with NP-CGG, and treated with tamoxifen at day 3 to activate Cre in *S1pr2*$^{+}$ GC B cells (Fig. 2.2F). We found that >70-80% of CD45.2 GC B cells were expressing tdTomato and HVEM surface expression was decreased to nearly *Hvem*$^{-/-}$ levels in the GC, but was unchanged in follicular B cells (Fig. S2C, S2D). Importantly, *Hvem*$^{f/f}$ *S1pr2*^{ERT2Cre} GC B cells had a 30-50% increase in their representation compared to their frequency amongst follicular B cells whereas the control *Hvem*$^{f/f}$ Cre$^{–}$ *and* *Hvem*$^{+/+}$ Cre^{+} GC B cells did not increase in their representation (Fig. 2.2G). A 1 hr EdU labeling analysis showed that a slightly greater fraction of HVEM-deficient than internal control GC B cells were in cell cycle (Fig. 2.2H). As another way to test the impact of HVEM loss at the GC stage, we crossed *Hvem* floxed animals to the *Cγ1*^{Cre} line, which acts earlier in the response and avoids the need for tamoxifen. In mixed BM chimeras, *Hvem*$^{f/f}$*Cγ1*^{Cre} GC B cells had a growth advantage over the control GC B cells (Fig. S2E, F). These findings indicate HVEM has a restraining influence on B cells during GC seeding and within the GC.

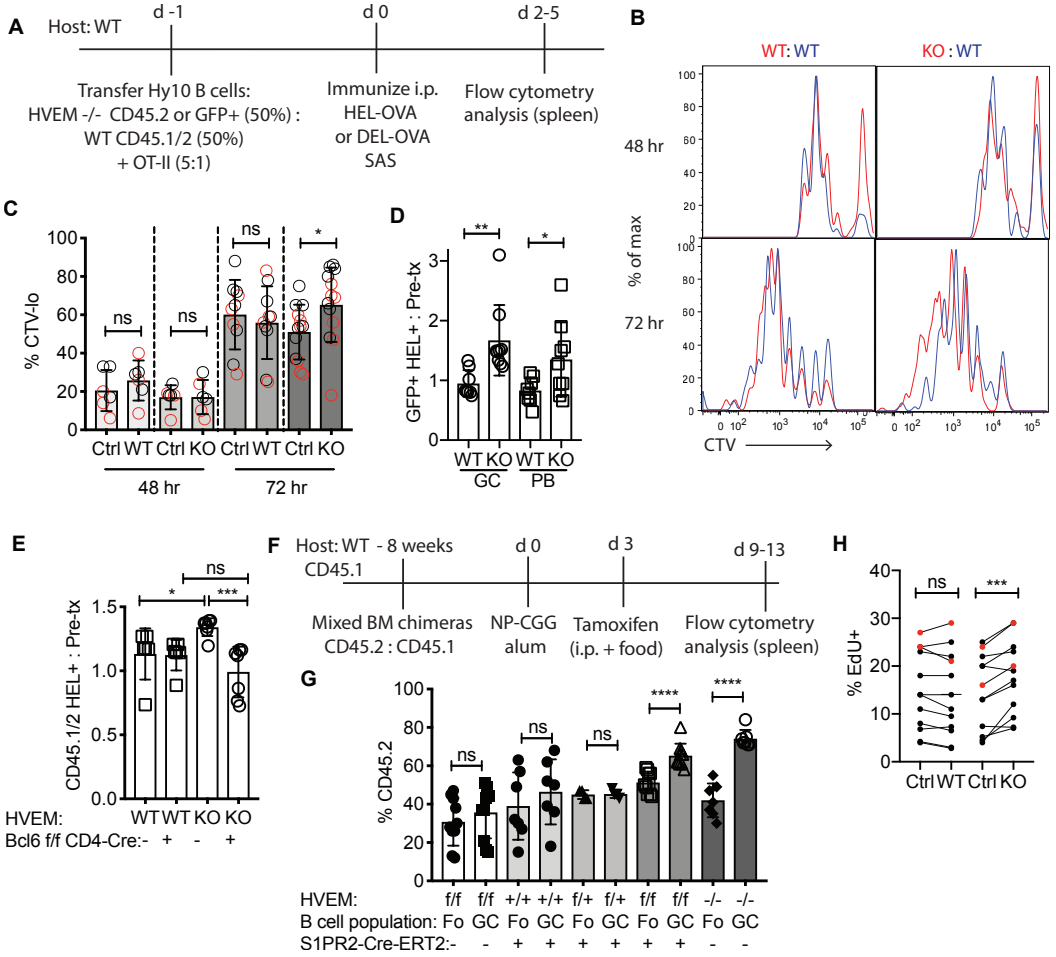

Figure 2.2. HVEM-deficiency provides B cells with a proliferation advantage early in the response and within the GC

(A) Experimental scheme and timeline for experiments in A-D. **(B)** Representative cell trace violet (CTV) dilution at 48 and 72 hr of Hy10 B cells compared to co-transferred WT Hy10 B cells after DEL-OVA. *Hvem*$^{+/+}$ or *Hvem*$^{-/-}$ Hy10 in red and WT mixing partner (Control) in blue. **(C)** Frequency of CTV-diluted (defined as >3 divisions at 48 hr and >4 divisions at 72 hr) Hy10 B cells compared to their WT mixing controls. Grey circles indicate HEL-OVA and red circles DEL-OVA immunization. Data are pooled from 3 experiments. **(D)** Ratio of the frequency of GFP^{+} HEL^{+} GC B cells or plasmablasts (PB) at days 4.5–5 after HEL-OVA immunization to pre-transfer frequency of GFP^{+} HEL^{+} B cells. Data are pooled from 3 experiments, with pre-transfer mixtures of GFP^{+} cells ~20-60%. **(E)** Mixed Hy10 transfer with endogenous T cell response into *Bcl6*$^{f/f}$ *Cd4*^{Cre} hosts and 2x-HEL SRBC immunization. Ratio of the frequency of CD45.1/2 *Hvem*$^{+/+}$ or *Hvem*$^{-/-}$ Hy10 to pre-transfer frequency. Tfh cell-deficient (*Bcl6*$^{f/f}$ *Cd4*^{Cre}) and controls hosts were analyzed at days 5–7. Data are pooled from 3 experiments. **(F)** Experimental scheme and timeline for experiments in F-G. **(G)** Frequency of CD45.2 Fo and GC B cells in the tamoxifen treated mixed BM chimeras. Data are pooled from 3 experiments and include chimeras with 10-60% CD45.2 Fo B cells. **(H)** Frequency of EdU^{+} IgD^{lo}EphrinB1^{+} GC

B cells in *Hvem*$^{+/+}$ and *Hvem*$^{-/-}$ mixed BM chimeras immunized with NP-CGG. Animals were treated with EdU 1 hr before analysis at days 6–7 (black circles) and day 21 (red circles). Data are pooled from 3 experiments. *P<0.05, **P<0.01, ***P<0.001, ****P<0.0001. Unpaired two-tailed Student's t test, C-E, G. Paired two-tailed Student's t test, H. See also Figure S2.

HVEM signaling intrinsic to the B cell is not required for GC B cell suppression

To test whether HVEM signaling into the B cell was required for HVEM-mediated restraint of the GC response, we used a gain-of-function approach. BM chimeric mice were generated using BM that had been transduced with MSCV-Thy1.1 retrovirus encoding full length or mutated forms of *Hvem* and the reconstituted mice were immunized with SRBC (Fig. 2.3A-C). Overexpression of WT HVEM suppressed the representation of Thy1.1 reporter^{+} GC B cells by 50% compared to follicular B cells while overexpression of an empty vector (EV) did not alter Thy1.1^{+} B cell participation in the GC (Fig. 2.3C, D).

To determine if loss of HVEM's ability to recruit TRAF2/5 impacted GC B cell participation, we introduced a point mutation in the HVEM cytoplasmic tail, E271A, that is known to disrupt TRAF recruitment (Hsu et al., 1997). This mutant form of HVEM was expressed on the cell surface and repressed B cell participation in the GC to the same extent as WT HVEM (Fig. 2.3B-D). To rule out signaling via other parts of the HVEM cytoplasmic tail, a mutant was generated harboring a stop codon at position 235 (Δ235) immediately after the transmembrane domain. This construct suppressed B cell participation in the GC to a similar extent as WT (Fig. 2.3B-D). The Δ235 mutant also restrained B cell participation in the GC when expressed in *Hvem*$^{-/-}$ cells (Fig. 2.3E). These data demonstrate that HVEM's intrinsic signaling into the B cell is not required for its ability to restrain B cell participation in the GC response.

A point mutation at Y61A within HVEM's CRD1 disrupts binding to BTLA and CD160 (Cheung et al., 2009a). Unlike WT HVEM, Y61A HVEM failed to reduce the participation of transduced B cells in the GC response, suggesting that HVEM's ability to bind a ligand through CRD1 is required (Fig. 2.3F, G).

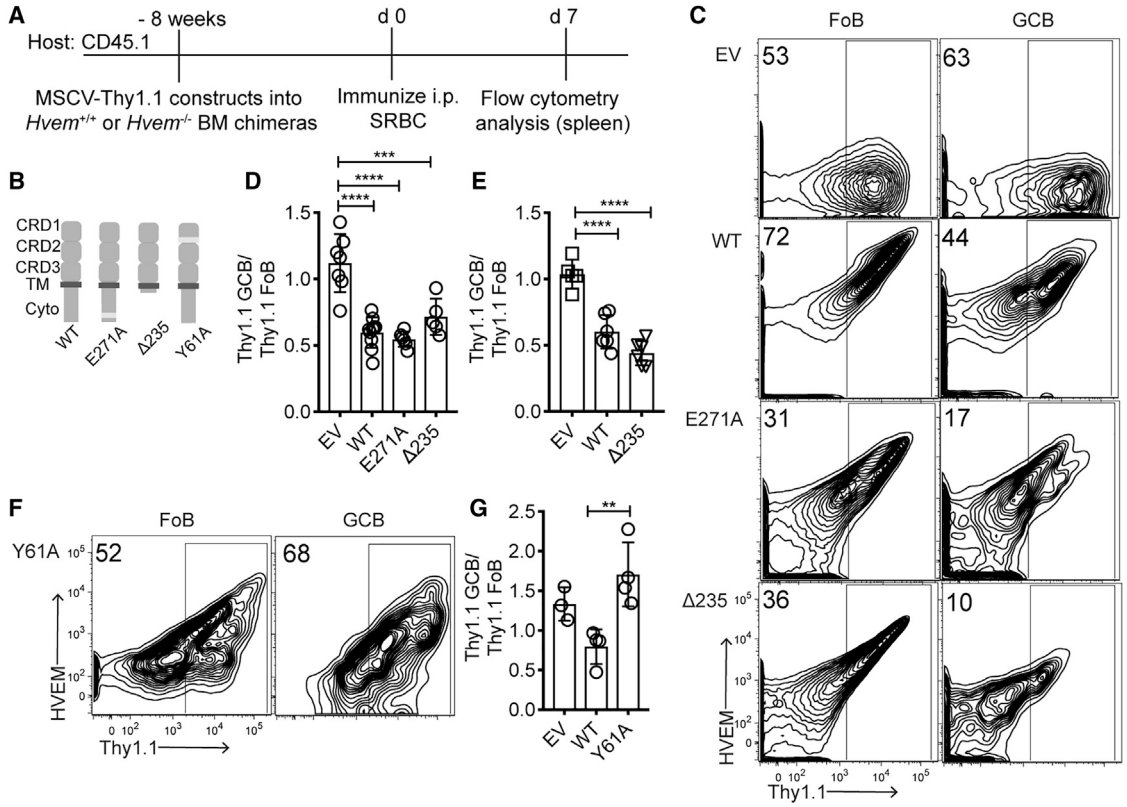

Figure 2.3. HVEM signaling intrinsic to the B cell is not required for GC B cell suppression **(A)** Experimental scheme and timeline for experiments in B-G. **(B)** Model of HVEM WT, E271A (TRAF2/5 binding mutant), Δ235 (cytoplasmic tail truncation), Y61A (CRD1 binding mutant). **(C)** Representative flow cytometric analysis of HVEM and Thy1.1 expression on Fo and GC B cells in empty vector (EV), HVEM WT, E271A and Δ235 transduced BM chimeras. **(D)** Frequency of Thy1.1$^+$ cells in GC compared to Fo in *Hvem*$^{+/+}$ BM chimeras in splenic response. Data are pooled from 3 experiments. **(E)** Frequency of Thy1.1$^+$ cells in GC compared to Fo in *Hvem*$^{-/-}$ BM chimeras in splenic response. Data are pooled from 2 experiments. **(F)** Representative flow cytometric analysis of HVEM and Thy1.1 expression on Fo and GC B cells in HVEM Y61A transduced BM chimeras. **(G)** Frequency of Thy1.1$^+$ cells in GC compared to Fo in *Hvem*$^{-/-}$ BM in pLN response. Data are pooled from 2 experiments. *P<0.05, **P<0.01, ***<P0.001, ****P<0.0001. Ordinary One-Way Anova with Bonferroni's multiple comparisons test, D, E, G.

BTLA on CD4$^+$ T cells is required for HVEM-deficient GC B cell competitiveness

Since BTLA is an inhibitory receptor highly expressed in the GC on both B cells and T cells (Fig. 2.4A), we tested if BTLA is required for HVEM's suppressive ability. When HVEM was overexpressed in *Btla*$^{-/-}$ BM chimeric mice, Thy1.1 reporter$^+$ GC B cells participated in the GC at the same frequency as in follicular B cells (Fig. 2.4B). This finding contrasted with the repressive effect of HVEM overexpression on B cells in WT BM chimeric mice (Fig. 2.3D) and suggested that BTLA was the relevant ligand for HVEM's ability to suppress participation in the GC.

In vitro studies have shown that BTLA in B cells can inhibit BCR signaling and it has been suggested that HVEM-BTLA can interact in *cis* within the same cell (Cheung et al., 2009a; Vendel et al., 2009), and a role for such *cis* interactions has been invoked to explain findings in a mouse FL model (Boice et al., 2016; Huet et al., 2018; Verdière et al., 2018). If the actions of HVEM in restraining B cell participation in the GC were dependent on *cis* engagement with BTLA, it would be predicted that B cells lacking BTLA would have a GC growth advantage similar to that observed for HVEM-deficient cells. Analysis of mice reconstituted with a mixture of WT and *Btla*$^{-/-}$ BM showed that cell intrinsic loss of BTLA did not alter the frequency of B cells in the GC (Fig. 2.4C). Similar results were obtained when mixed BM chimeras were made using BM from *Btla*$^{f/f}$ *Mb1*^{Cre} mice that selectively lack BTLA in B cells (Fig. S3A, B).

To determine if BTLA on bystander B cells was acting in *trans* to influence antigen-reactive B cells, *Hvem*$^{-/-}$ and WT Hy10 B cell mixes were transferred into *Btla*$^{f/f}$ *Mb1*^{Cre} or control hosts that were then immunized with 2x-HEL-SRBC (Fig. 2.4D). *Hvem*$^{-/-}$ Hy10 B cells maintained their growth advantage in the BTLA-B cell deficient hosts, suggesting bystander B

cells were not the cellular source of BTLA for HVEM-mediated suppression of GC B cell participation (Fig. 2.4E).

BTLA is a defining marker on Tfh cells compared to other $CD4^+$ T cells (Fig. 4A) (Chtanova et al., 2004; Kashiwakuma et al., 2010; Nurieva et al., 2009). To test if HVEM-deficient GC B cell competitiveness required BTLA-expressing T cells, *Hvem*$^{-/-}$ and WT Hy10 B cell mixes were transferred into *Btla*$^{f/f}$ *Cd4*^{Cre} hosts that lacked BTLA in all T cells (Fig. S3A). The hosts were immunized with 2x-HEL-SRBC and analyzed at day 3–6 of the response (Fig. 2.4D). The *Hvem*$^{-/-}$ Hy10 GC B cell growth advantage was abrogated in BTLA-T cell deficient mice at all timepoints analyzed (Fig. 2.4F and Fig. S3C). Tfh cells were present at similar frequencies in both types of recipient animal (Fig. S3D, E) and the frequency of HEL^+ responding B cells was also similar (Fig. S3F). BTLA was upregulated in T cells between day 2 and day 3 of the response (Fig. S3G, H), kinetics that matched the timing of when HVEM began to regulate the B cell proliferative response (Fig. 2.2B). These data indicate that BTLA-expressing T cells are required for the *Hvem*$^{-/-}$ GC B cell competitive advantage.

A previous study reported that BTLA deficiency led to increased IL-21 production by *in vitro* generated and restimulated Tfh cells (Kashiwakuma et al., 2010). However, when Tfh cells were generated *in vivo*, we did not observe a difference in *Il21* expression between BTLA-deficient and WT Tfh cells from the same animals (Fig. S3I).

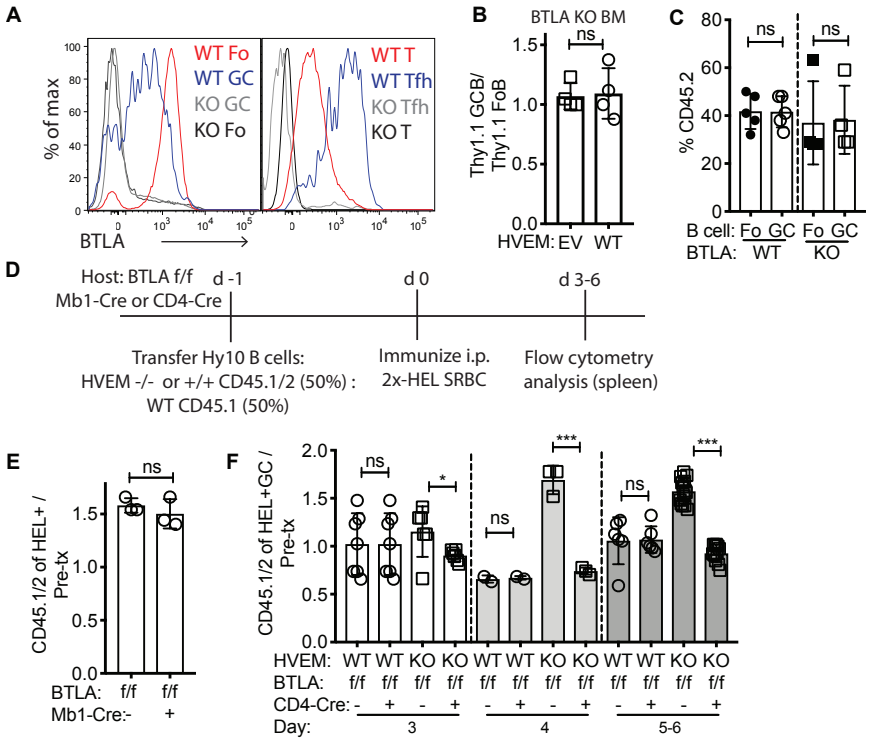

Figure 2.4. BTLA on T cells restrains GC B cell competitiveness
(A) Flow cytometric analysis of BTLA expression on B cells (left) and CD4$^+$ T cells (right) compared to *Btla*$^{-/-}$. **(B)** HVEM overexpression *Btla*$^{-/-}$ BM chimeras were made by transducing empty vector (EV) or HVEM (WT) MSCV-Thy1.1 constructs into *Btla*$^{-/-}$ BM and reconstituting CD4-depleted hosts. Chimeras were then immunized with SRBC and the participation of Thy1.1$^+$ cells in the GC compared to Fo B cell compartments was determined. **(C)** Contribution of *Btla*$^{+/+}$ or *Btla*$^{-/-}$ CD45.2 cells to Fo and GC populations in spleen of mixed BM chimeras made with ~40% of CD45.2 and ~60% of WT CD45.1 at day 7 after SRBC immunization. **(D)** Experimental scheme and timeline for experiments in E, F. **(E)** Ratio of the frequency of CD45.1/2 *Hvem*$^{-/-}$ HEL$^+$ B cells in BTLA-B cell deficient (*Btla*$^{f/f}$ *Mb1*^{Cre}) hosts at day 5 to the pre-transfer frequency. **(F)** Ratio of CD45.1/2 *Hvem*$^{+/+}$ or *Hvem*$^{-/-}$ HEL$^+$ GC B cells to pre-transfer mix in BTLA-T cell deficient (*Btla*$^{f/f}$ *Cd4*^{Cre}) hosts at day 3–6. Data pooled from 4 experiments. *P<0.05, **P<0.01, ***<P0.001, ****P<0.0001. Unpaired two-tailed Student's t test, B, C, E, F. See also Figure S3.

BTLA-HVEM at the immunological synapse recruits SHP1 to inhibit signaling in Tfh cells

To determine if BTLA can alter CD4$^+$ T cell signaling at the immunological synapse when engaging HVEM, we turned to the well-established supported lipid bilayer model (Dustin et al., 2007). Human CD4$^+$ T cell blasts were transfected with BTLA to mimic the surface expression in Tfh cells (Fig. S4A) and settled on supported lipid bilayers containing anti-CD3

(UCHT1) and ICAM1 for 15 min before fixation. When HVEM was added to the bilayers, BTLA and HVEM were recruited to the synapse, forming a ring around the central synaptic cleft in cases where a stable synapse was formed (Fig. 2.5A). In the presence of HVEM, there was a shift in interface organization from the stable synapse to the motile kinapse state (Mayya et al., 2018) where the TCR cluster is at one pole of the interface (Fig. 2.5B and Fig. S4B).

BTLA has been shown to recruit SHP1 and SHP2 biochemically through Y257 and Y282 (Gavrieli et al., 2003; Watanabe et al., 2003). BTLA demonstrated a strong colocalization with SHP1 at the synapse while SHP2 did not preferentially co-localize (Fig. 2.5C-F). When the $CD4^+$ T cells blasts were transfected with a BTLA Y257F/Y282F mutant, SHP1 colocalization was diminished and SHP2 was unchanged (Fig. 2.5C-F). The incomplete effect on SHP1 recruitment likely reflects the activity of endogenous BTLA in the blasts. These results are in contrast to the PD-1 molecule that colocalizes preferentially with SHP2 at the synapse (Fig. S4C-F).

In accord with SHP1 recruitment, inclusion of HVEM in the bilayer inhibited the amount of signaling downstream of the TCR as measured by pZAP70 and pPKCθ (Fig. 2.5G-J and Fig. S4G-H). This observation was made for both BTLA-transfected $CD4^+$ T cells and human tonsil-derived Tfh cells (Fig. 2.5G-J and Fig. S4G-H). Inclusion of the CD28 ligand CD80 in the bilayer led to an elevated amount of signaling and HVEM continued to reduce, in most cases significantly, the extent of ZAP70 and PKCθ activation (Fig. 2.5G-J and Fig. S4G-H). These data suggest that HVEM engagement of BTLA inhibits T cell activation through SHP1 at the immunological synapse.

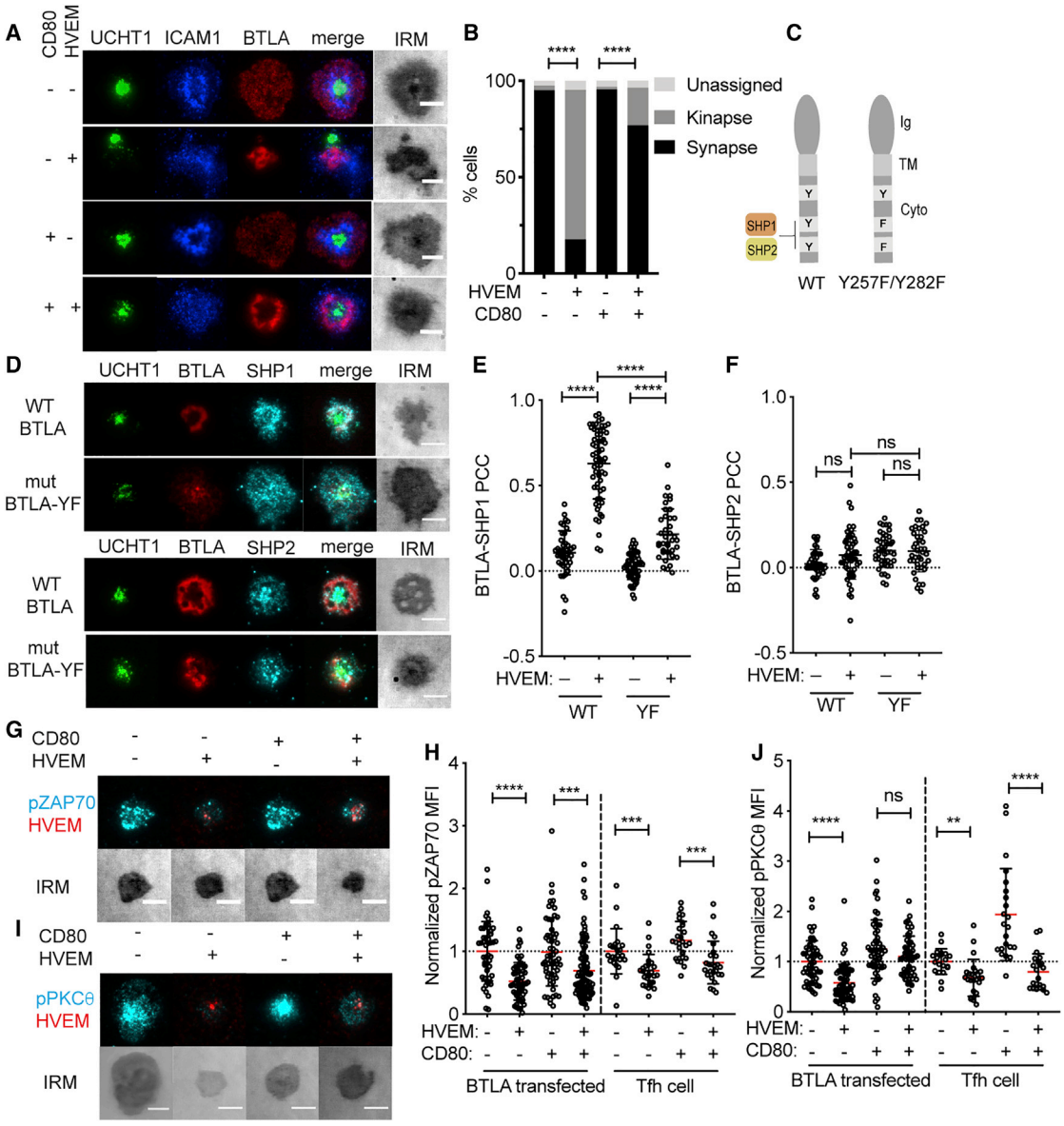

Figure 2.5. BTLA-HVEM at the immunological synapse recruits SHP1 to inhibit signaling in Tfh cells

(A) Example TIRF images of BTLA-transfected human CD4$^+$ T cell blasts on supported lipid bilayers containing anti-CD3, ICAM1 and, where indicated, HVEM and/or CD80. Staining for CD3 (UCHT1), ICAM1 and BTLA is shown. **(B)** Quantification of kinapse versus synapse state of cells imaged as in A. **(C)** Model of human BTLA binding mutant Y257F/Y282F designed to disrupt SHP1/2 recruitment to the last 2 of 4 cytosolic tyrosines. **(D)** Representative images of SHP1 and SHP2 recruitment to the synapse in relation to WT or mutant BTLA. **(E, F)** Quantification of SHP1 (E) and SHP2 (F) colocalization with WT or mutant BTLA with or without HVEM in the bilayer using Pearson's colocalization coefficient (PCC). **(G)** Representative images of pZAP70 in human Tfh cells in relation to HVEM in the bilayer after 15 min on the bilayer with standardized Lookup Table (LUT) across panels so fluorescence can be

directly compared. **(H)** Relative amount of pZAP70 in BTLA-transfected $CD4^+$ T cell blasts and Tfh cells with or without HVEM and CD80 in the bilayer normalized to no HVEM no CD80 condition. **(I)** Representative images of pPKCθ in human Tfh cells in relation to HVEM in the bilayer after 15 min on the bilayer with standardized LUT across panels so fluorescence can be directly compared. **(J)** Relative amount of pPKCθ in BTLA-transfected CD4+ T cell blasts and Tfh cells with or without HVEM and CD80 in the bilayer normalized to no HVEM no CD80 condition. Data pooled from 3 independent donors and experiments. Scale bars are 5 μm. *P<0.05, **P<0.01, ***<P0.001, ****P<0.0001. Chi-squared with Fischer's exact test, B, Mann-Whitney test E, F, H, J. See also Figure S4.

BTLA signaling into the T cell through SHP1 is required for HVEM-deficient GC B cell competitiveness

To test if BTLA signaling was restraining the help provided to B cells, we generated a mutant mouse line (termed BTLA Y3) that lacks the BTLA cytoplasmic tail (Fig. 2.6A and Fig. S5A). *Hvem*$^{-/-}$ Hy10 spleen cell mixes were then transferred into *Btla*$^{+/+}$, *Btla*$^{y3/y3}$, *Btla*$^{-/-}$ hosts, and the mice were immunized with 2x-HEL-SRBC and analyzed at day 5. *Btla*$^{y3/y3}$ hosts abrogated the *Hvem*$^{-/-}$ Hy10 GC B cell competitive advantage, phenocopying *Btla*$^{-/-}$ hosts (Fig. 2.6B). BTLA Y3 mutant protein was expressed at reduced levels on the T cell surface, comparable to those on *Btla*$^{+/-}$ Tfh cells (Fig. S5B). To control for possible effects of the reduced expression we also performed transfers into *Btla*$^{+/-}$ recipients. The *Hvem*$^{-/-}$ B cells showed a similar competitive advantage in heterozygous and WT hosts (Fig. 2.6B). These findings provide evidence that the BTLA cytoplasmic domain in host T cells is required for HVEM-mediated restraint of B cell participation in the GC response.

To test which of BTLA's intracellular binding partners in the T cell was restraining the signal to HVEM-expressing GC B cells, *Hvem*$^{-/-}$ and WT Hy10 B cell mixes were transferred into *Ptpn6*$^{fl/fl}$ (SHP1) and *Ptpn11*$^{fl/fl}$ (SHP2) *Cd4*^{Cre} or control hosts. Tfh cell frequencies in the SHP1 and SHP2 T cell-deficient hosts were comparable in the spleen compared to controls (Fig. S5C, D). The *Hvem*$^{-/-}$ GC B cell competitive advantage was lost in SHP1 T cell-deficient hosts,

while it was maintained in the SHP2 T cell-deficient hosts (Fig. 2.6C, D). The frequency of HEL-binding B cells in both types of host was comparable to controls (Fig. S5E, F). These data suggest that following HVEM engagement, BTLA recruits SHP1 to moderate the activation of the T cell and the amount of help provided to the HVEM-expressing B cell.

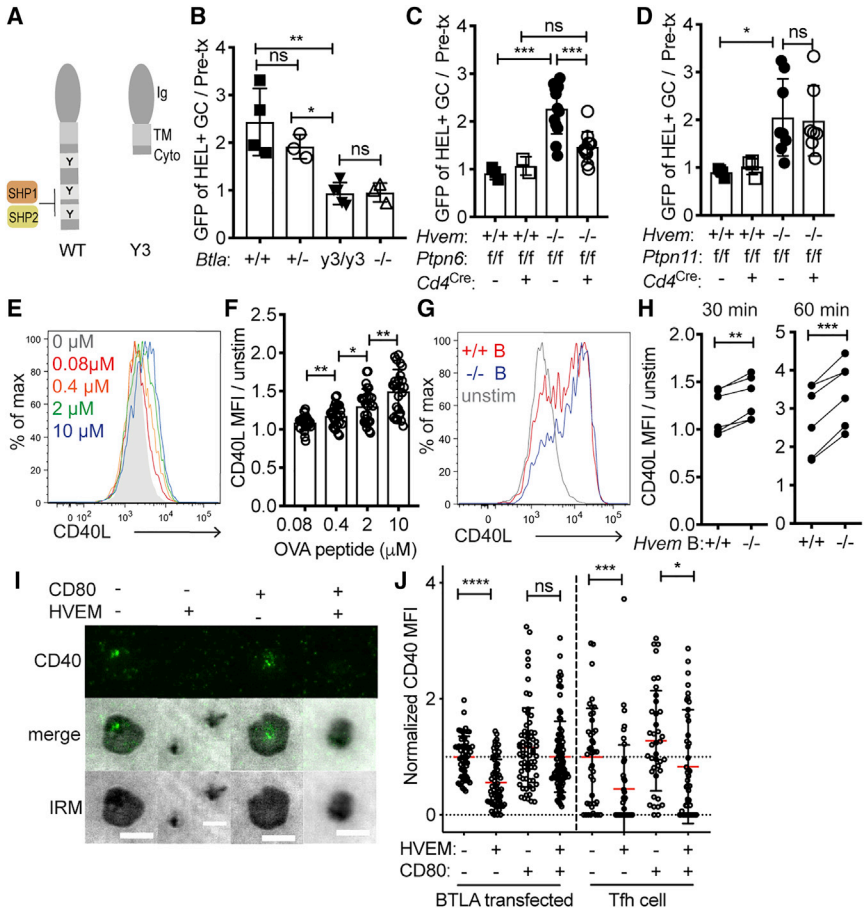

Figure 2.6. BTLA signaling into the T cell through SHP1 is required for HVEM-deficient GC B cell competitiveness

(A) Model of murine BTLA truncation termed Y3 in which all three cytoplasmic tyrosines have been removed. **(B)** Ratio of *Hvem*$^{-/-}$ GFP^{+} HEL^{+} GC (IgD^{lo}Fas^{+}) B cells compared to the pre-transfer mix (~20% *Hvem*$^{-/-}$ GFP^{+} Hy10 : ~80% WT CD45.1 Hy10) in *Btla*$^{+/+}$, *Btla*$^{+/-}$, *Btla*$^{y3/y3}$, *Btla*$^{-/-}$. Data pooled from 2 experiments. **(C)** Ratio of *Hvem*$^{+/+}$ or *Hvem*$^{-/-}$ GFP^{+} HEL^{+} GC B cells compared to the pre-transfer mix in *Ptpn6*$^{f/f}$ (SHP1) control or *Cd4*^{Cre} hosts. Data pooled from 4 experiments. **(D)** Ratio of *Hvem*$^{+/+}$ or *Hvem*$^{-/-}$ GFP^{+} HEL^{+} GC B cells compared to the pre-transfer mix in *Ptpn11*$^{f/f}$ (SHP2) control or *Cd4*^{Cre} hosts. Data pooled from 3 experiments. **(E)** Representative flow cytometric analysis of CD40L surface mobilization on OT-II Tfh cells after a 30 min incubation with B cells pulsed with a titration of OVA peptide (0-10 μM). **(F)** CD40L expression on OT-II Tfh cells stimulated as in E, normalized to unstimulated Tfh cells. Data

pooled from 3 experiments. **(G)** Representative flow cytometric analysis of CD40L surface mobilization on OT-II Tfh cells after 60 min stimulation on OVA peptide-pulsed *Hvem*$^{+/+}$ or *Hvem*$^{-/-}$ B cells. **(H)** Normalized CD40L MFI on OT-II Tfh cells 30 or 60 min after stimulation with OVA-loaded *Hvem*$^{+/+}$ or *Hvem*$^{-/-}$ B cells (2 μM or 10 μM). Data pooled from 2 experiments. **(I)** Representative images of CD40 recruitment to the immunological synapse with or without HVEM and CD80 present in the lipid bilayer after 15 min incubation with human Tfh cells with standardized LUT across panels so fluorescence can be directly compared. Upper images show IF, middle images overlayed IF and IRM and lower images IRM. **(J)** Relative CD40 accumulation at synaptic interface in BTLA-transfected CD4^{+} T cell blasts and Tfh cells with or without HVEM and CD80 in the bilayer, normalized to the no HVEM no CD80 condition. Data pooled from 3 independent donors and experiments. Scale bars are 5 μm. *P<0.05, **P<0.01, ***<P0.001, ****P<0.0001. Ordinary One-Way Anova with Bonferroni's multiple comparisons test B, C, D. Unpaired two-tailed Student's test panel, F. Paired two-tailed Student's test H. Mann-Whitney J. See also Figure S5.

HVEM-BTLA interaction reduces the amount of CD40-CD40L brought to synaptic interface

For a Tfh cell to provide greater help to HVEM-deficient versus HVEM-expressing B cells in the same GC microenvironment during interactions that often last only for minutes, Tfh cell BTLA likely had to regulate mobilization of a preformed mediator. The best defined pre-formed helper factor in Tfh cells is CD40L (Casamayor-Palleja et al., 1995; Koguchi et al., 2007; 2012). However, it has been unclear whether the amount of preformed CD40L displayed on the T cell surface can be tuned by the strength of the TCR signal. As one approach to test this, OVA-specific OT-II Tfh cells were incubated for 30 min with B cells that had been pulsed with a range of OVA-peptide concentrations. A 30 min incubation was chosen as a time that allowed cells to interact in the *in vitro* environment while being sufficiently short to ensure that only preformed CD40L could be mobilized. Although the B cells were not intentionally activated, they express ICOSL (Xu et al., 2013) and upregulated CD86 during the incubation (Fig. S5G), properties that may contribute to their ability to activate Tfh cells. Compared to unstimulated Tfh cell

expression of CD40L, B cells presenting increasing amounts of OVA-peptide led to an analog upregulation of CD40L on the Tfh cell surface by 30 min and this was further increased after 60 min (Fig. 2.6E, F and Fig. S5H, I).

We next tested whether HVEM-deficiency on the OVA-peptide pulsed B cell influenced CD40L upregulation on Tfh cells. Analysis at 30 and 60 min revealed a small but significant increase in CD40L exposure on Tfh cells interacting with HVEM-deficient B cells compared to Tfh cells interacting with WT B cells (Fig. 2.6G, H). Past studies have shown that CD40 is recruited to the immune synapse in a CD40L-dependent manner (Boisvert et al., 2004; Papa et al., 2017). We therefore returned to the supported lipid bilayer as another approach to test the ability of BTLA to regulate preformed CD40L upregulation. Human $CD4^+$ T cell blasts and human Tfh cells were plated on the bilayer containing anti-CD3, ICAM1, CD40 and in some cases CD80. When HVEM was added to the bilayer, the amount of CD40 recruited to the synapse in the 15 min assay was reduced in both the blasts and the Tfh cells (Fig. 2.6I, J and Fig. S5J). These data suggest that BTLA can restrain the amount of preformed CD40L that is mobilized to the immunological synapse, and thus the quality of T cell help.

To examine if increased T cell help could be read out in the *Hvem*$^{-/-}$ GC B cell as a transcriptional change, RNA-sequencing was performed on GC B cells from mixed BM chimeras. The top differentially expressed genes in *Hvem*$^{-/-}$ GC B cells compared to WT GC B cells corresponded to gene ontology biological processes for positive regulation of cell cycle progression (Fig. S5K). Previous studies have shown that Tfh cell help signals through CD40 to activate Myc and mTOR1 signaling in GC B cells that is required for clonal expansion (Calado et al., 2012; Dominguez-Sola et al., 2012; Ersching et al., 2017; Luo et al., 2018). GSEA analysis revealed that *Hvem*$^{-/-}$ GC B cells had increased Myc gene signatures compared to their WT

competitors (Fig. S5L) (Yu et al., 2005). *Hvem*$^{-/-}$ GC B cells were also enriched for a set of rapamycin-sensitive genes induced downstream of T cell help in GC B cells (Fig. S5M) (Ersching et al., 2017). These data are consistent with *Hvem*$^{-/-}$ B cells receiving increased T helper signals compared to their WT competitors.

BTLA-deficiency in T cells leads to GC B cell expansion in the setting of Bcl-2-overexpression

HVEM mutations in human GC-derived lymphomas often occur in the setting of Bcl-2-overexpression. To determine if the HVEM-deficient GC growth advantage occurred when B cells constitutively expressed Bcl-2, *Hvem*$^{-/-}$ *BCL-2*-tg mice were generated. Irradiated recipient mice were reconstituted with a mixture of CD45.2 *Hvem*$^{-/-}$ *BCL-2*-tg BM and congenically distinguished WT *BCL-2*-tg BM, and the chimeric animals were immunized with SRBC. The HVEM-deficient Bcl-2 GC B cells maintained their growth advantage compared to WT Bcl-2 competitors (Fig. 2.7A). These data indicate that the growth promoting pathway mediated by HVEM-deficiency is distinct from the pro-survival pathway mediated by Bcl-2.

Bcl-2 is very highly expressed in human FL and previous work has shown that lines of mice expressing higher amounts of Bcl-2 in B cells than the *BCL-2*-tg line have a higher propensity to form lymphomas (Ogilvy et al., 1999). To generate mice with higher expression of Bcl-2 in B cells, we transduced WT or *Hvem*$^{-/-}$ BM with a MSCV-*Bcl-2*-Thy1.1 construct. After reconstituting WT hosts, the Bcl-2 overexpressing BM chimeras generated large splenic GCs in unimmunized mice as early as week 6 after reconstitution and the GCs increased in size through 14 weeks (Fig. 2.7B, C). Compared to WT chimeras, *Hvem*$^{-/-}$ chimeras had increased GC B cell expansion, suggesting that HVEM-deficiency cooperates with strong Bcl-2 overexpression.

Based on our findings in the preceding sections, we hypothesized that BTLA in the T cell could restrain the amount of help provided to the GC B cell in the setting of Bcl-2 overexpression. To test this possibility, *Btla*$^{f/f}$ *Cd4*^{Cre} or control BM was transduced with the MSCV-*Bcl-2*-Thy1.1 construct and used to reconstitute *Rag2*$^{-/-}$ or *Tcrb*$^{-/-}$ mice. T cell-deficient mice were used as hosts to ensure an absence of radioresistant WT T cells. When Bcl-2-overexpressing B cells developed in an environment where all the T cells were BTLA-deficient, there was increased GC B cell expansion in the spleen (Fig. 2.7D-F). VH- and VL- region PCR analysis of GC B cells from two of the *Btla*$^{f/f}$ *Cd4*^{Cre} BM chimeras with GC B cell frequencies exceeding 20% of splenic B cells showed evidence of clonal outgrowths (Fig. 2.7G). Clonal dominance was not observable for the light chain, perhaps because even small numbers of polyclonal cells prevent an abundant clone from dominating this PCR reaction. Taken together, these data indicate that BTLA on the T cell acts as a cell-extrinsic suppressor of Bcl-2-overexpressing GC B cell expansion.

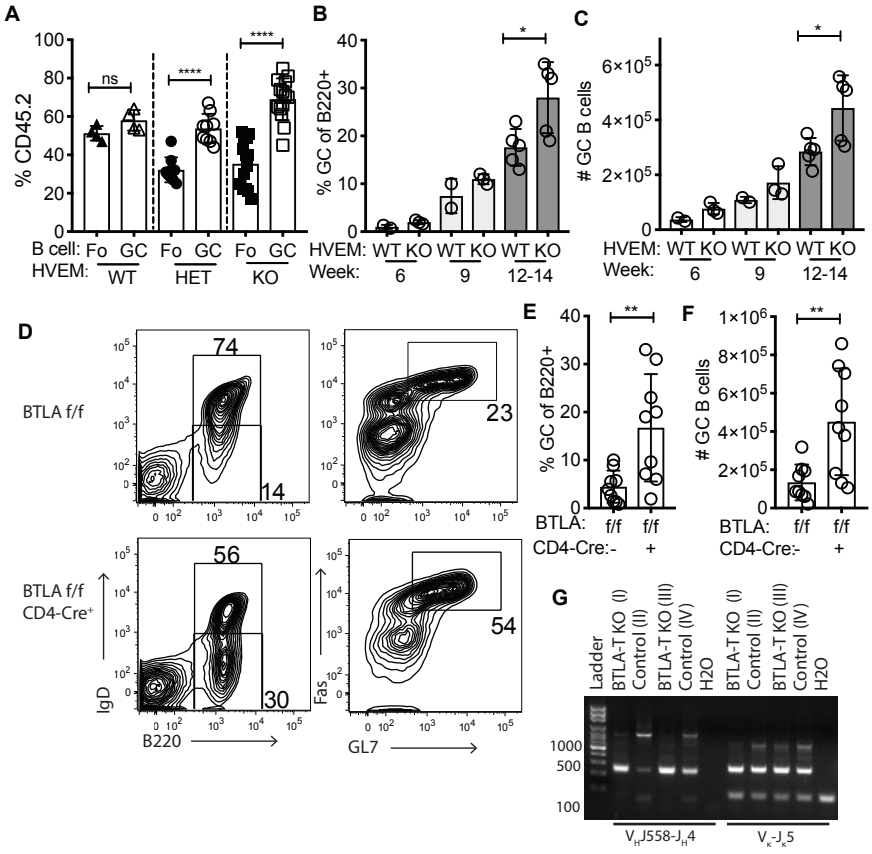

Figure 2.7. BTLA-deficiency in T cells leads to GC B cell expansion in the setting of Bcl-2-overexpression

(A) Frequency of CD45.2 splenic Fo and GC B cells of Bcl-2 transgenic origin in mixed BM chimeras reconstituted with 30-50% *Hvem*$^{+/+}$, *Hvem*$^{+/-}$, or *Hvem*$^{-/-}$ Eμ-BCL-2-tg CD45.2 BM and 50-70% WT Eμ-BCL-2-tg CD45.1/2 BM, 7d after immunization with SRBC. Data pooled from 3 experiments. **(B, C)** The frequency (B) and number (C) of spontaneously forming splenic GC B cells in mice reconstituted for 6-14 weeks with *Hvem*$^{+/+}$or *Hvem*$^{-/-}$ BM transduced with MSCV-Bcl-2-Thy1.1. Data from 2 experiments. **(D)** Representative flow cytometric analysis of spontaneous GC formation in the spleen at 8 weeks of reconstitution with *Btla*$^{f/f}$ or *Btla*$^{f/f}$ *Cd4*^{Cre} BM transduced with MSCV-Bcl-2-Thy1.1. Irradiated *Rag2*$^{-/-}$ or *Tcrb*$^{-/-}$ mice were used as hosts. **(E, F)** The frequency (E) and number (F) of spontaneously forming splenic GC B cells in BM chimeras from (D). Data pooled from 3 experiments. **(G)** V_H- and V_L- region PCR analysis of GC B cells from 2 *Btla*$^{f/f}$ *Cd4*^{Cre} chimeras with splenic GC outgrowths >20% and 2 *Btla*$^{f/f}$ control chimeras. *P<0.05, **<P0.01, ****P<0.0001. Unpaired two-tailed Student's test.

Discussion

The above findings establish that engagement of BTLA on helper T cells by HVEM on B cells signals to restrain B cell expansion during generation of GC cells and PBs, and also acts as

a restraint on B cells within the GC. The negative signaling into the T cell depends on the BTLA cytoplasmic domain and on SHP1 recruitment. HVEM engagement of BTLA reduces proximal TCR signaling and this reduces the output of CD40L and likely other preformed mediators from the T cell. HVEM thereby restrains B cell proliferation, differentiation and selection by reducing the delivery of helper signals from the T cell. We also find that the T helper signals restrained by the HVEM-BTLA interaction can exert their growth promoting effects on Bcl-2 overexpressing (pre-malignant) B cells, providing evidence that BTLA may act as a cell-extrinsic repressor of B cell lymphomagenesis.

Under competitive conditions, proliferation of HVEM-deficient B cells was favored over WT B cells, in agreement with other models of B cell competition for T cell help (Gitlin et al., 2014; Yeh et al., 2018). When C57BL/6 mice were deficient in HVEM in all B cells or BTLA in all T cells, while there was a trend for increased GC frequencies, there was not a significant enlargement of the GC response. A study in BALB/c mice reported an enlarged GC response when BTLA was absent, suggesting that the extent of BTLA-mediated regulation of GC B cells may be influenced by background genes (Kashiwakuma et al., 2010). Although we observed a slight increase in *Hvem*$^{-/-}$ GC B cell proliferation in mixed settings across several time points, we did not observe a progressive increase in *Hvem*$^{-/-}$ B cell representation within the GC over time, suggesting there should be increased output of *Hvem*$^{-/-}$ cells from the GC that accounts for the extra cells generated by proliferation. Our inability to detect increased GC B cell death or increased Bmem or PC compared to B cell representation in the GC may be because of a small effect size and the possibility that more than one of these output parameters is affected. As much as leading to increased proliferation of HVEM-deficient cells, lack of HVEM on some B cells appeared to reduce proliferation of competing WT B cells in the same animal. The exact

mechanism of the diminished response of the WT cells is unclear, but one possibility might be that Tfh cells harbor a limited amount of preformed helper factors (such as CD40L) and when greater amounts are delivered to some cells (*Hvem*$^{-/-}$ in this case) then less is available for the other cells present in the same microenvironment. A related possibility, suggested by the propensity of HVEM to convert stable synapses to motile kinapses, is that the increased stability of *Hvem*$^{-/-}$ B cell interactions with Tfh cells diminishes the contact of WT B cells with Tfh cells.

B-T interactions generally occur over periods of minutes, making it unlikely that there is sufficient time for B cell-triggered induction of new transcription to impact the T cell help delivered during a given contact. Although previous work has shown that CD40L can be upregulated in a graded manner in proportion to the amount of TCR engagement, these studies were done over periods of 16-20 hrs and most likely involved transcriptional induction (Iezzi et al., 2009; Ruedl et al., 2000). In this study, we show that the rapid display of preformed CD40L protein on Tfh cells occurs in a manner proportional to the amount of MHC-peptide on the B cells. In accord with stronger signaling into the T cell mobilizing more preformed CD40L, previous work found that co-engagement of ICOS and the TCR enhanced CD40L externalization (Liu et al., 2014b; Papa et al., 2017). Based on these combined observations it can be suggested that the BTLA-mediated restraint of TCR-induced CD40L mobilization in T cells is due to the negative regulation of proximal TCR signaling.

BTLA has been shown in biochemical studies to co-immunoprecipitate with SHP1 and SHP2 (Gavrieli et al., 2003; Watanabe et al., 2003). The molecular basis for the preferential coupling to SHP1 observed here in Tfh cells is not yet known and will need further investigation. These observations contrast with findings for PD-1, which preferentially associates with SHP2 in immune synapse studies with $CD4^+$ and $CD8^+$ T cells (Hui et al., 2017; Yokosuka et al., 2012)

and this study). However, an *in vivo* study has suggested that PD-1 function in effector CD8 T cells is not fully dependent on SHP2 (Rota et al., 2018). Given that PD-1 and BTLA are both highly expressed on Tfh cells, it will be important to determine whether PD-1 in Tfh cells *in vivo* depends on SHP2 since this may indicate qualitative differences in the type of regulation exerted in Tfh cells by these related checkpoint-family proteins.

HVEM-mediated restraint of the B cell response did not begin immediately, suggesting that some temporal event needs to take place before HVEM-BTLA signaling becomes influential. We speculate that this may at least in part reflect the need for Bcl6 and BTLA upregulation in the activated T cell since the influence of HVEM-deficiency was lost in mice lacking Bcl6 in T cells. It is notable that HVEM surface levels are decreased on both mouse and human GC B cells compared to naïve and early activated B cells. Given the strong growth-repressive effects observed in HVEM gain-of-function experiments, the reduced HVEM levels may be important in permitting transmission of the helper signals needed to support the strong proliferative responses of GC B cells.

The impact of greater T cell help (indiscriminate of the amount of MHC-peptide presented) on the repertoire of B cells selected in the GC is not straightforward to predict. Our findings show that selection of NP-binding B cells is disfavored in HVEM-deficient B cells, perhaps indicating an increased competitiveness of carrier-specific B cells that would normally receive inadequate T cell help and be outcompeted by B cells responding to the readily accessible and highly multivalent NP hapten. Our inability to detect a differential effect of HVEM-deficiency on the proliferative response of Hy10 B cells responding to DEL (K_A 10^7 M^{-1}) versus HEL (K_A 10^{10} M^{-1}) (Lavoie et al., 1992) may be because both antigens are in the high affinity range and the oligomeric state of the OVA conjugates may further diminish

differences in antigen capture and MHC-peptide presentation. In the context of NP-based immunizations, a similar increase in representation of non-NP binding B cells was seen in immunized PD-L1-deficient mice (Shi et al., 2018). Within the NP-binding *Hvem*$^{-/-}$ GC B cell population, there was a reduction in the fraction of cells harboring the affinity improving W33L mutation compared to the internal control WT cells. When compared to the WT control mixed chimeras, it was notable that there was an increase in the frequency of W33L mutations in the WT cells competing with *Hvem*$^{-/-}$ cells compared to those competing with other WT cells. One interpretation of these findings is that by diminishing the helper signals available to WT B cells, the HVEM-deficient B cells promote stronger selection for those WT B cells that are able to present the highest amounts of antigen. The combined observations suggest that negative costimulatory molecule signaling in Tfh cells is necessary to maintain the stringency of GC selection. A reduction in B cell selection stringency may explain the autoantibody production occurring in aged BTLA-deficient 129/SvEV mice (Oya et al., 2008)

In agreement with a previous Bcl-2-overexpression BM chimera study (Boice et al., 2016), where *Hvem* shRNA-targeted B cells preferentially contributed to GC-derived lymphomas, we found that B cell HVEM-deficiency cooperated with Bcl-2-overexpression in promoting GC outgrowth. The previous work also found that shRNA-targeting of *Btla* in hematopoietic cells (HSCs) led to GC outgrowth and this was attributed to a role for *cis* engagement of BTLA by HVEM leading to BTLA-mediated down-regulation of tumor-promoting BCR signals (Boice et al., 2016; Huet et al., 2018; Verdière et al., 2018). In the experiments here, we did not observe any evidence for *cis* or *trans* effects of deleting BTLA from B cells, as measured by participation in the GC response. Instead, we found that deletion of BTLA from T cells led to a HVEM-expressing B cell growth advantage, including in

experiments with Bcl-2-overexpressing B cells. Although an important distinction between studies is that we measured GC participation and Boice et al., measured B cell lymphomagenesis, we believe that the different conclusions can be reconciled. Specifically, Boice et al., did not observe enrichment of BTLA-reduced B cells over control B cells in shRNA BM chimeras, making it unlikely that *cis* HVEM-BTLA interaction could be the principle mechanism of HVEM-mediated tumor suppression. While *trans* engagement by HVEM expressed in other B cells was also proposed (Boice et al., 2016), we believe the more likely explanation for the lymphomas arising in some of the mice reconstituted with BTLA knockdown HSCs is that a high knockdown efficiency was achieved in the Tfh cell compartment. Taking Boice et al., shRNA chimera data together with our findings, we believe that a revised model is supported in which *HVEM* mutation in B cells leads to a loss of negative signaling into Tfh cells, allowing *HVEM* mutant B cells to receive exaggerated helper signals that promote proliferation and accrual of AID-mediated mutations. In this regard, it is notable that FL has been highlighted for its rich presence of Tfh cells (de Jong and Fest, 2011; Huet et al., 2018; Verdière et al., 2018). Importantly, the therapeutic benefit of elevating HVEM levels in the FL setting, as achieved by Boice et al., using CAR T cells (Boice et al., 2016), might act by diminishing Tfh cell function and thus support of FL cell growth. Future studies are needed to test if soluble HVEM can reduce Tfh cell function during GC responses and in lymphoma models where B cell HVEM has been mutated.

SUPPLEMENTAL FIGURES AND LEGENDS

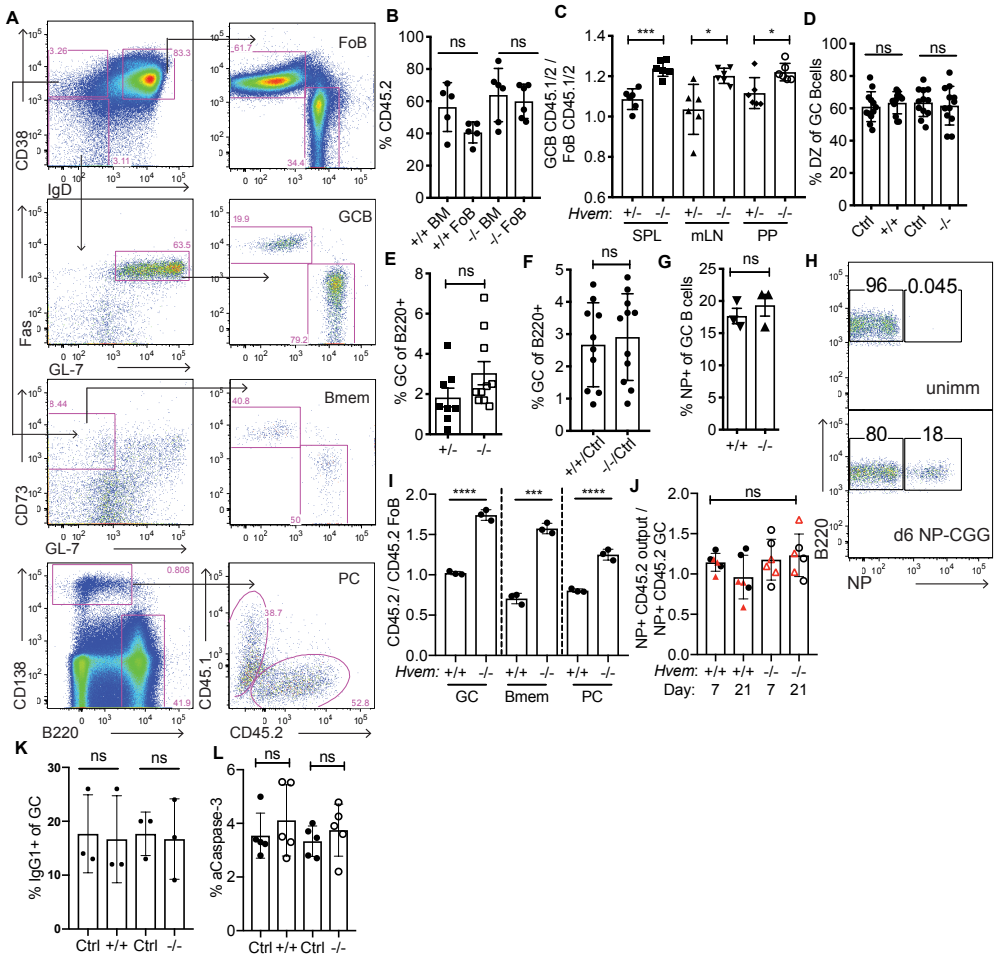

Figure S1. HVEM-deficiency increases GC B cell competitiveness in chronic GCs and GC output after an acute immune response. Related to Figure 1.

(A) Representative flow cytometric analysis of spleen Fo, GC, Bmem, and PC populations from mixed BM chimeras after SRBC immunization. (B) Contribution of CD45.2 cells to CD93^{+} immature BM B cells and splenic Fo B cells in mixed BM chimeras. Data pooled from 2 experiments. (C) Ratio of CD45.1/2 GC to CD45.1/2 Fo B cells in mixed chimeras made with ~70% of CD45.1/2 *Hvem*$^{+/-}$ or *Hvem*$^{-/-}$ BM with ~30% CD45.1 WT BM in Spleen (SPL), mesenteric LN (mLN) and Peyer's Patches (PP), after intraperitoneal (i.p.) SRBC immunization. Data pooled from 2 independent experiments. (D) Frequency of GC B cells from mixed BM chimeras in dark zone (DZ) state (CXCR4^{high}CD86^{low}) after SRBC immunization. Data pooled from 3 experiments. (E) Frequency of GC B cells in full *Hvem*$^{+/-}$ or *Hvem*$^{-/-}$ animals 6–8 days after SRBC immunization. Data pooled from 3 experiments. (F) Frequency of GC B cells in *Hvem*$^{+/+}$ and *Hvem*$^{-/-}$ mixed BM chimeras after SRBC immunization. Data pooled from 3 experiments. (G) Frequency of NP^{+} GC B cells in full, non-competitive *Hvem*$^{+/+}$ or *Hvem*$^{-/-}$ chimeras. (H) Representative flow cytometric analysis for splenic NP^{+} GC B cell gating on day 6 NP-CGG alum response compared to unimmunized control. (I) Ratio of CD45.2 GC, memory B cells (Bmem), and plasma cells (PC) to CD45.2 Fo B cells at day 8 after SRBC immunization. *Hvem*$^{-/-}$ mixed chimera example shown in panel A. (J) Ratio of CD45.2 NP^{+} splenic Bmem (black circles) or PC (red triangles) to CD45.2 NP^{+} GC B cells at day 7 and 21 after NP-CGG immunization. Data from 1 experiment and representative of 3 experiments. (K) Frequency IgG1^{+} of GC B cells in *Hvem*$^{-/-}$ mixed chimeras at day 8 after SRBC. (L) Frequency of anti-active Caspase-3^{+} GC B cells from NP-CGG alum immunized mixed BM chimeras day 6-7 directly ex vivo. Data pooled from 2 experiments. 'Ctrl' refers to the respective WT CD45.1 competitor. *P<0.05, **P<0.01, ***P<0.001, ****P<0.0001. Unpaired two-tailed Student's t test (B-G, I, K-L), Ordinary One-Way Anova with Bonferroni's multiple comparisons test (J).

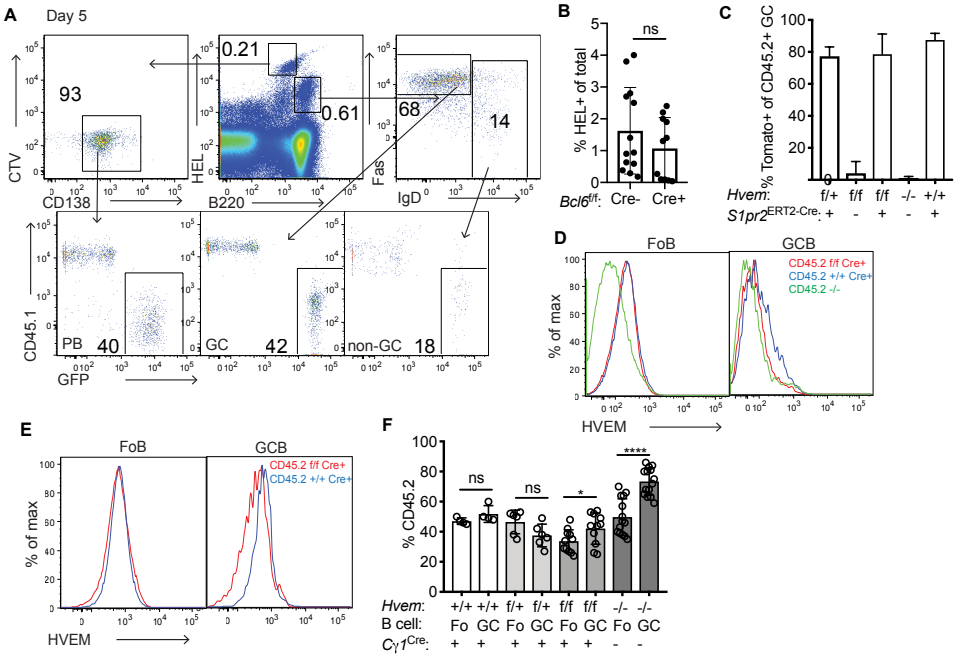

Figure S2. HVEM-deficiency provides B cells with a proliferation advantage early in the response and within the GC. Related to Figure 2.

(A) Representative flow cytometric analysis for gating GFP$^+$ HEL$^+$ B cells as HEL-intracellular-high CD138$^+$ plasmablasts (PB) and HEL-intermediate IgD^{lo}Fas$^+$ GC B cells at days 4.5–5. (B) Frequency of HEL$^+$ cells of total spleen in *Bcl6*$^{f/f}$ *Cd4*^{Cre} or controls at day 5–7 after 2x-HEL-SRBC. Data pooled from 3 experiments. (C) Frequency of tdTomato$^+$ of CD45.2 GC B cells after tamoxifen treatment. Data are pooled from 3 experiments. (D) Representative flow cytometric analysis of HVEM surface levels on Fo and GC B cells in CD45.2 compartment. Red *Hvem*$^{f/f}$ *S1pr2*^{ERT2Cre}, blue *Hvem*$^{+/+}$ *S1pr2*^{ERT2Cre}, and green *Hvem*$^{-/-}$. (E) Representative flow cytometric analysis of HVEM surface levels in *Hvem*$^{f/f}$ *Cγ1*^{Cre} Fo and GC B cells in red and *Hvem*$^{+/+}$ *Cγ1*^{Cre} in blue. (F) *Hvem*$^{f/f}$ *Cγ1*^{Cre} and respective control CD45.2 mixed BM chimeras immunized with NP-CGG and analyzed day 10–13 for the frequency of CD45.2 cells in the Fo and GC compartments. Data are pooled from 3 experiments. *P<0.05, ***P<0.001, ****P<0.0001. Unpaired two-tailed Student's t test (B, F).

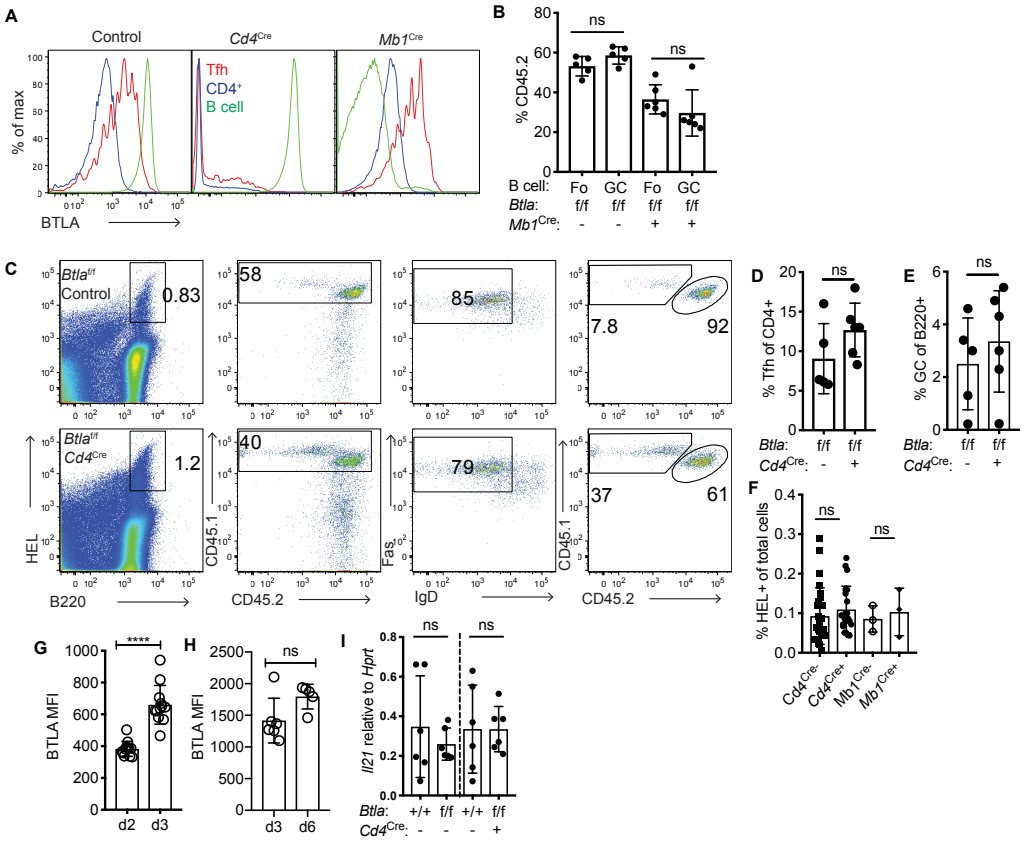

Figure S3. Conditional deletion of BTLA in T cells abrogates HVEM-deficient GC advantage. Related to Figure 4.

(A) BTLA MFI B220$^+$ B cells (green), CD4$^+$TCRβ$^+$CXCR5$^+$PD-1$^+$ Tfh cells (red), and CD4$^+$TCRβ$^+$CXCR5$^-$PD1$^-$ non-Tfh CD4$^+$ T cells (blue) in *Btla*$^{f/f}$ animals. Cre$^-$ left, *Cd4*^{Cre} middle, and *Mb1*^{Cre} right. (B) Contribution of CD45.2 *Btla*$^{f/f}$ control or BTLA-B cell-deficient *Btla*$^{f/f}$ *Mb1*^{Cre} CD45.2 cells to Fo and GC populations in spleen of mixed BM chimeras made with ~50% CD45.2 and ~50% WT CD45.1 BM at day 7 after SRBC immunization. Data are pooled from 2 experiments. (C) Representative flow cytometric analysis of the frequency of *Hvem*$^{-/-}$ CD45.1/2 HEL$^+$ GC B cells in *Btla*$^{f/f}$ control (top) and *Cd4*^{Cre} (bottom) recipients at day 6 after 2x-HEL-SRBC. (D) Frequency of Tfh cells of CD4$^+$ T cells in *Btla*$^{f/f}$ *Cd4*^{Cre} animals in the spleen after SRBC. Data are pooled from 2 experiments. (E) Frequency of GC B cells of B cells in *Btla*$^{f/f}$ *Cd4*^{Cre} animals in the spleen after SRBC. Data are pooled from 2 experiments. (F) Frequency of HEL$^+$ B cells of total splenocytes after Hy10 transfer and 2x-HEL-SRBC immunization. Data are pooled from 4 experiments. (G) BTLA MFI on OT-II T cells at 48 hr and 72 hr after HEL-OVA or DEL-OVA immunization. Data are pooled from 2 experiments. (H) BTLA MFI on Tfh cells at 3 days and 6 days after 2x-HEL-SRBC immunization. (I) *Il21* mRNA transcript relative to *Hprt* from sorted splenic Tfh cells from *Btla*$^{f/f}$ control CD45.2 or *Cd4*^{Cre} mixed CD45.1/2 WT BM chimeras at day 7 SRBC immunization. Data are pooled from 2 experiments. ****P<0.0001. Unpaired two-tailed Student's t test (B, D-I).

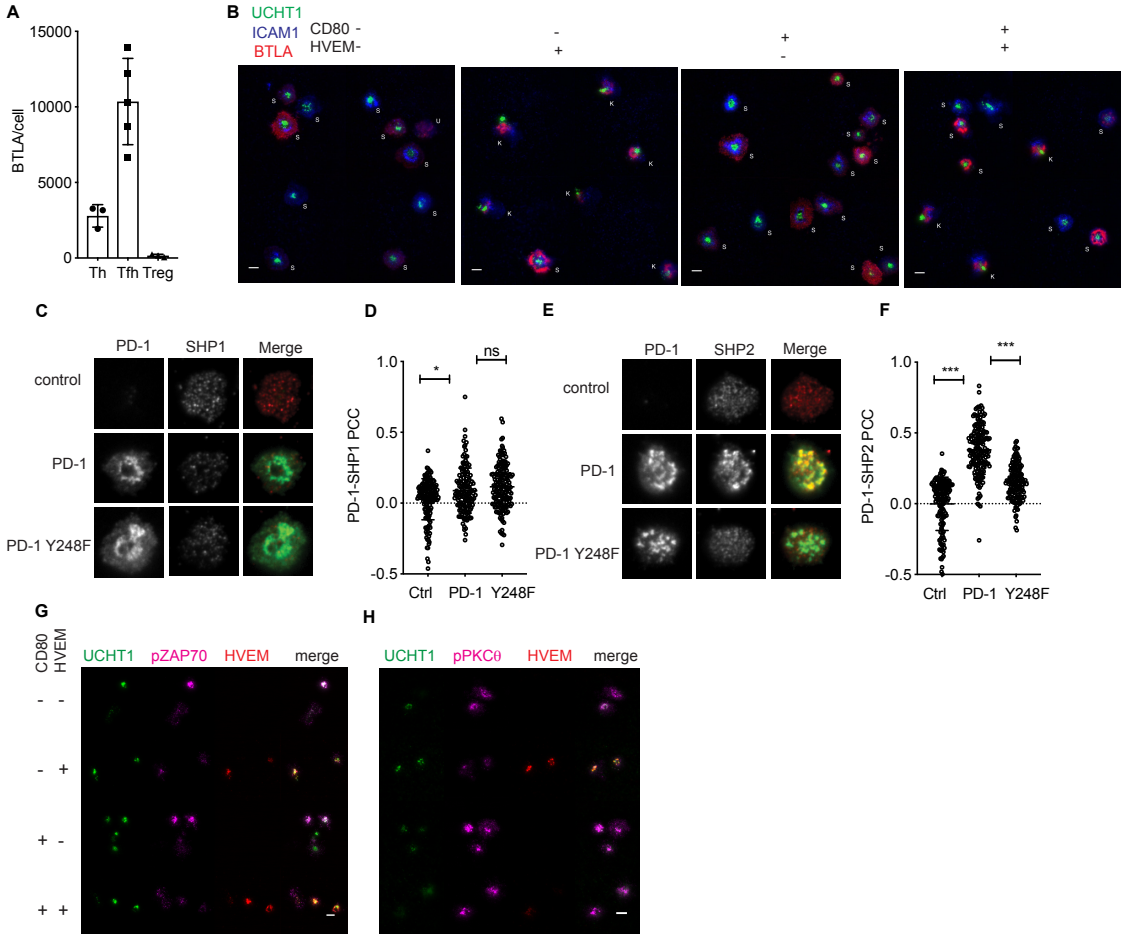

Figure S4. BTLA-HVEM at the immunological synapse recruits SHP1 to inhibit signaling in Tfh cells. Related to Figure 5.

(A) Expression of BTLA on human tonsil Tfh cells, Treg cells and untransfected CD4⁺ blasts (Th). (B) Representative images of synapse (s) or kinapse (k) states in BTLA-transfected human CD4⁺ T cell blasts on supported lipid bilayers containing anti-CD3 (UCHT1), ICAM1 and/or HVEM, CD80 as indicated. (C) Representative images of SHP1 recruitment to the synapse in relation to PD-1 or mutant PD-1 Y248F. (D) Quantification of SHP1 colocalization with WT PD-1 or mutant Y248F with or without (Ctrl) PDL-1 in the bilayer. (E) Representative images of SHP2 recruitment to the synapse in relation to PD-1 or mutant PD-1 Y248F. (F) Quantification of SHP2 colocalization with PD-1 or mutant Y248F with or without (Ctrl) PDL-1 in the bilayer. (G) Representative images of p-ZAP70 and (H) p-PKCθ in human CD4⁺ T cell blasts transfected with BTLA shown at the same LUT. Scale bars are 5 μm. *P<0.05, **P<0.01, ***<P0.001, ****P<0.0001. Mann-Whitney test (D, F.)

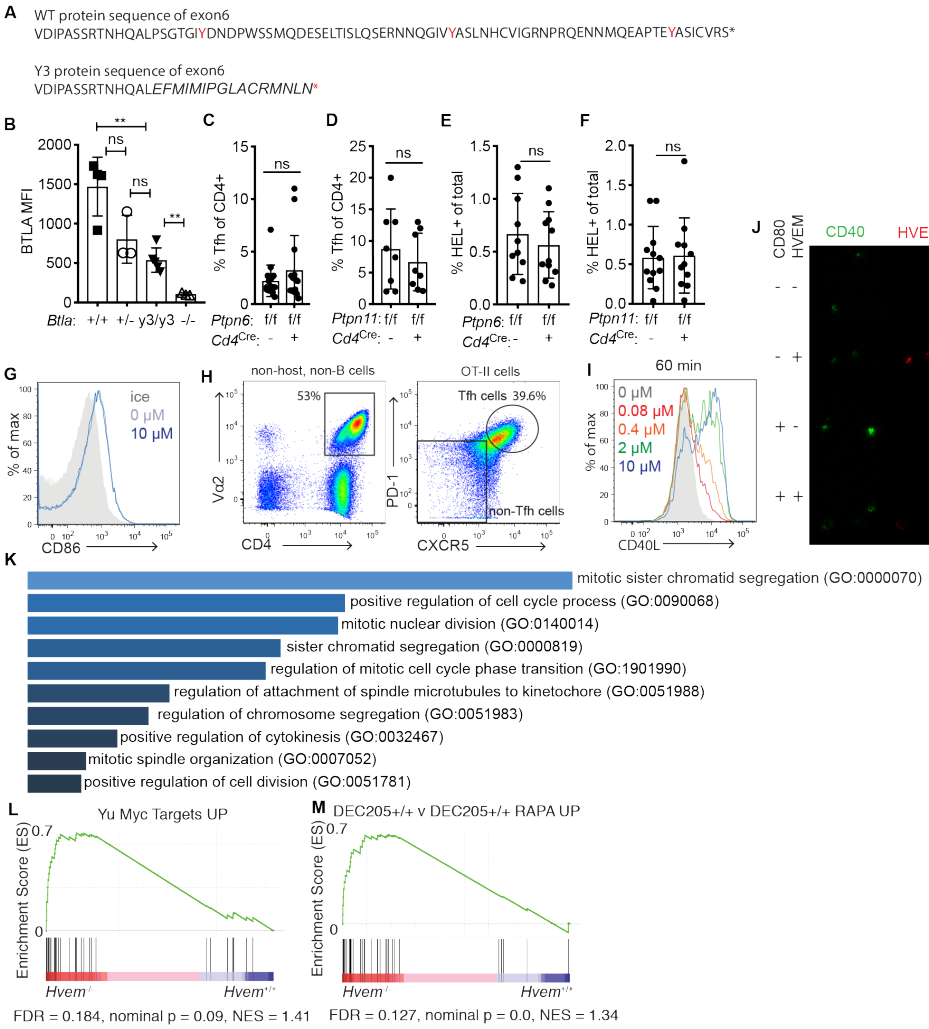

Figure S5. BTLA signaling into the T cell through SHP1 is required for HVEM-deficient GC B cell competitiveness. Related to Figure 6.

(A) Protein sequence of exon 6 of WT BTLA and mutant BTLA Y3. A short out-of-frame deletion was introduced at position 38 of exon 6 using CRISPR mutagenesis in the mouse embryo. Italics indicates nonsense sequence occurring after the deletion. * denotes stop codon. (B) BTLA expression on *Btla*$^{+/+}$, *Btla*$^{+/-}$, *Btla*$y^{3/y3}$, *Btla*$^{-/-}$ Tfh cells. Data pooled from 2 experiments. (C, D) Frequency of Tfh cells in *Ptpn6*$^{f/f}$ (SHP1) (C) and *Ptpn11*$^{f/f}$ (SHP2) (D) control and *Cd4*^{Cre} animals. Data pooled from 2 experiments. (E, F) Frequency of HEL^{+} cells in *Ptpn6*$^{f/f}$ (E) and *Ptpn11*$^{f/f}$ (F) control and *Cd4*^{Cre} animals. Data pooled from 2 experiments. (G) Representative flow cytometric analysis of CD86 surface expression on B cells after a 2 hr pulse with or without OVA peptide (10 μM) and incubation with OT-II Tfh cells for 30 min compared to B cells kept on ice directly ex vivo. (H) Gating strategy for OT-II Tfh cells at d3 after HEL-OVA-SRBC + poly-I:C. (I) Representative flow cytometric analysis of CD40L surface mobilization on OT-II Tfh cells after a 60 min incubation with B cells pulsed with a titration of OVA peptide (0-10 μM). (J) Representative images of CD40 recruitment to the immunological synapse with or without HVEM and CD80 present in the lipid bilayer after 15 min incubation with blasting human CD4^{+} T cells with standardized LUT across panels so fluorescence can be directly compared. Scale bars are 5 μm. (K) Gene ontology (GO) biological processes of genes significantly (padj <0.01) upregulated in *Hvem*$^{+/+}$ v *Hvem*$^{-/-}$ GC B cells at d11 after NP-CGG from RNA-sequencing through Enrichr. Sorted by p-value. (L) GSEA of differentially expressed genes from RNA-sequencing of *Hvem*$^{+/+}$ v *Hvem*$^{-/-}$ mixed BM chimeras at d11 of the NP-CGG alum response compared to Yu Myc targets UP gene set. (M) GSEA of differentially expressed genes from RNA-sequencing of *Hvem*$^{+/+}$ v *Hvem*$^{-/-}$ mixed BM chimeras at d11 of the NP-CGG alum response compared to significant genes (<0.01 padj) with >2 fold increased gene expression in DEC205-WT GC B cells 24 hr after anti-DEC205-OVA compared to DEC205-WT Rapamycin treated. *P<0.05, **P<0.01, ***<P0.001, ****P<0.0001. Unpaired two-tailed Student's test (B-F).

MATERIALS AND METHODS

Mice

Adult C57BL6 CD45.1 mice at least 7 weeks of age were from the National Cancer Institute. *Hvem* flox animals (JAX stock 030862) and *Hvem*-deficient animals (Seo et al., 2018) were used in most studies. In one experiment mixed chimeras were generated from a separate *Hvem*-deficient line (Wang et al., 2005). *Btla* flox animals have loxp sites flanking exons 4 and 5 of BTLA gene (J.-W.S., M.K. unpublished data). Full *Btla* deficient mice were from JAX stock 006353 (Watanabe et al., 2003). Other lines included *Ptpn6* flox (JAX stock 008336), *Ptpn11* flox (JAX stock 025758), *Bcl6* flox (JAX 023727), *Cγ1*-Cre (JAX stock 010611), *S1pr2*-ERT2Cre tdTomato Flox (Shinnakasu et al., 2016), *Mb1*-Cre (JAX stock 020505), *Cd4*-Cre (JAX stock 022071), Hy10 (Allen et al., 2007), OT-II (MGI 4836972), and *Rag2*-/- (JAX stock 008449), *Tcrb*-/- (JAX stock 002118), Eμ-BCL-2-tg (JAX stock 002319), and *Btla*-y3/y3 animals were generated and maintained in our laboratory. In most experiments, littermates were used as controls and experimental animals were co-caged in groups of 2-6 whenever possible. Male and female mice were used as both donors and recipients, except for OT-II animals, which required male donors. Animals were housed in specific pathogen free environment in the Laboratory Animal Research Center at UCSF and all experiments conformed to ethical principles and guidelines approved by the UCSF Institutional Animal Care and Use Committee.

Generation of BTLAY3 mice

Btla-y3/y3 animals were generated using crRNA1:TCATAAATTCCAGTTCCTGA targeting guide. The protocol followed Chen et al (Chen et al., 2016) with the main exception that the

standard square curve electroporation was performed twice with an interval of 3 seconds. RNP assembly followed standard protocol: 160 µM tracrRNA + 160 µM crRNA (Dharmacon), equal volume mix well 37°C, 30 min (80 µM sgRNA); 80 µM sgRNA + 40 µM Cas9 Protein equal volume, mix well 37°C 10 min (20 µM RNPs); leave on ice, each electroporation 10 µl of RNPs mix with 10 µl Opti-MEM with C57B6/J embryos. Standard electroporation: two pulses 30V for 3 ms interval 100 ms. Embryos were transferred into pseudo-pregnant females.

Bone marrow chimeras

WT CD45.1, *Rag2*-/-, or *Tcrb*-/- where indicated were lethally irradiated with 1,100 rads gamma-irradiation (split dose separated by 3 h) and then i.v. injected with relevant BM cells. BM was harvested by flushing the tibia and femurs. For T cell depletion (when necessary), 250 µg of anti-CD4 GK1.5 (BioXcell) was injected I.V. at day -1 and day 0.

Retroviral constructs and transductions

Murine HVEM and Bcl-2 retroviral constructs were made by inserting the mouse open reading frame into the MSCV2.2 retroviral vector followed by an internal ribosome entry site (IRES) and Thy1.1 as an expression marker. *Hvem* point mutations were introduced by quick-change PCR and *Hvem* truncation was introduced by PCR. Retrovirus was generated by transfecting PLAT-E packaging cell line with 10 µg plasmid DNA and 10 µg Lipofectamine 2000 (Fischer). For transduction of BM, WT, $Hvem^{-/-}$, or $Btla^{-/-}$ mice were injected I.V. with 3 mg 5-fluorouracil (Sigma). BM was collected after 4 d and cultured in DMEM containing 15% (vol/vol) FBS, antibiotics (penicillin (50 IU/ml) and streptomycin (50 µg/ml); Cellgro) and 10 mM HEPES, pH 7.2 (Cellgro), supplemented with IL-3, IL-6 and stem cell factor (at concentrations of 20, 50 and

100 ng/ml, respectively; Peprotech). Cells were 'spin-infected' twice at days 1 and 2 and were transferred into irradiated recipients on day 3.

Cell isolation, adoptive transfer

Spleens were macerated and resulting cell suspensions were filtered through a 70 µm mesh into PBS supplemented with 2% FCS and 1mM EDTA. Cells were counted on a hemocytometer and frequency of HEL+ Hy10 B cell was determined by staining of HEL-AlexaFluor647 (made using Invitrogen Alexa Fluor 647 antibody labeling kit) positive B cells on the flow cytometer. Mixes of *Hvem*$^{-/-}$ or *Hvem*$^{+/+}$ Hy10 and WT Hy10 congenically mismatched B cells were made at ratios of 1:4-1:1 as indicated in the figures. In some experiments OT-II T cells were co-transferred at a ratio of 1:5 Hy10 B cell as indicated in the figures. Mixtures of $5x10^4$-$2x10^5$ cells were transferred i.v. in a volume of 200 µl into the retroorbital venous sinus. To visualize cell proliferation, cells were labeled with Cell Trace violet (Invitrogen).

Immunizations

Hosts were immunized with an intermediate affinity mutant 2x-HEL (Paus et al., 2006) (Gift of R. Brink) conjugated to SRBC (Colorado Serum Company) (Yi and Cyster, 2013) intraperitoneally (i.p.). If Hy10 B cells were co-transferred with OT-II, hosts were immunized with 50 µg of HEL-OVA or DEL-OVA (Yi and Cyster, 2013) mixed 1:1 with Sigma Adjuvant System (SAS, previously Sigma RIBI adjuvant) for a total volume of 200 µl. Animals were immunized with 100 µg NP-(20-29)-CGG (Biosearch technologies) mixed with 1:1 Alum (Alhydrogel) for a total of 200 µl volume. $2x10^8$ SRBC (Colorado Serum Company) were injected in a volume of 300 µl. Tamoxifen (Sigma) was dissolved in Corn Oil (Sigma) at 20

mg/ml and injected at 2 mg/20g mouse i.p. TAM diet (Envigo) containing chow replaced normal chow when indicated.

Flow cytometry

Cells were stained on ice, in 96 round bottom plates in PBS supplements with 2% FBS and 1mM EDTA. The following antibodies were used: B220 APC-CY7 or BV785 (clone RA3-6B2), IgD FITC (clone 11-26c.2a), GL-7 Pacific Blue (clone GL7), FAS PE-CY7 (clone Jo2), CD38 AlexaFluor647 (clone 90), CD45.1 PERCP-CY5.5, APC (clone A20), CD45.2 BV605, APC-CY7 (clone 104), HVEM PE (clone LH1), BTLA AlexaFluor 647 (8F4), Ephrin-B1 Biotin (polyclonal, R&D), CXCR4 Biotin (clone 2B11/CXCR4), CD86 AlexaFluor647 (clone GL-1), IgG1 FITC (clone RMG1-1), CD138 BV421 (clone 281-2), CD73 PERCP-CY5.5 (clone TY/11.8), CD4 PE-CY7 (clone GK1.5), TCRβ Pacific Blue (clone H57-597), CXCR5 BV605 (clone L138D7), PD-1 PE or FITC (clone 29F.1A12), CD40L PE (clone MR1), Vα2 PERCP-CY5.5 (clone B20.1), Active caspase-3 (clone C92-605), Fixable viability dye eFluor780 (eBioscience). NP-47-PE (Biosearch technologies). For intracellular staining, cells were fixed and permeabilized using BD Cytofix/Cytoperm kit. EdU detection was with Click-IT Plus EdU kit (Invitrogen). Data were collected on a BD LSRII and analyzed on FlowJo Software.

qPCR and RNA-sequencing

Hvem primers F: GGAGCTGGGATAGCTGGATTC R: TCTCCTGTTGTTCCTGGAAAGG, *Il21* primers F: GCTCCACAAGATGTAAAGGG R: TTATTGTTTCCAGGGTTTGA. Cells were sorted using BD FACS ARAII. 10^4 cells or greater were sorted for qPCR and $5x10^4$ cells were sorted for RNA-sequencing. RNA sequencing was prepared using Ovation RNA-seq

System V2 from Nugen, KAPA Hyper prep labeling kit, NEXTflex DNA barcodes Adapter kit from Bioo Scientific. 100 bp paired end was run on HiSeq4000 at UCSF Institute for Human Genetics. Data was run through STAR alignment and Deseq2.

GSEA and Gene Ontology

GSEA analysis (v3.0) through the BROAD was performed using standard settings: 1000 number of permutations, collapsed data to gene symbols, permutation type phenotype, enrichment statistic weighted. Data for Rapamycin sensitive DEC205-WT GC B cell genes was accessed (Ersching et al., 2017) and significant genes, defined as padj <0.01 with >2 fold increased in untreated v. Rapa treated, were made into a manually curated gene list. Yu Myc targets UP was a premade GSEA gene list. Gene ontology was performed using Enrichr platform (Kuleshov et al., 2016).

NP V_H186.2 mutation analysis

For bulk GC sequencing- PCR reaction 1. PCR1 For primer: CATGGGATGGAGCTGTATCATGC Rev primer: CTCACAAGAGTCCGATAGACCCTG PCR2 (nested) For primer: GGTGACAATGACATCCACTTTGC Rev primer: GACTGTGAGAGTGGTGCCTTG and the blunt end cloned into TOPO vector. Plates were sent to TacGen for plasmid prep and Sanger sequencing (Bannard et al., 2016). For single cell sequencing- NP^+ cells were sorted into lysis buffer and frozen in 96U bottom plates. Nested PCR with primers and sent for sequencing. 186-EF: GTATCATGCTCTTCTTGGCAGC 186-IF: ACAGTAGCAGGCTTGAGGTCTG 186-IR: CCCAATGACCCTTTCTGACTC 186-ER:

TGAGGATGTCTGTCTGCGTCA (Yang et al., 2012). Data was analyzed using IgBLAST and the frequency of W33L were counted in non-frame shifted IGHV1-72*01 sequences.

Tfh cell CD40L surface mobilization

Tfh cells were generated by transferring OT-II into WT mice on day -1 and immunizing retro-orbitally with 2 x 10^8 SRBCs (Colorado Serum Company) conjugated to 10 μg (0.85 mg/mL) HEL-OVA and mixed with 150 μg (1mg/mL) poly I:C (GE Healthcare) pre-heated for 10 min at 60ºC in a total volume of 350 μL on day 0. On day 3, spleens were harvested and $CD4^+$ T cells were isolated through negative selection by depletion with anti-CD8a biotin, anti-CD11c biotin, and anti-CD19 biotin antibodies and EasySep Mouse Streptavidin RapidSpheres (Stemcell) in complete RPMI. For B cells, spleens were harvested from WT or *Hvem*$^{-/-}$ mice. Splenocytes were CTV labeled at 0.5 μM and pulsed with 10 μM, 2 μM, 0.4 μM, or 0.08 μM OVA 323-339 peptide (GenScript) antigen or no antigen for 2 h at 37°C. The splenocytes were all washed three times and 8 x 10^5 splenocytes were combined with 4 x 10^5 $CD4^+$ T cells in a 96-well round bottom plate. To facilitate detection of surface exposed CD40L the cells were incubated in the presence of 1 μg/ml anti-CD40L PE antibody as previously described (Gardell and Parker, 2016; Koguchi et al., 2007). After 30 or 60 min incubation at 37°C, T cells were harvested, stained, and analyzed on the LSRII flow cytometer. Anti-CD11c biotin antibody and EasySep Mouse Streptavidin RapidSpheres (Stemcell) were used to deplete dendritic cells in two experiments with no differing results.

Assessment of BCR clonality by PCR

Assessment of clonality by PCR of J558 heavy chain, and κ light chains from genomic DNA from $2x10^4$ FACS sorted GC B cells from 8 week old *Btla*$^{f/f}$ *Cd4*^{Cre} and *Btla*$^{f/f}$ control chimeras (Cobaleda et al., 2007; Muppidi et al., 2014). Primers:

V_HJ558 CGAGCTCTCCARCACAGCCTWCATGCARCTCARC,

J_H4 CGAGCTCTCCARCACAGCCTWCATGCARCTCARC,

V_κ GGCTGCAGSTTCAGTGGCAGTGGRTCWGGRAC,

J_κ5 GGCTGCAGSTTCAGTGGCAGTGGRTCWGGRAC.

Human CD4$^+$ T cell isolation, stimulation, and transfection

Primary human CD4$^+$ T cells were isolated using the RosetteSep Human CD4$^+$ T Cell Enrichment Cocktail (StemCell Technologies) as per the manufacturer's instructions from leukocyte cones provided by UK National Health Service Blood and Transplant. Isolated cells were cultured in RPMI-1640 supplemented with 10% FCS, 4 mM L-glutamine, 10 mM HEPES, 1% non-essential amino acid solution (Gibco), and 1% penicillin-streptomycin solution (Gibco) at 37°C, 5% CO_2 for between 24 and 72 h before stimulating. Cells were diluted to $1x10^6$/ml in supplemented RPMI-1640 containing 50 U/ml recombinant IL-2 (PeproTech) and anti-human CD3/CD28 Dynabeads (Gibco) at $1x10^6$/ml. Cells were cultured for 3 days before the beads were removed by magnetic separation and the medium replaced with fresh supplemented RPMI-1640 + 50 U/ml IL-2. Cells were cultured for a further 4 days with medium replaced and cells diluted to $1x10^6$/ml as required.

Human BTLA was cloned into pGEM-SnapTag vector. This vector was used to produce mRNA

in vitro using the mMESSAGE mMACHINE T7 Transcription Kit (Thermo Fisher Scientific) as per the manufacturer's instructions. Transfection was performed 24 h before imaging. Cells were washed 3 times with OptiMEM (Gibco) at room temperature and resuspended at $2.5x10^6$ cells/100 µl. 2.5 – 7.5 µg mRNA encoding WT or mutant BTLA-SNAP-tag was added to $2.5x10^6$ cells, which were gently mixed, transferred to a Gene Pulser cuvette (BioRad) and pulsed for 2 ms at 300 V in an ECM 830 Square Wave Electroporation System (BTX). Cells were then immediately transferred to supplemented RPMI-1640 at $1x10^6$/ml and cultured for 24 h. The amount of mRNA used was optimized for each T cell donor and mRNA preparation by performing multiple transfections with titrated mRNA amounts, then assessing total BTLA expression after 24 h by staining with AlexaFluor 647-conjugated anti-BTLA (BioLegend, 344520) and comparing to Quantum AlexaFluor 647 MESF calibration beads (Bangs Laboratories) by flow cytometry. Conditions giving ~10,000 transfected BTLA/cell were selected for imaging.

Human Tfh cell isolation

Human Tfh cells were isolated from tonsils provided by UK National Health Service Blood and Transplant. Tissue was kept on ice prior to use and processed within 3 h of surgery. Tonsils were washed in ice-cold Hank's balanced salt solution (HBSS; Gibco) supplemented with 2% FCS, 5% penicillin-streptomycin solution (Gibco), and 500 µg/ml normocin (Invivogen). Whole tonsils were partially submerged in cold, supplemented HBSS and dissected into pieces 1-5mm in size using a sterile scalpel. Tissue fragments were separated into multiple 70 µm cell strainers and crushed using a 20 ml syringe plunger, then washed with cold, supplemented HBSS. Strained samples were pooled and passed through a 40 µm cell strainer then pelleted at 400 g for

10 min and resuspended in 15 ml cold, supplemented HBSS. Peripheral blood mononuclear cells (PBMCs) were isolated by Ficoll-Paque density gradient centrifugation. Total $CD4^+$ T cells were isolated from the PBMC fraction using the EasySep $CD4^+$ isolation kit (StemCell Technologies) and kept on ice in supplemented HBSS. Cells were immediately stained with anti-CXCR5 conjugated to either AlexaFluor 488 (BD Biosciences, 558112) or PE/Cy7 (BioLegend, 356923) depending on the downstream application, washed, and the $CXCR5^{high}$ population sorted using a FACSAria III cell sorter (BD Biosciences). Isolated Tfh cells were resuspended at $5x10^6$/ml in supplemented RPMI-1640 and cultured for 3 h at 37°C, 5% CO_2 before being used for imaging. A small number of cells were retained and stained with anti-CXCR5 and anti-PD1 conjugated to AlexaFluor 488 (BioLegend, 329935) or AlexaFluor 647 (BioLegend, 329910), washed, and analysed by flow cytometry to confirm the purity of the $CXCR5^{high}$ $PD1^+$ population.

Quantification of BTLA and HVEM surface expression

Isolated whole $CD4^+$ populations or isolated Tfh cells were stained with with AlexaFluor 647-conjugated anti-BTLA (BioLegend, 344520) and compared to Quantum AlexaFluor 647 MESF calibration beads (Bangs Laboratories) by flow cytometry. HVEM levels on B cells were determined by staining PBMCs from whole blood with anti-CD19-PE-Cy7 (BD Biosciences; 560911), anti-CD38-AlexaFluor 488 (BioLegend; 303511), anti-CD27-BrilliantViolet421 (BioLegend; 356417), anti-CD20-PE (BioLegend; 302305), and anti-HVEM-AlexaFluor 647 (BD Biosciences; 564411). B cell subsets were gated as follows: Activated (CD19+ CD20+ CD27+ CD38+), Memory (CD19+ CD20+ CD27+ CD38-), immature/transitional (CD19+ CD20+ CD27- CD38+), and plasmablasts (CD19+ CD20- CD27+ CD38+). HVEM intensity on each cell subset was converted to absolute protein numbers by reference to Quantum AlexaFluor 647 MESF calibration beads (Bangs Laboratories). Based on the mean HVEM expression on

activated B cells of ~35,000/cell, minimum surface density was estimated at ~35 molecules/μm^2 assuming an upper limit of ~1000 μm^2 total area.

Supported lipid bilayer preparation and use

Supported lipid bilayers (SLB) were prepared as described previously (Choudhuri et al., 2014). Briefly, micelles of 1,2-dioleoyl-sn-glycero-3-phosphocholine (Avanti Polar Lipids Inc.) supplemented with 12.5% 1,2-dioleoyl-sn-glycero-3-[(N-(5-amino-1-carboxypentyl) iminodiacetic acid) succinyl]-Ni (Avanti Polar Lipids Inc.) were flowed onto glass coverslips hydroxylated with piranha solution, plasma cleaned, and affixed with adhesive 6-lane chambers (Ibidi). SLBs were blocked and washed, then incubated with recombinant His-tagged proteins of interest (produced in-house with the exception of HVEM-Fc-His, which was a gift from Prof. Simon Davis, University of Oxford) at the requisite concentrations to achieve the desired density: 30 molecules/μm^2 for UCHT1-FaB, 200 molecules/μm^2 for ICAM1, 100 molecules/μm^2 for CD80, 35 molecules/μm^2 for HVEM-Fc-His, and 100 molecules/μm^2 for CD40. The specific combination of unconjugated proteins or proteins conjugated to different dyes (AlexaFluors 405, 488, 568, and 657) was varied to suit the demands of each experiment. Within 2 h of preparation, SLBs were pre-warmed to 37°C and cells were infused into the SLB chambers at ~$5x10^5$/lane for $CD4^+$ cells or ~$1x10^5$/lane for Tfh cells. Samples were either incubated for 3 or 15 min at 37°C then fixed with warm 4% para-formaldehyde in PHEM buffer (60 mM PIPES, 25 mM HEPES, 10 mM EGTA, 2 mM $MgCl_2$, pH 6.9) for 10 min, or imaged live. In experiments involving labelling of transfected BTLA-SNAP-tag, cells were incubated with 0.5 µM SNAP-Cell 647-SiR ligand (New England BioLabs) in supplemented RPMI-1640 for 30 min at 37°C, washed 3 times, and incubated for a further 30 min prior to addition to SLBs.

Immunofluorescence staining

Fixed cell samples were exposed to a second round of fixation in PHEM buffer with 2% PFA and 3% BSA (bovine serum albumin) for 10 min at room temperature in order to reduce non-specific adsorption of probing antibodies to the coverslip. Samples were washed 3 times with PHEM buffer, permeabilised with 0.1% saponin in PHEM buffer for 15 min, then washed 3 more times with PHEM buffer. Samples were then quenched with 100mM glycine for 20 min and blocked with 6% BSA in PHEM buffer for 1 h before washing 3 times with PHEM buffer. Samples were then incubated with the appropriate primary rabbit antibody (anti-SHP1, Santa Cruz Biotechnology, sc-287; anti-SHP2, Santa Cruz Biotechnology, sc-280; anti-pY493 ZAP70, Cell Signaling Technology, 2704; anti-pT538 PKCθ, Cell Signaling Technology, 9377) in PHEM buffer with 0.02% saponin, 3% BSA for 1 h. Washing was performed 3 times with PHEM buffer, 0.1% saponin, 3% BSA with 2 min between each wash, before incubating with goat anti-rabbit F(ab')2 conjugated to AlexaFluor 568 (ThermoFisher Scientific, A-21069) in PHEM buffer with 0.02% saponin, 3% BSA for 45 min. Samples were finally washed 5 times with PHEM buffer, 0.1% saponin, 3% BSA with 2 min between each wash before imaging. A sample stained using only secondary antibody was included in each experiment as a background control.

TIRF and confocal imaging

TIRF imaging was performed on an Olympus cellTIRF-4Line system using a 150x (NA 1.45) oil objective. Imaging of live samples was performed at 37°C, and of fixed samples at room temperature. Confocal imaging was performed on a 37°C-controlled Olympus FV1200 confocal microscope using a 20x (NA 0.75) air objective.

Image analysis

All image analysis was performed using the ImageJ software. Thresholded IRM images were used to define the contact area of each cell, and all pixels therein used to calculate the mean fluorescence intensity (MFI) for a given channel. Pearson colocalization coefficients (PCCs) were also calculated only for IRM-defined contact areas using the Coloc 2 plugin to perform pixel intensity correlation between channels. Identification and tracking of cells for comparison of adhesion and movement was performed using the TrackMate plugin, with total cells detected from bright field images and those forming contacts identified through IRM images. Cells were qualitatively assigned as forming synapses or kinapses based on the relative centrality and symmetry of the predominant UCHT1 and ICAM1 signals. Synapses were defined as having approximately central UCHT1 accumulations completely surrounded by a ring of ICAM1; kinapses as having a highly polarized UCHT1 accumulation with ICAM1 adjacent but not surrounding. Cells not fitting either category were defined as unassigned.

In-situ analysis of interaction of SHP1 and SHP2 with PD-1

Supported lipid bilayers presenting relevant ligands were prepared as described above. Biotin-CAP-phosphatidylethanolamine was used at a 0.04 molar percentage to that of dioleoylphosphatidylcholine (DOPC). Monobiotinylated Okt3 (anti-CD3 antibody, from Ebiosciences) was used at 0.5 µg/ml. The following ligands were presented on the bilayer by means of coordination chemistry between DOGS-NTA and poly-Histidine tag: 12x-His ICAM1 ectodomain at ~200 molecules/µm2; 12x-His CD58 ectodomain at ~300 molecules/μm^2; and 12x-His PDL1 ectodomain at ~300 molecules/μm^2. Freshly isolated human CD8 T cells were electroporated with mRNA encoding PD-1 GFP or PD-1 Y248F GFP and cultured for ~8 h

(Zhao et al., 2005). Cells were introduced into the flow-cells containing lipid bilayers at 37 °C and fixed after 10 min by flowing in pre-warmed 2% EM-grade formic acid in PBS. SHP1/2 staining was performed as described above. Images were acquired on a Nikon Eclipse Ti inverted fluorescence microscope using an Apo TIRF 100x 1.49 NA oil objective. Diode lasers (488 nm, 561 nm and 641 nm, from Coherent) were used for TIRF illumination at the plane of bilayer. An AOTF (from Solamere Technologies) was used for choosing appropriate excitation wavelengths. A xenon arc lamp (from Newport) filtered at 490nm was used for reflection imaging of cell contacts with the bilayer. Nikon perfect focus system® was used to achieve consistent illumination and also to compensate for axial chromatic aberration. NIS-Elements software (from Nikon) was used for hardware control of the microscope, filter and shutter wheels, AOTF, and the EMCCD camera (Andor DU-897 X-4654) during image acquisition. EMCCD camera was operated in the normal gain mode and well under saturation. Custom written macros were used for automated image analysis in ImageJ 1.44o (from NIH). Cell-boundaries were defined based on segmented ('Default' algorithm in ImageJ) reflection images. Back-ground subtracted images were used for calculating average fluorescence intensity from each cell. Pearson Cross-correlation Coefficient (PCC) values between thresholded green and far-red channels ('MaxEntropy' algorithm in ImageJ) were calculated for each cell to quantitatively measure the extent of colocalization. Cluster statistics were computed using the 'Analyze Particles' routine in ImageJ after thresholding the images using the 'MaxEntropy' algorithm. Statistical significance was assessed by Mann-Whitney test using the GraphPad Prism5 software.

Quantification and statistical analysis

All statistical tests were done with GraphPad Prism software. The appropriate statistical test for each experiment is noted in the figures.

Data availability

Raw and processed data files for RNA sequencing analysis have been deposited in the NCBI Gene Expression Omnibus under accession number GSE130095.

Acknowledgements

We thank C. Allen, J. Bluestone, J. Rubenstein for mice, S. Davis for HVEM-Fc-His and 6x-His PDL1, K. Wucherpfennig for 10x-His-CD58, R. Brink for 2x-HEL, N. Strauli for assistance running MIXCR, D. Parker and J. Gardell for advise on detecting CD40L, E. Dang, E. Lu and A. Reboldi for helpful discussions, and M. Meyer-Hermann, O. Bannard and J. Muppidi for helpful discussions and critical reading of the manuscript. M.A.M. was supported by 5F30AI131496-02, J.G.C. is a HHMI Investigator. J.H.F. is a Wellcome Trust Sir Henry Wellcome Fellow (107375/Z/15/Z), M.L.D is a Wellcome Trust Principal Research Fellow (100262Z/12/Z), A.M. holds a Career Award for Medical Scientists from the Burroughs Wellcome Fund, is an investigator at the Chan Zuckerberg Biohub, a PICI investigator, and has received funding from IGI. This work was supported in part by NIH grant R01 AI045073 (J.G.C), a European Research Council Advanced Grant ERC-2014-AdG_670930 (M.L.D), NIH P01 DK46763 (M.K).

Author Contributions: M.A.M. and J.G.C. conceptualized the project, designed the experiments, interpreted the results and wrote the manuscript. M.A.M performed the

experiments. J.H.F., V.M. and M.L.D. designed and performed the lipid bilayer experiments, interpreted the results and helped prepare the manuscript. M.Y.C. performed CD40L induction studies, interpreted data and helped prepare the manuscript. Y.X. performed molecular biology experiments. J.A. genotyped mice. Z.L. and A.M. generated the BTLA Y3 mutant mouse line. T.O., J-W.S., C.F.W. and M.K. provided gene targeted mouse lines and provided input on the manuscript.

Declaration of interests

A.M. is a co-founder of Arsenal Biosciences, Spotlight Therapeutics and Sonoma Biotherapeutics. A.M. serves as on the scientific advisory board of PACT Pharma and was a former advisor to Juno Therapeutics. The Marson Laboratory has received sponsored research support from Juno Therapeutics, Epinomics, Sanofi and a gift from Gilead. J.G.C. is on the SAB of ALX Oncology Ltd and is a consultant for Corvus Pharmaceuticals.

CHAPTER 3: CONCLUSION

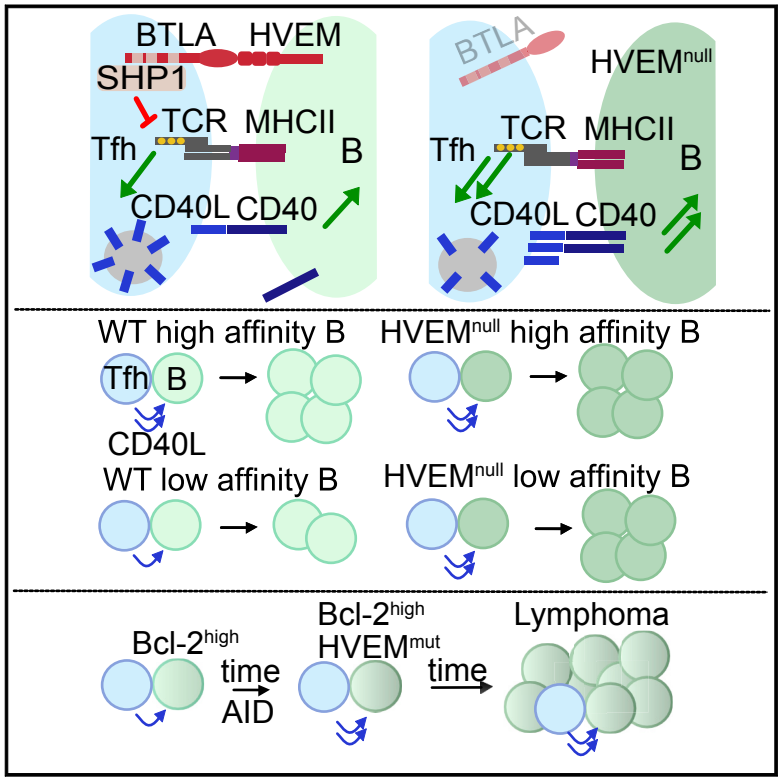

Figure 3.1. Model
(Top) HVEM-expressing GC B cell recruits BTLA to immunological synapse. BTLA signals into Tfh cell through SHP1, which inhibits the strength of TCR signal and amount of preformed CD40L mobilized to the cell surface. In the absence of HVEM, BTLA is not recruited to the immune synapse and the amount of preformed CD40L mobilized to the surface is increased. The HVEM-deficient B cell receives increased CD40 signaling. **(Middle)** When a high affinity B cell presents antigen to a Tfh cell, it receives stronger helper signals compared to a low affinity B cell. However, when a HVEM-deficient low affinity B cell presents antigens it receives helper signals more similar to a high affinity B cell. **(Bottom)** Bcl-2 overexpressing B cells encounter antigen and enter the GC. Over time and accumulating AID-induced mutations, HVEM is mutated and the HVEM-deficient Bcl-2-high GC B cells receive more T cell helper cues that in combination with their enhanced survival lead to lymphomagenesis.

In this study, we aimed to show how HVEM regulates the GC B cell response in mice (Fig. 3.1). We found that HVEM is an intrinsic negative regulator of GC B cell responses. HVEM engages BTLA in *trans* on the T cell. BTLA recruits SHP1 which negatively regulates T cell signaling and the amount of preformed CD40L mobilized to the surface of the Tfh cell.

Thus, the HVEM-deficient GC B cell receives stronger CD40 signals when BTLA is not recruited to the immune interface.

While *Tnfrsf14* transcripts are expressed at similar levels in naïve and GC B cells in mouse, HVEM surface protein is reduced on GC B cells (Mintz et al., 2019). A similar pattern of HVEM mRNA and protein expression is evident in human follicular and GC B cells (Duhen et al., 2004)(unpublished observations). A study of FL has confirmed the specificity of this low-level staining by identifying some cases that are surface positive and others (most likely HVEM mutant) that are surface negative (Kotsiou et al., 2016). The apparent post-transcriptional downregulation of HVEM in GC B cells suggests these cells need to have tight control of HVEM protein abundance. However, what regulates HVEM protein expression in GC B cells remains unknown and is an area that merits future investigation.

Using a mixed chimeric mouse system, HVEM-deficiency was found to provide B cells with a competitive advantage in the GC compared to the follicular compartment (Mintz et al., 2019). HVEM haploinsufficiency provided GC B cells with an intermediate advantage, suggesting that the amount of HVEM expressed on the B cell regulates competitiveness. HVEM-deficient B cells showed a competitive advantage at both the pre-GC and GC stages (Mintz et al., 2019). HVEM-deficiency led to a small increase in the frequency of pre-GC and GC B cells entering into the cell cycle, providing at least a partial explanation for their increased representation. Following immunization with an NP-haptenated protein, HVEM-deficient GC B cells showed preferential expansion of the non-NP binding relative to the NP-binding B cells. Since the NP-binding cells tend to rapidly achieve high affinity, these data suggested HVEM-deficient B cells with lower affinity were being preferentially selected. In additional support for this model, HVEM-deficient NP-specific GC B cells had reduced high affinity W33L mutations

compared to HVEM-expressing competitors in the same mice. Comparison with W33L mutation frequencies in control chimeras suggested that the most prominent effect was an increased stringency of selection for W33L mutations in wild-type cells that were in competition with HVEM-deficient cells. One model to explain these observations is that the wild-type GC B cells needed to acquire more antigen through a higher affinity BCR in order to receive competitive T helper cell positive selection signals. These data are similar to what was observed in chimeric PD-L1-deficient GCs, where PD-L1-deficient GC B cells were preferentially expanded amongst the non-NP binding cells and had reduced high affinity mutations (Shi et al., 2018). While the data together suggest that negative regulators maintain the stringency of Tfh cell selection of GC B cells, the PD-L1 study did not observe an increase in high affinity mutations in the PD-L1-expressing GC B cells competing with the PD-L1 deficient GC B cells, suggesting that these regulatory molecules do not act in an identical manner.

Using gain and loss of function approaches, we demonstrated that the growth restraining actions of HVEM in GC B cells depended on BTLA expression by T cells (Mintz et al., 2019). Although BTLA is highly expressed in B cells and HVEM–BTLA have been shown to engage in *cis* interactions in HEK-293t cells (Cheung et al., 2009a; Watanabe et al., 2003), BTLA-deficient B cells were not over-represented in GCs, suggesting BTLA is not acting in *cis* to regulate B cell responses (Mintz et al., 2019). HVEM-BTLA *cis*-interactions were presented to explain Boice et al.'s finding that sh-RNA targeting of *Btla* phenocopied the increased GC lymphomagenesis seen in *Tnfrsf14*-targeted Vav-Bcl-2 BM chimeras (Boice et al., 2016; Huet et al., 2018; Verdière et al., 2018). The authors, however, did not report a preferential enrichment of BTLA-knock-down cells in the B cell compartment as they did for HVEM-knockdown cells. We reconcile the findings by noting that the global hematopoietic shRNA knockdown approach would be

expected to reduce BTLA in Tfh cells as well as in B cells. In accord with the model that BTLA acts in *trans*, no mutations have been reported in the coding region of BTLA in B cell lymphomas. It has been suggested that BTLA expression is lost in a significant fraction of FLs through epigenetic regulation of KMT2D methylation (Boice et al., 2016), and an additional report observed a diversity of BTLA expression in FL samples (Carreras et al., 2019). Further work will be needed to understand if heterogeneity of human BTLA expression in the GC and follicular B cell compartments is relevant to lymphomagenesis.

Early evidence that HVEM mutations may be enhancing the ability of FL cells to present antigen to T cells came from the observation that FL patients with BM transplantation had increased rates of graft versus host disease (Kotsiou et al., 2016). Using FL cells as antigen presenting cells in allogeneic mixed lymphocyte reactions, they found HVEM-mutated FL cells induced more division in both $CD4^+$ and $CD8^+$ T cells than HVEM-expressing FL cells. When HVEM-expressing FL cells were incubated with a BTLA antagonist both allogeneic $CD4^+$ and $CD8^+$ T cell proliferation increased, while the antagonist had no effect on the response elicited by HVEM-mutated FL cells. These findings suggest that HVEM on FL cells inhibits signaling in allogeneic T cells through engagement of BTLA (Kotsiou et al., 2016).

Planar lipid bilayer imaging of human T cells showed co-localization of SHP1 with BTLA that was largely reversed when BTLA's ITIM/ITSM motif was mutated; BTLA did not colocalize with SHP2 (Mintz et al., 2019). These results have been supported by two independent studies finding BTLA preferentially recruits SHP1 in mouse $CD4^+$ T cells (Celis-Gutierrez et al., 2019). In addition to its ability to directly dephosphorylate CD3-zeta, BTLA inhibited phosphorylation of ZAP-70 and PKC-theta in human Tfh cells. Analysis of mice homozygous for a cytoplasmic domain mutant of BTLA that lacks all three tyrosines including

its SHP1 recruiting ITIM/ITSM motif, confirmed that BTLA reverse signaling was required for HVEM function in B cells. These data suggest that HVEM-expressing cells are selected through *trans* signaling into BTLA expressing Tfh cells during cell-cell contacts. Experiments in mice lacking SHP1 or SHP2 in T cells further supported the conclusion that BTLA signaling via SHP1 into the Tfh cell modulates the amount of help provided to HVEM-expressing B cells (Mintz et al., 2019).

While early T cell-B cell interactions can last for an hour, in the GC the majority of interactions take place on the range of minutes. Based on finding that HVEM-deficiency led to an intrinsic growth advantage in B cells, it was inferred that HVEM-deficient B cells must receive greater help than their wild-type counterparts during these brief interactions. CD40L is the main helper factor known to be preformed in Tfh cells. When Tfh cells were exposed in vitro to B cells presenting increasing amounts of MHC-peptide complexes, an analog upregulation of CD40L was observed (Mintz et al., 2019), indicating that the extent of mobilization of preformed CD40L to the Tfh cell surface is tuned to the TCR signal strength. In accord with this notion, HVEM-deficient B cells induced greater CD40L surface mobilization in Tfh cells when compared to HVEM-expressing B cells displaying the same amount of MHC-peptide. Furthermore, CD40 recruitment to the immune synapse was decreased when HVEM was included in lipid bilayers, suggesting that CD40L mobilization to the synapse is reduced by HVEM-BTLA interactions. While these data do not rule out additional factors that HVEM-BTLA may be regulating, such as cytokines, they suggest that BTLA inhibits Tfh cell help by restraining the amount of CD40 signals delivered to GC B cells. In further support of this model, HVEM-deficient GC B cells competing with wild-type GC B cells exhibited an increased Myc gene signature (Mintz et al., 2019).

In planar lipid bilayer studies, the presence of HVEM in the bilayer transformed the stable, centered immune synapse into a motile, polarized kinapse structure (Mintz et al., 2019). These results suggested that BTLA inhibits strong contacts with HVEM-expressing cells. Surprisingly, 2-photon microscopy-based imaging of Tfh cells interacting with HVEM-deficient and wild-type GC B cells in intact lymph nodes did not reveal differences in the time of contact or surface area of interactions (unpublished observations). Further work is needed to determine if there are differences in interaction stability early versus late in the GC response.

In models of Bcl-2-overexpression, HVEM-deficiency continued to provide GC B cells with an advantage and it led to accelerated lymphomagenesis, suggesting that HVEM deficiency was acting in a separate pathway from Bcl-2 (Boice et al., 2016). Overexpression of Bcl-2 in mice lacking BTLA in T cells led to similar pre-malignant outgrowths as occurred in HVEM-deficient Bcl-2 over-expressing Bcl-2 mice. These data provide some of the first evidence of a cell-extrinsic tumor suppressor distinct from the mechanism of $CD8^+$ and NK cell immune surveillance. The ways in which increased signaling via CD40 and other T cell-derived helper factors cooperates with Bcl-2-overexpression in lymphoma development remains to be fully elucidated.

Given HVEM's complex signaling biology and the expression of several of HVEM's ligands on cells in immune microenvironments, it remains to be determined if loss of HVEM in GC-derived lymphomas alters parameters in addition to the BTLA-HVEM axis. While a third of *TNFRSF14* mutations are truncating, the remaining two-thirds may still preserve HVEM protein expression but alter its ability to engage ligands. For instance, HVEM-Y61A, a mutation that disrupts binding to BTLA and CD160, is found in FL patients. In particular, it will be interesting to learn if loss of HVEM or particular mutations alter FL cell interactions with CD160

expressing cytotoxic $CD8^+$ T cells or NK cells and immune surveillance in the tumor microenvironment. It will also be interesting to learn if LIGHT engages with HVEM on B cells to determine GC B cell outcomes, and if HVEM can signal into the B cell. Lastly, given BTLA's high expression on B cells it will be important to better understand if the ability of this molecule to negatively regulate BCR signaling is relevant to lymphomagenesis or other B cell-mediated diseases.

The HVEM—BTLA axis may be a regulatory pathway suppressing Tfh cell lymphomas. Interestingly, high expression of BTLA correlated with a positive clinical outcomes in AITL through RNA sequencing of the entire tumor (Iqbal et al., 2010). We hypothesize that the high levels of BTLA mRNA could be maintained on the Tfh cells to inhibit TCR signaling strength when interacting with HVEM-expressing B cells, thereby limiting tumor growth. In accord with this logic, a *TNFRSF14* mutation has been found in one AITL sample in which the entire tumor was sequenced (Cannons et al., 2010). These data raise the possibility that loss of HVEM in B cells in the tumor environment could be driving Tfh cell outgrowth. Interestingly, AITL cells continue to express high levels of PD-1 (Odejide et al., 2014).

Therapeutic approaches

The work in this dissertation adds to other studies discussed in the introduction in pointing to possible novel therapies to stop lymphoma progression. Blunt approaches can be considered if a patient it at high risk of developing GC-derived lymphomas or failed prior therapies. These include depleting Tfh cells through anti-CD4 antibodies and blocking CD40-CD40L, ICOS-ICOSL and IL4-IL4R signaling axes. More modest approaches could be to augment SLAMF receptor function in T cells. Restoring negative regulation of GC B cell responses by enhancing PD-1-PD-L1 and BTLA-HVEM axes could inhibit GC B cell outgrowth.

This has been demonstrated in a mouse model of FL where anti-CD19 CAR-T cells delivered soluble HVEM to the tumor microenvironment and likely inhibited Tfh cell help to FL B cells by engaging BTLA. Augmenting FasL-Fas interaction in lymphomas that retain this pathway could have therapeutic benefit. Better definition of the dependency of some GC lymphomas on T cells, and of tumor suppressors that are acting in *trans*, may identify more opportunities for restoring those tumor suppressors using CAR T cell-type approaches or other surface receptor-targeted therapeutic strategies. It is also possible that targeting the cues that organize GCs and foster interactions between GC B cells and Tfh cells, such as CXCL13 and CXCR5, may be an approach to interrupt T cell support of lymphoma cells.

Concluding remarks

The study of mutations arising in B and T cell lymphomas is providing important insights about the normal mechanisms acting in GC responses and this work in turn is proving informative about the drivers of lymphomagenesis. While the tumor microenvironment is unquestionably crucial for lymphomagenesis (Basso and Dalla-Favera, 2015), the potential of a supportive T cells to be targeted during lymphomagenesis is only just beginning to be appreciated. The evidence discussed in this review suggests that targeting T cell help during GC-derived lymphomagenesis can provide a complementary approach to B cell targeted therapies for treating these lymphomas.

REFERENCES

Allen, C.D.C., Okada, T., Tang, H.L., and Cyster, J.G. (2007). Imaging of germinal center selection events during affinity maturation. Science *315*, 528–531.

Ame-Thomas, P., Le Priol, J., Yssel, H., Caron, G., Pangault, C., Jean, R., Martin, N., Marafioti, T., Gaulard, P., Lamy, T., et al. (2012). Characterization of intratumoral follicular helper T cells in follicular lymphoma: role in the survival of malignant B cells. Leukemia *26*, 1053–1063.

Auguste, T., Travert, M., Tarte, K., Ame-Thomas, P., Artchounin, C., Martin-Garcia, N., de Reynies, A., de Leval, L., Gaulard, P., and Delfau-Larue, M.-H. (2013). ROQUIN/RC3H1 Alterations Are Not Found in Angioimmunoblastic T-Cell Lymphoma. PLoS ONE *8*, e64536–4.

Álvarez-Prado, Á.F., Pérez-Durán, P., Pérez-García, A., Benguria, A., Torroja, C., de Yébenes, V.G., and Ramiro, A.R. (2018). A broad atlas of somatic hypermutation allows prediction of activation-induced deaminase targets. Journal of Experimental Medicine *215*, 761–771.

Bannard, O., and Cyster, J.G. (2017). ScienceDirect Germinal centers: programmed for affinity maturation and antibody diversification. Current Opinion in Immunology *45*, 21–30.

Bannard, O., McGowan, S.J., Ersching, J., Ishido, S., Victora, G.D., Shin, J.-S., and Cyster, J.G. (2016). Ubiquitin-mediated fluctuations in MHC class II facilitate efficient germinal center B cell responses. Journal of Experimental Medicine *213*, 993–1009.

Basso, K., and Dalla-Favera, R. (2015). Germinal centres and B cell lymphomagenesis. Nat. Rev. Immunol. *15*, 172–184.

Bende, R.J., Smit, L.A., and van Noesel, C.J.M. (2007). Molecular pathways in follicular lymphoma. Leukemia *21*, 18–29.

Berkova, Z., Tao, R.-H., and Samaniego, F. (2009). Milatuzumab – a promising new immunotherapeutic agent. Expert Opinion on Investigational Drugs *19*, 141–149.

Béguelin, W., Popovic, R., Teater, M., Jiang, Y., Bunting, K.L., Rosen, M., Shen, H., Yang, S.N., Wang, L., Ezponda, T., et al. (2013). EZH2 Is Required for Germinal Center Formation and Somatic EZH2 Mutations Promote Lymphoid Transformation. Cancer Cell *23*, 677–692.

Béguelin, W., Rivas, M.A., Fernández, M.T.C., Teater, M., Purwada, A., Redmond, D., Shen, H., Challman, M.F., Elemento, O., Singh, A., et al. (2017). EZH2 enables germinal centre formation through epigenetic silencing of CDKN1A and an Rb-E2F1 feedback loop. Nat Commun 1–16.

Boice, M., Salloum, D., Mourcin, F., Sanghvi, V., Amin, R., Oricchio, E., Jiang, M., Mottok, A., Denis-Lagache, N., Ciriello, G., et al. (2016). Loss of the HVEM Tumor Suppressor in Lymphoma and Restoration by Modified CAR-T Cells. Cell *167*, 405–418.e413.

Boisvert, J., Edmondson, S., and Krummel, M.F. (2004). Immunological Synapse Formation Licenses CD40-CD40L Accumulations at T-APC Contact Sites. The Journal of Immunology *173*, 3647–3652.

Bolotin, D.A., Poslavsky, S., Mitrophanov, I., Shugay, M., Mamedov, I.Z., Putintseva, E.V., and Chudakov, D.M. (2015). MiXCR: software for comprehensive adaptive immunity profiling. Nature Publishing Group *12*, 380–381.

Bouska, A., Bi, C., Lone, W., Zhang, W., Kedwaii, A., Heavican, T., Lachel, C.M., Yu, J., Ferro, R., Eldorghamy, N., et al. (2017). Adult high-grade B-cell lymphoma with Burkitt lymphoma signature: genomic features and potential therapeutic targets. Blood *130*, 1819–1831.

Bride, K., and Teachey, D. (2017). Autoimmune lymphoproliferative syndrome: more than a FAScinating disease. F1000Res *6*, 1928–16.

Butt, D., Chan, T.D., Bourne, K., Hermes, J.R., Nguyen, A., Statham, A., O'Reilly, L.A., Strasser, A., Price, S., Schofield, P., et al. (2015). FAS Inactivation Releases Unconventional Germinal Center B Cells that Escape Antigen Control and Drive IgE and Autoantibody Production. Immunity *42*, 890–902.

Calado, D.P., Sasaki, Y., Godinho, S.A., Pellerin, A., Köchert, K., Sleckman, B.P., de Alborán, I.M., Janz, M., Rodig, S., and Rajewsky, K. (2012). The cell-cycle regulator c-Myc is essential for the formation and maintenance of germinal centers. Nat Immunol *13*, 1092–1100.

Calvo, K.R., Dabir, B., Kovach, A., Devor, C., Bandle, R., Bond, A., Shih, J.H., and Jaffe, E.S. (2008). IL-4 protein expression and basal activation of Erk in vivo in follicular lymphoma. Blood *112*, 3818–3826.

Cannons, J.L., Qi, H., Lu, K.T., Dutta, M., and Gomez-Rodriguez, J. (2010). Optimal germinal center responses require a multistage T cell: B cell adhesion process involving integrins, SLAM-associated protein, and CD84. Immunity *32*, 253–265.

Carbone, A., Gloghini, A., Gruss, H.J., and Pinto, A. (1995). CD40 ligand is constitutively expressed in a subset of T cell lymphomas and on the microenvironmental reactive T cells of follicular lymphomas and Hodgkin's disease. Am. J. Pathol. *147*, 912–922.

Carreras, J., Lopez-Guillermo, A., Kikuti, Y.Y., Itoh, J., Masashi, M., Ikoma, H., Tomita, S., Hiraiwa, S., Hamoudi, R., Rosenwald, A., et al. (2019). High TNFRSF14 and low BTLA are associated with poor prognosis in Follicular Lymphoma and in Diffuse Large B-cell Lymphoma transformation. Jceh *59*, 1–16.

Casamayor-Palleja, M., Khan, M., and MacLennan, I.C. (1995). A subset of CD4+ memory T cells contains preformed CD40 ligand that is rapidly but transiently expressed on their surface after activation through the T cell receptor complex. Journal of Experimental Medicine *181*, 1293–1301.

Celis-Gutierrez, J., Blattmann, P., Zhai, Y., Jarmuzynski, N., Ruminski, K., Grégoire, C., Ounoughene, Y., Fiore, F., Aebersold, R., Roncagalli, R., et al. (2019). Quantitative Interactomics in Primary T Cells Provides a Rationale for Concomitant PD-1 and BTLA Coinhibitor Blockade in Cancer Immunotherapy. Cell Rep *27*, 3315–3330.e3317.

Challa-Malladi, M., Lieu, Y.K., Califano, O., Holmes, A.B., Bhagat, G., Murty, V.V., Dominguez-Sola, D., Pasqualucci, L., and Dalla-Favera, R. (2011). Combined genetic inactivation of β2-Microglobulin and CD58 reveals frequent escape from immune recognition in diffuse large B cell lymphoma. Cancer Cell *20*, 728–740.

Chang, K.-C., Huang, X., Medeiros, L.J., and Jones, D. (2003). Germinal centre-like versus undifferentiated stromal immunophenotypes in follicular lymphoma. J. Pathol. *201*, 404–412.

Chao, M.P., Alizadeh, A.A., Tang, C., Myklebust, J.H., Varghese, B., Gill, S., Jan, M., Cha, A.C., Chan, C.K., Tan, B.T., et al. (2010). Anti-CD47 antibody synergizes with rituximab to promote phagocytosis and eradicate non-Hodgkin lymphoma. Cell *142*, 699–713.

Chemnitz, J.M., Parry, R.V., Nichols, K.E., June, C.H., and Riley, J.L. (2004). SHP1 and SHP2 Associate with Immunoreceptor Tyrosine-Based Switch Motif of Programmed Death 1 upon Primary Human T Cell Stimulation, but Only Receptor Ligation Prevents T Cell Activation. The Journal of Immunology *173*, 945–954.

Chen, S., Lee, B., Lee, A.Y.-F., Modzelewski, A.J., and He, L. (2016). Highly Efficient Mouse Genome Editing by CRISPR Ribonucleoprotein Electroporation of Zygotes. J. Biol. Chem. *291*, 14457–14467.

Cheung, K.-J.J., Johnson, N.A., Affleck, J.G., Severson, T., Steidl, C., Ben-Neriah, S., Schein, J., Morin, R.D., Moore, R., Shah, S.P., et al. (2010). Acquired TNFRSF14 mutations in follicular lymphoma are associated with worse prognosis. Cancer Res *70*, 9166–9174.

Cheung, T.C., Oborne, L.M., Steinberg, M.W., Macauley, M.G., Fukuyama, S., Sanjo, H., D'Souza, C., Norris, P.S., Pfeffer, K., Murphy, K.M., et al. (2009a). T Cell Intrinsic Heterodimeric Complexes between HVEM and BTLA Determine Receptivity to the Surrounding Microenvironment. The Journal of Immunology *183*, 7286–7296.

Cheung, T.C., Steinberg, M.W., Oborne, L.M., Macauley, M.G., Fukuyama, S., Sanjo, H., D'Souza, C., Norris, P.S., Pfeffer, K., Murphy, K.M., et al. (2009b). Unconventional ligand activation of herpesvirus entry mediator signals cell survival. Proc. Natl. Acad. Sci. U.S.a. *106*, 6244–6249.

Chevrier, S., Kratina, T., Emslie, D., Tarlinton, D.M., and Corcoran, L.M. (2017). IL4 and IL21 cooperate to induce the high Bcl6 protein level required for germinal center formation. Immunol. Cell Biol. *95*, 925–932.

Choudhuri, K., Llodrá, J., Roth, E.W., Tsai, J., Gordo, S., Wucherpfennig, K.W., Kam, L.C., Stokes, D.L., and Dustin, M.L. (2014). Polarized release of T-cell-receptor-enriched microvesicles at the immunological synapse. Nature *507*, 118–123.

Chtanova, T., Tangye, S.G., Newton, R., Frank, N., Hodge, M.R., Rolph, M.S., and Mackay, C.R. (2004). T Follicular Helper Cells Express a Distinctive Transcriptional Profile, Reflecting Their Role as Non-Th1/Th2 Effector Cells That Provide Help for B Cells. The Journal of Immunology *173*, 68–78.

Cobaleda, C., Jochum, W., and Busslinger, M. (2007). Conversion of mature B cells into T cells by dedifferentiation to uncommitted progenitors. Nature *449*, 473–477.

Cortes, J.R., Ambesi-Impiombato, A., Couronné, L., Quinn, S.A., Kim, C.S., da Silva Almeida, A.C., West, Z., Belver, L., Martin, M.S., Scourzic, L., et al. (2018). RHOA G17V Induces T Follicular Helper Cell Specification and Promotes Lymphomagenesis. Cancer Cell *33*, 259–273.e7.

Crotty, S. (2019). T Follicular Helper Cell Biology: A Decade of Discovery and Diseases. Immunity *50*, 1132–1148.

de Jong, D., and Fest, T. (2011). The microenvironment in follicular lymphoma. Best Practice & Research Clinical Haematology *24*, 135–146.

Dominguez-Sola, D., Victora, G.D., Ying, C.Y., Phan, R.T., Saito, M., Nussenzweig, M.C., and Dalla-Favera, R. (2012). The proto-oncogene MYC is required for selection in the germinal center and cyclic reentry. Nat Immunol *13*, 1083–1091.

Duhen, T., Pasero, C., Mallet, F.O., Barbarat, B., Olive, D., and Costello, R.G.T. (2004). LIGHT costimulates CD40 triggering and induces immunoglobulin secretion; a novel key partner in T cell-dependent B cell terminal differentiation. Eur. J. Immunol. *34*, 3534–3541.

Dustin, M.L., Starr, T., Varma, R., and Thomas, V.K. (2007). Supported Planar Bilayers for Study of the Immunological Synapse. Current Protocols in Immunology *76*, 18.13.1–18.13.35.

Egle, A. (2004). VavP-Bcl2 transgenic mice develop follicular lymphoma preceded by germinal center hyperplasia. Blood *103*, 2276–2283.

Ellyard, J.I., Chia, T., Rodriguez-Pinilla, S.-M., Martin, J.L., Hu, X., Navarro-Gonzalez, M., Garcia, J.F., Delfau-Larue, M.-H., Montes-Moreno, S., Gaulard, P., et al. (2012). Heterozygosity for Roquinsan leads to angioimmunoblastic T-cell lymphoma-like tumors in mice. Blood *120*, 812–821.

Engel, P., Eck, M.J., and Terhorst, C. (2003). The SAP and SLAM families in immune responses and X-linked lymphoproliferative disease. Nat. Rev. Immunol. *3*, 813–821.

Ersching, J., Efeyan, A., Mesin, L., Jacobsen, J.T., Pasqual, G., Grabiner, B.C., Dominguez-Sola, D., Sabatini, D.M., and Victora, G.D. (2017). Germinal Center Selection and Affinity Maturation Require Dynamic Regulation of mTORC1 Kinase. Immunity *46*, 1045–1058.e1046.

Fanale, M., Assouline, S., Kuruvilla, J., Solal-Céligny, P., Heo, D.S., Verhoef, G., Corradini, P., Abramson, J.S., Offner, F., Engert, A., et al. (2013). Phase IA/II, multicentre, open-label study of the CD40 antagonistic monoclonal antibody lucatumumab in adult patients with advanced non-Hodgkin or Hodgkin lymphoma. British Journal of Haematology *164*, 258–265.

Fouquet, G., Marcq, I., Debuysscher, V., Bayry, J., Rabbind Singh, A., Bengrine, A., Nguyen-Khac, E., Naassila, M., and Bouhlal, H. (2018). Signaling lymphocytic activation molecules Slam and cancers: friends or foes? Oncotarget *9*, 16248–16262.

Gardell, J.L., and Parker, D.C. (2016). CD40L is transferred to antigen-presenting B cells during delivery of T-cell help. Eur. J. Immunol. *47*, 41–50.

Gavrieli, M., and Murphy, K.M. (2006). Association of Grb-2 and PI3K p85 with phosphotyrosile peptides derived from BTLA. Biochem. Biophys. Res. Commun. *345*, 1440–1445.

Gavrieli, M., Watanabe, N., Loftin, S.K., Murphy, T.L., and Murphy, K.M. (2003). Characterization of phosphotyrosine binding motifs in the cytoplasmic domain of B and T lymphocyte attenuator required for association with protein tyrosine phosphatases SHP1 and SHP2. Biochem. Biophys. Res. Commun. *312*, 1236–1243.

Ghia, P., Boussiotis, V.A., Schultze, J.L., Cardoso, A.A., Dorfman, D.M., Gribben, J.G., Freedman, A.S., and Nadler, L.M. (1998). Unbalanced expression of bcl-2 family proteins in follicular lymphoma: contribution of CD40 signaling in promoting survival. Blood *91*, 244–251.

Gitlin, A.D., Shulman, Z., and Nussenzweig, M.C. (2014). Clonal selection in the germinal centre by regulated proliferation and hypermutation. Nature *509*, 637–640.

Godfrey, J., Tumuluru, S., Bao, R., Leukam, M., Venkataraman, G., Phillip, J., Fitzpatrick, C., McElherne, J., MacNabb, B.W., Orlowski, R., et al. (2019). PD-L1 gene alterations identify a subset of diffuse large B-cell lymphoma harboring a T-cell–inflamed phenotype. Blood *133*, 2279–2290.

Gonzalez, D.G., Cote, C.M., Patel, J.R., Smith, C.B., Zhang, Y., Nickerson, K.M., Zhang, T., Kerfoot, S.M., and Haberman, A.M. (2018). Nonredundant Roles of IL-21 and IL-4 in the Phased Initiation of Germinal Center B Cells and Subsequent Self-Renewal Transitions. J. Immunol. *201*, 3569–3579.

Good-Jacobson, K.L., Szumilas, C.G., Chen, L., Sharpe, A.H., Tomayko, M.M., and Shlomchik, M.J. (2010). PD-1 regulates germinal center B cell survival and the formation and affinity of long-lived plasma cells. Nat Immunol *11*, 535–542.

Green, J.A., Suzuki, K., Cho, B., Willison, L.D., Palmer, D., Allen, C.D.C., Schmidt, T.H., Xu, Y., Proia, R.L., Coughlin, S.R., et al. (2011). The sphingosine 1-phosphate receptor S1P2 maintains the homeostasis of germinal center B cells and promotes niche confinement. Nat Immunol *12*, 672–680.

Hams, E., McCarron, M.J., Amu, S., Yagita, H., Azuma, M., Chen, L., and Fallon, P.G. (2011). Blockade of B7-H1 (programmed death ligand 1) enhances humoral immunity by positively regulating the generation of T follicular helper cells. J. Immunol. *186*, 5648–5655.

Hao, Z., Duncan, G.S., Seagal, J., Su, Y.-W., Hong, C., Haight, J., Chen, N.-J., Elia, A., Wakeham, A., Li, W.Y., et al. (2008). Fas Receptor Expression in Germinal-Center B Cells Is Essential for T and B Lymphocyte Homeostasis. Immunity *29*, 615–627.

Hashwah, H., Schmid, C.A., Kasser, S., Bertram, K., Stelling, A., Manz, M.G., and Müller, A. (2017). Inactivation of CREBBP expands the germinal center B cell compartment, down-regulates MHCII expression and promotes DLBCL growth. Proc. Natl. Acad. Sci. U.S.a. *114*, 9701–9706.

Hömig-Hölzel, C., Hojer, C., Rastelli, J., Casola, S., Strobl, L.J., Müller, W., Quintanilla-Martinez, L., Gewies, A., Ruland, J., Rajewsky, K., et al. (2008). Constitutive CD40 signaling in B cells selectively activates the noncanonical NF-κB pathway and promotes lymphomagenesis. Journal of Experimental Medicine *205*, 1317–1329.

Hsu, H., Solovyev, I., Colombero, A., Elliott, R., Kelley, M., and Boyle, W.J. (1997). ATAR, a novel tumor necrosis factor receptor family member, signals through TRAF2 and TRAF5. J. Biol. Chem. *272*, 13471–13474.

Huang, B., Gomez-Rodriguez, J., Preite, S., Garrett, L.J., Harper, U.L., and Schwartzberg, P.L. (2016). CRISPR-Mediated Triple Knockout of SLAMF1, SLAMF5 and SLAMF6 Supports Positive Signaling Roles in NKT Cell Development. PLoS ONE *11*, e0156072–19.

Huet, S., Sujobert, P., and Salles, G. (2018). From genetics to the clinic: a translational perspective on follicular lymphoma. Nature Publishing Group *18*, 224–239.

Hui, E., Cheung, J., Zhu, J., Su, X., Taylor, M.J., Wallweber, H.A., Sasmal, D.K., Huang, J., Kim, J.M., Mellman, I., et al. (2017). T cell costimulatory receptor CD28 is a primary target for PD-1–mediated inhibition. Science *355*, 1428–1433.

Iezzi, G., Sonderegger, I., Ampenberger, F., Schmitz, N., Marsland, B.J., and Kopf, M. (2009). CD40–CD40L cross-talk integrates strong antigenic signals and microbial stimuli to induce development of IL-17-producing CD4+ T cells. Proceedings of the National Academy of Sciences *106*, 876–881.

Iqbal, J., Meyer, P.N., Smith, L.M., Johnson, N.A., Vose, J.M., Greiner, T.C., Connors, J.M., Staudt, L.M., Rimsza, L., Jaffe, E., et al. (2011). BCL2 Predicts Survival in Germinal Center B-

cell-like Diffuse Large B-cell Lymphoma Treated with CHOP-like Therapy and Rituximab. Clinical Cancer Research *17*, 7785–7795.

Iqbal, J., Weisenburger, D.D., Greiner, T.C., Vose, J.M., McKeithan, T., Kucuk, C., Geng, H., Deffenbacher, K., Smith, L., Dybkær, K., et al. (2010). Molecular signatures to improve diagnosis in peripheral T-cell lymphoma and prognostication in angioimmunoblastic T-cell lymphoma. Blood *115*, 1026–1036.

Kasahara, H., Kakimoto, T., Saito, H., Akuta, K., Yamamoto, K., Ujiie, H., Sugahara, H., Hoshida, Y., and Sakoda, H. (2013). Successful treatment with rituximab for angioimmunoblastic T-cell lymphoma. Leukemia Research Reports *2*, 36–38.

Kashiwakuma, D., Suto, A., Hiramatsu, Y., Ikeda, K., Takatori, H., Suzuki, K., Kagami, S.-I., Hirose, K., Watanabe, N., Iwamoto, I., et al. (2010). B and T lymphocyte attenuator suppresses IL-21 production from follicular Th cells and subsequent humoral immune responses. J. Immunol. *185*, 2730–2736.

Kishi, Y., Aiba, Y., Higuchi, T., Furukawa, K., Tokuhisa, T., Takemori, T., and Tsubata, T. (2010). Augmented Antibody Response with Premature Germinal Center Regression in CD40L Transgenic Mice. The Journal of Immunology *185*, 211–219.

Koguchi, Y., Thauland, T.J., Slifka, M.K., and Parker, D.C. (2007). Preformed CD40 ligand exists in secretory lysosomes in effector and memory CD4+ T cells and is quickly expressed on the cell surface in an antigen-specific manner. Blood *110*, 2520–2527.

Koguchi, Y., Buenafe, A.C., Thauland, T.J., Gardell, J.L., Bivins-Smith, E.R., Jacoby, D.B., Slifka, M.K., and Parker, D.C. (2012). Preformed CD40L Is Stored in Th1, Th2, Th17, and T

Follicular Helper Cells as Well as CD4+8− Thymocytes and Invariant NKT Cells but Not in Treg Cells. PLoS ONE *7*, e31296–14.

Koncz, G., and Hueber, A.-O. (2012). The Fas/CD95 Receptor Regulates the Death of Autoreactive B Cells and the Selection of Antigen-Specific B Cells. Front Immunol *3*, 207.

Kondo, E., Yoshino, T., Nishiuchi, R., Sakuma, I., Nishizaki, K., Kayagaki, N., Yagita, H., and Akagi, T. (1997). Expression of Fas ligand mRNA in germinal centres of the human tonsil. J. Pathol. *183*, 75–79.

Kopf, M., Le Gros, G., Coyle, A.J., Kosco-Vilbois, M., and Brombacher, F. (1995). Immune responses of IL-4, IL-5, IL-6 deficient mice. Immunological Reviews *148*, 45–69.

Kotsiou, E., Okosun, J., Besley, C., Iqbal, S., Matthews, J., Fitzgibbon, J., Gribben, J.G., and Davies, J.K. (2016). TNFRSF14 aberrations in follicular lymphoma increase clinically significant allogeneic T-cell responses. Blood 1–40.

Kuleshov, M.V., Jones, M.R., Rouillard, A.D., Fernandez, N.F., Duan, Q., Wang, Z., Koplev, S., Jenkins, S.L., Jagodnik, K.M., Lachmann, A., et al. (2016). Enrichr: a comprehensive gene set enrichment analysis web server 2016 update. Nucleic Acids Res. *44*, W90–W97.

Lackraj, T., Goswami, R., and Kridel, R. (2018). Pathogenesis of follicular lymphoma. Best Practice & Research Clinical Haematology *31*, 2–14.

Launay, E., Pangault, C., Bertrand, P., Jardin, F., Lamy, T., Tilly, H., Tarte, K., Bastard, C., and Fest, T. (2012). High rate of TNFRSF14 gene alterations related to 1p36 region in de novo follicular lymphoma and impact on prognosis. Leukemia *26*, 559–562.

Lavoie, T.B., Drohan, W.N., and Smith-Gill, S.J. (1992). Experimental analysis by site-directed mutagenesis of somatic mutation effects on affinity and fine specificity in antibodies specific for lysozyme. The Journal of Immunology *148*, 503–513.

Le, K.S., Thibult, M.L., Just-Landi, S., Pastor, S., Gondois-Rey, F., Granjeaud, S., Broussais, F., Bouabdallah, R., Colisson, R., Caux, C., et al. (2016). Follicular B Lymphomas Generate Regulatory T Cells via the ICOS/ICOSL Pathway and Are Susceptible to Treatment by Anti-ICOS/ICOSL Therapy. Cancer Res *76*, 4648–4660.

Lesley, R., Kelly, L.M., Xu, Y., and Cyster, J.G. (2006). Naive CD4 T cells constitutively express CD40L and augment autoreactive B cell survival. Proceedings of the National Academy of Sciences *103*, 10717–10722.

Liu, D., Xu, H., Shih, C., Wan, Z., Ma, X., Ma, W., Luo, D., and Qi, H. (2014). T-B-cell entanglement and ICOSL-driven feed-forward regulation of germinal centre reaction. Nature.

Liu, Y., Hernandez, A.M., Shibata, D., and Cortopassi, G.A. (1994). BCL2 translocation frequency rises with age in humans. Proceedings of the National Academy of Sciences *91*, 8910–8914.

Losman, J.A., Chen, X.P., Hilton, D., and Rothman, P. (1999). Cutting edge: SOCS-1 is a potent inhibitor of IL-4 signal transduction. The Journal of Immunology *162*, 3770–3774.

Lossos, I.S., and Gascoyne, R.D. (2011). Transformation of follicular lymphoma. Best Practice & Research Clinical Haematology *24*, 147–163.

Lu, E., Wolfreys, F.D., Muppidi, J.R., Xu, Y., and Cyster, J.G. (2019). S-Geranylgeranyl-L-glutathione is a ligand for human B cell-confinement receptor P2RY8. Nature *567*, 244–248.

Luo, W., Weisel, F., and Shlomchik, M.J. (2018). B Cell Receptor and CD40 Signaling Are Rewired for Synergistic Induction of the c-Myc Transcription Factor in Germinal Center B Cells. Immunity *48*, 313–326.e315.

MacLennan, I.C. (1994). Germinal centers. Annu. Rev. Immunol. *12*, 117–139.

Manso, B.A., Wenzl, K., Asmann, Y.W., Maurer, M.J., Manske, M., Yang, Z.-Z., Slager, S.L., Nowakowski, G.S., Ansell, S.M., Witzig, T.E., et al. (2017). Whole-exome analysis reveals novel somatic genomic alterations associated with cell of origin in diffuse large B-cell lymphoma. Blood Cancer J *7*, e553–e553.

Martinov, T., Swanson, L.A., Breed, E.R., Tucker, C.G., Dwyer, A.J., Johnson, J.K., Mitchell, J.S., Sahli, N.L., Wilson, J.C., Singh, L.M., et al. (2019). Programmed Death-1 Restrains the Germinal Center in Type 1 Diabetes. J. Immunol. *203*, 844–852.

Mayer, C.T., Gazumyan, A., Kara, E.E., Gitlin, A.D., Golijanin, J., Viant, C., Pai, J., Oliveira, T.Y., Wang, Q., Escolano, A., et al. (2017). The microanatomic segregation of selection by apoptosis in the germinal center. Science *358*.

Mayya, V., Judokusumo, E., Shah, E.A., Peel, C.G., Neiswanger, W., Depoil, D., Blair, D.A., Wiggins, C.H., Kam, L.C., and Dustin, M.L. (2018). Durable Interactions of T Cells with T Cell Receptor Stimuli in the Absence of a Stable Immunological Synapse. Cell Rep *22*, 340–349.

Mesin, L., Ersching, J., and Victora, G.D. (2016). Germinal Center B Cell Dynamics. Immunity *45*, 471–482.

Milpied, P., Cervera-Marzal, I., Mollichella, M.-L., Tesson, B., Brisou, G., Traverse-Glehen, A., Salles, G., Spinelli, L., and Nadel, B. (2018). Human germinal center transcriptional programs are de-synchronized in B cell lymphoma. Nat Immunol 1–19.

Mintz, M.A., Felce, J.H., Chou, M.Y., Mayya, V., Xu, Y., Shui, J.-W., An, J., Li, Z., Marson, A., Okada, T., et al. (2019). The HVEM-BTLA Axis Restrains T Cell Help to Germinal Center B Cells and Functions as a Cell- Extrinsic Suppressor in Lymphomagenesis. Immunity *51*, 310–323.e317.

Mlynarczyk, C., Fontán, L., and Melnick, A. (2019). Germinal center-derived lymphomas: The darkest side of humoral immunity. Immunological Reviews *288*, 214–239.

Mulder, T.A., Wahlin, B.E., Österborg, A., and Palma, M. (2019). Targeting the Immune Microenvironment in Lymphomas of B-Cell Origin: From Biology to Clinical Application. Cancers (Basel) *11*.

Muppidi, J.R., Schmitz, R., Green, J.A., Xiao, W., Larsen, A.B., Braun, S.E., An, J., Xu, Y., Rosenwald, A., Ott, G., et al. (2014). Loss of signalling via Gα13 in germinal centre B-cell-derived lymphoma. Nature *516*, 254–258.

Murphy, K.M., Nelson, C.A., and Sedy, J.R. (2006). Balancing co-stimulation and inhibition with BTLA and HVEM. Nat. Rev. Immunol. *6*, 671–681.

Müschen, M., Rajewsky, K., Krönke, M., and Küppers, R. (2002). The origin of CD95-gene mutations in B-cell lymphoma. Trends Immunol. *23*, 75–80.

Myklebust, J.H., Irish, J.M., Brody, J., Czerwinski, D.K., Houot, R., Kohrt, H.E., Timmerman, J., Said, J., Green, M.R., Delabie, J., et al. (2013). High PD-1 expression and suppressed cytokine signaling distinguish T cells infiltrating follicular lymphoma tumors from peripheral T cells. Blood *121*, 1367–1376.

Nurieva, R.I., Chung, Y., Martinez, G.J., Yang, X.O., Tanaka, S., Matskevitch, T.D., Wang, Y.-H., and Dong, C. (2009). Bcl6 mediates the development of T follicular helper cells. Science *325*, 1001–1005.

Ochando, J., and Braza, M.S. (2017). T follicular helper cells: a potential therapeutic target in follicular lymphoma. Oncotarget *8*, 112116–112131.

Odejide, O., Weigert, O., Lane, A.A., Toscano, D., Lunning, M.A., Kopp, N., Kim, S., van Bodegom, D., Bolla, S., Schatz, J.H., et al. (2014). A targeted mutational landscape of angioimmunoblastic T-cell lymphoma. Blood *123*, 1293–1296.

Ogilvy, S., Metcalf, D., Print, C.G., Bath, M.L., Harris, A.W., and Adams, J.M. (1999). Constitutive Bcl-2 expression throughout the hematopoietic compartment affects multiple lineages and enhances progenitor cell survival. Proceedings of the National Academy of Sciences *96*, 14943–14948.

Owada, T., Watanabe, N., Oki, M., Oya, Y., Saito, Y., Saito, T., Iwamoto, I., Murphy, T.L., Murphy, K.M., and Nakajima, H. (2010). Activation-induced accumulation of B and T

lymphocyte attenuator at the immunological synapse in CD4+ T cells. Journal of Leukocyte Biology *87*, 425–432.

Oya, Y., Watanabe, N., Owada, T., Oki, M., Hirose, K., Suto, A., Kagami, S.-I., Nakajima, H., Kishimoto, T., Iwamoto, I., et al. (2008). Development of autoimmune hepatitis-like disease and production of autoantibodies to nuclear antigens in mice lacking B and T lymphocyte attenuator. Arthritis & Rheumatism *58*, 2498–2510.

Paiva, C., Godbersen, J.C., Rowland, T., Danilova, O.V., Danes, C., Berger, A., and Danilov, A.V. (2017). Pevonedistat, a Nedd8-activating enzyme inhibitor, sensitizes neoplastic B-cells to death receptor-mediated apoptosis. Oncotarget *8*, 21128–21139.

Pangault, C., Ame-Thomas, P., Ruminy, P., Rossille, D., Caron, G., Baia, M., De Vos, J., Roussel, M., Monvoisin, C., Lamy, T., et al. (2010). Follicular lymphoma cell niche: identification of a preeminent IL-4-dependent T(FH)-B cell axis. Leukemia *24*, 2080–2089.

Papa, I., Saliba, D., Ponzoni, M., Bustamante, S., Canete, P.F., Gonzalez-Figueroa, P., McNamara, H.A., Valvo, S., Grimbaldeston, M., Sweet, R.A., et al. (2017). TFH-derived dopamine accelerates productive synapses in germinal centres. Nature *547*, 318–323.

Paul, W.E. (2015). History of interleukin-4. Cytokine *75*, 3–7.

Paus, D., Phan, T.G., Chan, T.D., Gardam, S., Basten, A., and Brink, R. (2006). Antigen recognition strength regulates the choice between extrafollicular plasma cell and germinal center B cell differentiation. Journal of Experimental Medicine *203*, 1081–1091.

Qi, H., Cannons, J.L., Klauschen, F., Schwartzberg, P.L., and Germain, R.N. (2008). SAP-controlled T–B cell interactions underlie germinal centre formation. Nature *455*, 764–769.

Rabkin, C.S., Hirt, C., Janz, S., and Dolken, G. (2008). t(14;18) Translocations and Risk of Follicular Lymphoma. JNCI Monographs *2008*, 48–51.

Rawal, S., Chu, F., Zhang, M., Park, H.J., Nattamai, D., Kannan, S., Sharma, R., Delgado, D., Chou, T., Lin, H.Y., et al. (2013). Cross Talk between Follicular Th Cells and Tumor Cells in Human Follicular Lymphoma Promotes Immune Evasion in the Tumor Microenvironment. The Journal of Immunology *190*, 6681–6693.

Reinhardt, R.L., Liang, H.-E., and Locksley, R.M. (2009). Cytokine-secreting follicular T cells shape the antibody repertoire. Nat Immunol *10*, 385–393.

Ritthipichai, K., Haymaker, C.L., Martinez, M., Aschenbrenner, A., Yi, X., Zhang, M., Kale, C., Vence, L.M., Roszik, J., Hailemichael, Y., et al. (2017). Multifaceted Role of BTLA in the Control of CD8+ T-cell Fate after Antigen Encounter. Clinical Cancer Research *23*, 6151–6164.

Rota, G., Niogret, C., Dang, A.T., Barros, C.R., Fonta, N.P., Alfei, F., Morgado, L., Zehn, D., Birchmeier, W., Vivier, E., et al. (2018). Shp2 Is Dispensable for Establishing T Cell Exhaustion and for PD-1 Signaling In Vivo. Cell Rep *23*, 39–49.

Ruedl, C., Bachmann, M.F., and Kopf, M. (2000). The antigen dose determines T helper subset development by regulation of CD40 ligand. Eur. J. Immunol. *30*, 2056–2064.

Sacco, M.G., Ungari, M., Catò, E.M., Villa, A., Strina, D., Notarangelo, L.D., Jonkers, J., Zecca, L., Facchetti, F., and Vezzoni, P. (2000). Lymphoid abnormalities in CD40 ligand transgenic

mice suggest the need for tight regulation in gene therapy approaches to hyper immunoglobulin M (IgM) syndrome. Cancer Gene Ther. *7*, 1299–1306.

Sage, P.T., Francisco, L.M., Carman, C.V., and Sharpe, A.H. (2012). The receptor PD-1 controls follicular regulatory T cells in the lymph nodes and blood. Nat Immunol *14*, 152–161.

Schmitz, N., and de Leval, L. (2016). How I manage peripheral T-cell lymphoma, not otherwise specified and angioimmunoblastic T-cell lymphoma: current practice and a glimpse into the future. British Journal of Haematology *176*, 851–866.

Schmitz, R., Wright, G.W., Huang, D.W., Johnson, C.A., Phelan, J.D., Wang, J.Q., Roulland, S., Kasbekar, M., Young, R.M., Shaffer, A.L., et al. (2018). Genetics and Pathogenesis of Diffuse Large B-Cell Lymphoma. N. Engl. J. Med. *378*, 1396–1407.

Schmitz, R., Young, R.M., Ceribelli, M., Jhavar, S., Xiao, W., Zhang, M., Wright, G., Shaffer, A.L., Hodson, D.J., Buras, E., et al. (2012). Burkitt lymphoma pathogenesis and therapeutic targets from structural and functional genomics. Nature *490*, 116–120.

Sedy, J.R., Gavrieli, M., Potter, K.G., Hurchla, M.A., Lindsley, R.C., Hildner, K., Scheu, S., Pfeffer, K., Ware, C.F., Murphy, T.L., et al. (2004). B and T lymphocyte attenuator regulates T cell activation through interaction with herpesvirus entry mediator. Nat Immunol *6*, 90–98.

Seo, G.-Y., Shui, J.-W., Takahashi, D., Song, C., Wang, Q., Kim, K., Mikulski, Z., Chandra, S., Giles, D.A., Zahner, S., et al. (2018). LIGHT-HVEM Signaling in Innate Lymphoid Cell Subsets Protects Against Enteric Bacterial Infection. Cell Host and Microbe *24*, 249–260.e4.

Shi, J., Hou, S., Fang, Q., Liu, X., Liu, X., and Qi, H. (2018). PD-1 Controls Follicular T Helper Cell Positioning and Function. Immunity *49*, 264–274.e264.

Shinnakasu, R., Inoue, T., Kometani, K., Moriyama, S., Adachi, Y., Nakayama, M., Takahashi, Y., Fukuyama, H., Okada, T., and Kurosaki, T. (2016). Regulated selection of germinal-center cells into the memory B cell compartment. Nat Immunol *17*, 1–11.

Shui, J.-W., Larange, A., Kim, G., Vela, J.L., Zahner, S., Cheroutre, H., and Kronenberg, M. (2012). HVEM signalling at mucosal barriers provides host defence against pathogenic bacteria. Nature *488*, 222–225.

Shulman, Z., Gitlin, A.D., Weinstein, J.S., Lainez, B., Esplugues, E., Flavell, R.A., Craft, J.E., and Nussenzweig, M.C. (2014). Dynamic signaling by T follicular helper cells during germinal center B cell selection. Science *345*, 1058–1062.

Smeltzer, J.P., Jones, J.M., Ziesmer, S.C., Grote, D.M., Xiu, B., Ristow, K.M., Yang, Z.Z., Nowakowski, G.S., Feldman, A.L., Cerhan, J.R., et al. (2014). Pattern of CD14+ follicular dendritic cells and PD1+ T cells independently predicts time to transformation in follicular lymphoma. Clinical Cancer Research *20*, 2862–2872.

Steinberg, M.W., Cheung, T.C., and Ware, C.F. (2011). The signaling networks of the herpesvirus entry mediator (TNFRSF14) in immune regulation. Immunological Reviews *244*, 169–187.

Straus, S.E., Jaffe, E.S., Puck, J.M., Dale, J.K., Elkon, K.B., Rösen-Wolff, A., Peters, A.M., Sneller, M.C., Hallahan, C.W., Wang, J., et al. (2001). The development of lymphomas in

families with autoimmune lymphoproliferative syndrome with germline Fas mutations and defective lymphocyte apoptosis. Blood *98*, 194–200.

Sugiura, D., Maruhashi, T., Okazaki, I.-M., Shimizu, K., Maeda, T.K., Takemoto, T., and Okazaki, T. (2019). Restriction of PD-1 function by cis-PD-L1/CD80 interactions is required for optimal T cell responses. Science *364*, 558–566.

Sungalee, S., Mamessier, E., Morgado, E., Grégoire, E., Brohawn, P.Z., Morehouse, C.A., Jouve, N., Monvoisin, C., Menard, C., Debroas, G., et al. (2014). Germinal center reentries of BCL2-overexpressing B cells drive follicular lymphoma progression. J. Clin. Invest. *124*, 5337–5351.

Takahashi, Y., Ohta, H., and Takemori, T. (2001). Fas is required for clonal selection in germinal centers and the subsequent establishment of the memory B cell repertoire. Immunity *14*, 181–192.

Tang, J., Zha, J., Guo, X., Shi, P., and Xu, B. (2017). CXCR5+CD8+ T cells present elevated capacity in mediating cytotoxicity toward autologous tumor cells through interleukin 10 in diffuse large B-cell lymphoma. International Immunopharmacology *50*, 146–151.

Totten, S., Gaucher, D., Morin, R.D., Assouline, S., Connors, J.M., Marra, M.A., Scott, D.W., Gascoyne, R.D., Pelletier, J., Mann, K.K., et al. (2014). FAS Mutations Accelerate Lymphoma Growth and Induce Therapeutic Resistance. Blood *124*, 3018.

Travert, M., Ame-Thomas, P., Pangault, C., Morizot, A., Micheau, O., Semana, G., Lamy, T., Fest, T., Tarte, K., and Guillaudeux, T. (2008). CD40 ligand protects from TRAIL-induced apoptosis in follicular lymphomas through NF-kappaB activation and up-regulation of c-FLIP and Bcl-xL. J. Immunol. *181*, 1001–1011.

Tsukamoto, T., Nakano, M., Sato, R., Adachi, H., Kiyota, M., Kawata, E., Uoshima, N., Yasukawa, S., Chinen, Y., Mizutani, S., et al. (2017). High-risk follicular lymphomas harbour more somatic mutations including those in the AID-motif. Scientific Reports 1–10.

Turqueti-Neves, A., Otte, M., da Costa, O.P., Höpken, U.E., Lipp, M., Buch, T., and Voehringer, D. (2014). B-cell-intrinsic STAT6 signaling controls germinal center formation. Eur. J. Immunol. *44*, 2130–2138.

Vendel, A.C., Calemine-Fenaux, J., Izrael-Tomasevic, A., Chauhan, V., Arnott, D., and Eaton, D.L. (2009). B and T lymphocyte attenuator regulates B cell receptor signaling by targeting Syk and BLNK. J. Immunol. *182*, 1509–1517.

Verdière, L., Mourcin, F., and Tarte, K. (2018). Microenvironment signaling driving lymphomagenesis. Current Opinion in Hematology *25*, 335–345.

Vijayanand, P., Seumois, G., Simpson, L.J., Abdul-Wajid, S., Baumjohann, D., Panduro, M., Huang, X., Interlandi, J., Djuretic, I.M., Brown, D.R., et al. (2012). Interleukin-4 Production by Follicular Helper T Cells Requires the Conserved Il4 Enhancer Hypersensitivity Site V. Immunity *36*, 175–187.

Wakamatsu, E., Mathis, D., and Benoist, C. (2013). Convergent and divergent effects of costimulatory molecules in conventional and regulatory CD4+ T cells. Proceedings of the National Academy of Sciences *110*, 1023–1028.

Wan, Z., Lin, Y., Zhao, Y., and Qi, H. (2019). TFH cells in bystander and cognate interactions with B cells. Immunological Reviews *288*, 28–36.

Wang, Y., Subudhi, S.K., Anders, R.A., Lo, J., Sun, Y., Blink, S., Wang, Y., Wang, J., Liu, X., Mink, K., et al. (2005). The role of herpesvirus entry mediator as a negative regulator of T cell-mediated responses. J. Clin. Invest. *115*, 711–717.

Ward-Kavanagh, L.K., Lin, W.W., Sedy, J.R., and Ware, C.F. (2016). The TNF Receptor Superfamily in Co-stimulating and Co-inhibitory Responses. Immunity *44*, 1005–1019.

Watanabe, N., Gavrieli, M., Sedy, J.R., Yang, J., Fallarino, F., Loftin, S.K., Hurchla, M.A., Zimmerman, N., Sim, J., Zang, X., et al. (2003). BTLA is a lymphocyte inhibitory receptor with similarities to CTLA-4 and PD-1. Nat Immunol *4*, 670–679.

Weber, J.P., Fuhrmann, F., Feist, R.K., Lahmann, A., Baz, Al, M.S., Gentz, L.-J., Vu Van, D., Mages, H.W., Haftmann, C., Riedel, R., et al. (2015). ICOS maintains the T follicular helper cell phenotype by down-regulating Krüppel-like factor 2. Journal of Experimental Medicine *212*, 217–233.

Weinstein, J.S., Herman, E.I., Lainez, B., Licona-Limón, P., Esplugues, E., Flavell, R., and Craft, J. (2016). TFH cells progressively differentiate to regulate the germinal center response. Nat Immunol *17*, 1197–1205.

Wu, T.-H., Zhen, Y., Zeng, C., Yi, H.-F., and Zhao, Y. (2007). B and T lymphocyte attenuator interacts with CD3ζ and inhibits tyrosine phosphorylation of TCRζ complex during T-cell activation. Immunol. Cell Biol. *85*, 590–595.

Xu, H., Li, X., Liu, D., Li, J., Zhang, X., Chen, X., Hou, S., Peng, L., Xu, C., Liu, W., et al. (2013). Follicular T-helper cell recruitment governed by bystander B cells and ICOS-driven motility. Nature *496*, 523–527.

Xu-Monette, Z.Y., Xiao, M., Au, Q., Padmanabhan, R., Xu, B., Hoe, N., Rodríguez-Perales, S., Torres-Ruiz, R., Manyam, G.C., Visco, C., et al. (2019). Immune Profiling and Quantitative Analysis Decipher the Clinical Role of Immune-Checkpoint Expression in the Tumor Immune Microenvironment of DLBCL. Cancer Immunology Research *7*, 644–657.

Xu-Monette, Z.Y., Li, L., Byrd, J.C., Jabbar, K.J., Manyam, G.C., Maria de Winde, C., van den Brand, M., Tzankov, A., Visco, C., Wang, J., et al. (2016). Assessment of CD37 B-cell antigen and cell of origin significantly improves risk prediction in diffuse large B-cell lymphoma. Blood *128*, 3083–3100.

Yang, Z.Z., Kim, H.J., Villasboas, J.C., Price-Troska, T., Jalali, S., Wu, H., Luchtel, R.A., Polley, M.-Y.C., Novak, A.J., and Ansell, S.M. (2019). Mass Cytometry Analysis Reveals that Specific Intratumoral CD4+ T Cell Subsets Correlate with Patient Survival in Follicular Lymphoma. Cell Rep *26*, 2178–2193.e3.

Yang, Z., Sullivan, B.M., and Allen, C.D.C. (2012). Fluorescent In Vivo Detection Reveals that IgE+ B Cells Are Restrained by an Intrinsic Cell Fate Predisposition. Immunity *36*, 857–872.

Yeh, C.-H., Nojima, T., Kuraoka, M., and Kelsoe, G. (2018). Germinal center entry not selection of B cells is controlled by peptide-MHCII complex density. Nat Commun *9*, 928.

Yi, T., and Cyster, J.G. (2013). EBI2-mediated bridging channel positioning supports splenic dendritic cell homeostasis and particulate antigen capture. eLife *2*, 309–319.

Yokosuka, T., Takamatsu, M., Kobayashi-Imanishi, W., Hashimoto-Tane, A., Azuma, M., and Saito, T. (2012). Programmed cell death 1 forms negative costimulatory microclusters that

directly inhibit T cell receptor signaling by recruiting phosphatase SHP2. Journal of Experimental Medicine *209*, 1201–1217.

Yu, D., Cozma, D., Park, A., and Thomas-Tikhonenko, A. (2005). Functional validation of genes implicated in lymphomagenesis: an in vivo selection assay using a Myc-induced B-cell tumor. Ann. N. Y. Acad. Sci. *1059*, 145–159.

Yusuf, I., Kageyama, R., Monticelli, L., Johnston, R.J., DiToro, D., Hansen, K., Barnett, B., and Crotty, S. (2010). Germinal Center T Follicular Helper Cell IL-4 Production Is Dependent on Signaling Lymphocytic Activation Molecule Receptor (CD150). The Journal of Immunology *185*, 190–202.

Zhao, Y., Zheng, Z., Cohen, C.J., Gattinoni, L., Palmer, D.C., Restifo, N.P., Rosenberg, S.A., and Morgan, R.A. (2005). High-Efficiency Transfection of Primary Human and Mouse T Lymphocytes Using RNA Electroporation. Molecular Therapy *13*, 151–159.

Zhu, Y., Yao, S., Augustine, M.M., Xu, H., Wang, J., Sun, J., Broadwater, M., Ruff, W., Luo, L., Zhu, G., et al. (2016). Neuron-specific SALM5 limits inflammation in the CNS via its interaction with HVEM. Science Advances *2*, e1500637–e1500637.

Zotos, D., Coquet, J.M., Zhang, Y., Light, A., D'Costa, K., Kallies, A., Corcoran, L.M., Godfrey, D.I., Toellner, K.-M., Smyth, M.J., et al. (2010). IL-21 regulates germinal center B cell differentiation and proliferation through a B cell-intrinsic mechanism. J. Exp. Med. *207*, 365–378.

Publishing Agreement

It is the policy of the University to encourage the distribution of all theses, dissertations, and manuscripts. Copies of all UCSF theses, dissertations, and manuscripts will be routed to the library via the Graduate Division. The library will make all theses, dissertations, and manuscripts accessible to the public and will preserve these to the best of their abilities, in perpetuity.

Please sign the following statement:

I hereby grant permission to the Graduate Division of the University of California, San Francisco to release copies of my thesis, dissertation, or manuscript to the Campus Library to provide access and preservation, in whole or in part, in perpetuity.

DocuSigned by:
Michelle Amy Mintz
90EDD263E42B439...
Author Signature

11/30/2019
Date